PARTON FRAGMENTATION AND STRING DYNAMICS

B. ANDERSSON, G. GUSTAFSON, G. INGELMAN and T. SJÖSTRAND
Lund, Sweden

CLASSICAL STRING PHENOMENOLOGY. HOW STRINGS WORK

X. ARTRU
Orsay, France

NORTH-HOLLAND PUBLISHING COMPANY - AMSTERDAM

PHYSICS REPORTS (Review Section of Physics Letters) 97, Nos. 2 & 3 (1983) 31–145. North-Holland Publishing Company

PARTON FRAGMENTATION AND STRING DYNAMICS

B. ANDERSSON, G. GUSTAFSON, G. INGELMAN* and T. SJÖSTRAND**

Department of Theoretical Physics, Sölvegatan 14A, S-223 62 Lund, Sweden

Contents:

1. Introduction

The quark-parton model is still at the basis of most of our attempts to describe hadronic phenomena. It is surprising that a model with essentially noninteracting *parts* describes so many properties which are not so easy to address in terms of the *entities*, i.e. the hadrons themselves. There is a simple and beautiful explanation by the notion of asymptotic freedom [1] for nonabelian gauge theories, in particular for quantum chromodynamics (QCD). It does, however, imply that the space-time scale where theory dwells is rather different from the one where the experimental detector setups are working. Thus while perturbative QCD-calculations can be trusted on the scale of maybe fractions of a fermi, the outcome of the hard processes are measured very far away, indeed. In the meantime a large amount of frustrating changes seems to have occurred. The main observation seems to be that there is no longer a partonic picture around. Nevertheless, one may hope that there are more or less pronounced traces of the basic dynamics available in the final state hadron distributions. Many of the

* Present address: CERN, Theory Division, CH-1211 Geneva 23, Switzerland.
** Present address: DESY, Theory Group, Notkestrasse 85, D-2000 Hamburg 52, Germany.

0 370-1573/83/0000–0000/$34.50

PARTON FRAGMENTATION AND STRING DYNAMICS

B. ANDERSSON, G. GUSTAFSON, G. INGELMAN and T. SJÖSTRAND

Lund, Sweden

CLASSICAL STRING PHENOMENOLOGY. HOW STRINGS WORK

X. ARTRU

Orsay, France

Received March 1983

Contents:

Abstract:

While much has been learned recently about quark and gluon interactions in the framework of perturbative Quantum Chromodynamics, the relation between calculated parton properties and observed hadron densities involves models where dynamics and jet empirical rules have to be combined. The purpose of this article is to describe a presently successful approach which is based on a cascade jet model using String dynamics. It can readily lead to Monte Carlo jet programmes of great use when analyzing data. Production processes in an iterative cascade approach, with tunneling in a constant force field, are reviewed. Expected differences between quark and gluon jets are discussed. Low transverse momentum phenomena are also reviewed with emphasis on hyperon polarization. In so far as this approach uses a fragmentation scheme based on String dynamics, it was deemed appropriate to also include under the same cover a special report on the Classical theory of relativistic Strings, seen as the classical limit of the Dual Resonance model. The Equations of motion and interaction among strings are presented.

tests of the theory, in particular of the perturbative QCD structure, contains e.g. nonscaling deviations from the parton model.

There are at this point already some difficulties because it is well-known that any finite energy hadronic distribution will contain nonscaling contributions, sometimes to an even larger degree than the inherent scale breaking effects of the theory. Further the pencilsharp energy and momentum distributions from the single partons are essentially distorted, widened in transverse directions and even the basic quantum numbers like charge and strangeness etc. seem to have been transported sometimes rather far away in longitudinal rapidity space. It has therefore become increasingly obvious over the years that in order to compare experiment to basic theory, it is necessary to have reliable descriptions of the transfer from the partonic stage to the hadronic one, i.e. to have consistent models for the process of parton fragmentation.

Such models may on the one hand be looked upon solely as phenomenological parametrizations and rules of thumb in order to obtain a translation from one language to another. As such they are useful for analysis of experiment as well as for the planning. On the other hand one may as always in connection with phenomenology try to obtain a dynamical framework that serves as a motivation and a generalizing principle for the constructions.

It should be kept in mind, however, that there are no easily available measures of the success of such a venture. As Bacon told us a long time ago, it is actually only possible to learn that one is wrong by a comparison between model calculations and experimental findings. If the prediction agrees there is no reassurance that one is even working in the right basic direction (although there is evidently a possible reason to feel some confidence!).

A modest measure of success would be a demand that the number of phenomenological parameters and the variation in size of their values are nonincreasing functions of time as well as the number of independent experimental findings. It is also of evident interest that the same basic scheme is applicable in different contexts such as different partonic processes and different parts of phase-space. Several schemes with a more or less profound theoretical foundation have been suggested but we will in this review be concerned only with iterative cascade jet models based upon string dynamics. The present experience from these models shows that at least the above-mentioned criteria for success are fulfilled.

We will in this review mostly discuss a possible dynamical framework behind the models and we will only use comparisons to data in order to demonstrate matters of principle. One of the nice features of the models is their stochastic structure which readily lends itself to an implementation in terms of computer generation. Several such Monte Carlo jet programs are available [2] for the interested reader to make much more detailed comparisons.

Our approach will primarily be of a semi-classical nature, i.e. we will at most places make use of a classical dynamical framework for our considerations. We will, however, at all necessary places point to the basic quantum mechanical constraints.

It is well-known that by means of a careful choice of dynamical variables it is often possible to circumvent such constraints. As an example we note that it is in general not possible to give independent values to canonically conjugate variables such as momentum (p) and position (x) due to Heisenberg's uncertainty principle:

$$\Delta p \cdot \Delta x \gtrsim 1 . \tag{1.1}$$

It is on the other hand for a large energy (E) particle possible to give values to rapidity ($\Delta y = \Delta p/E$) and

position [3] up to a degree of precision determined by the size of $1/E$:

$$\Delta x \cdot \Delta y \geq 1/E . \tag{1.2}$$

Therefore, in general longitudinal degrees of freedom may in high energy experiments be described essentially in a classical language. For transverse momentum properties and for spin it is necessary, however, to keep track of quantum mechanics. Further, for questions related to the density of states and the level schemes, it is also necessary to take quantum mechanics fully into account. Fortunately, it is well-known ever since the first cosmic ray interactions in emulsion plates became available, that the main dynamics seem to be of a one-dimensional nature.

A word of warning may, however, once again be in place. As long as only the properties of "all particles", "all charged particles" or "all pions" in hadronic events are considered, it is seldom necessary to go outside the time-honoured incoherent longitudinal phase-space dynamics to describe the data. Features of the fragmentation dynamics which contains more information and necessitates a more sophisticated description are e.g.

1. Strangeness–antistrangeness, baryon–antibaryon and heavy quark production (in particular correlation studies). Because strange particles and baryons are more rare, such pairs are often correlated and can exhibit the local properties of the production process. Also the larger masses imply that the particles carry more information on the force fields between the partons.

2. Vector meson production studies, which more directly exhibit the quantum number and energy-momentum flow of the original partons than their final decay products.

3. Transverse momentum correlations, in particular in connection with heavy particles, which should exhibit degrees of freedom in the force fields like soft gluon emission etc.

4. Polarization properties, which exhibit further degrees of freedom than the purely kinematical energy momentum flows.

This part is organized into five sections besides this Introduction.

In section 2 we discuss in some detail the properties of iterative cascade jets, with emphasis on the longitudinal degrees of freedom. We provide a dynamical picture in space-time and energy-momentum space, based upon string dynamics and we compare to different schemes that have been suggested. We also consider in some detail a scheme which is symmetric with respect to particle generation from the quark and antiquark ends in a two-jet system.

In section 3 we consider the production as a tunneling process in a constant force field. We also discuss the ratio of vector to pseudoscalar meson production in a jet as well as a simple mechanism for the production of baryon–antibaryon pairs.

In section 4 we extend the model to processes containing gluons and consider different models for hard and soft gluon emission as well as the dynamical implications. We discuss the possibility to construct observables which are insensitive to the fragmentation process, and the possibility to determine the strong coupling constant α_s from the hadronization properties.

In section 5 we exhibit a possible dynamical mechanism in low-$p_\perp$ hadronic interactions and discuss in some detail the ensuing model which usually is referred to as the fragmentation model. We consider a simple mechanism for polarization in hyperon production and the consequences of it.

In section 6 we point to an inherent property of fragmentation schemes based upon string dynamics, i.e. that the final state particles stem from the confined force fields between the partons. The fact that the properties of a confined force field are not determined solely by the position of the charges means

that it is necessary to consider field topological properties, i.e. the way the fields are spanned and the way the colour flow is directed along the fields, in order to describe the fragmentation in complicated partonic events like high-$p_\perp$ etc. Since the investigations of these features have just started, we only comment upon a few results for the total ensuing event structure in high-$p_\perp$ events.

2. Jet fragmentation in 1 + 1 dimensions

Consider a quark q and an antiquark $\bar{q}$ going out back-to-back in the overall CM frame, i.e. the typical situation in an e^+e^--annihilation event. Because of the three-gluon coupling (or vacuum pressure, depending on the point of view), the colour flux lines will not spread out over all space, as the electromagnetic field lines do, but rather be constrained to a thin tubelike region.

Within this tube, new $q\bar{q}$-pairs can be created from the available field energy. Thus the original system breaks into smaller and smaller pieces, until only ordinary hadrons remain. Some of these so-called primary hadrons may be unstable and decay further into the stable hadrons, leptons and photons that are actually observed. In the end, these particles come out essentially aligned along the original $q\bar{q}$-axis, with transverse momenta of around 400 MeV.

In section 3 we will argue that transverse momentum arises naturally from a tunneling mechanism for $q\bar{q}$-pair production. The resulting $p_\perp$-spectrum for the quarks becomes a Gaussian, with the transverse momenta of the q and $\bar{q}$ of a pair balancing each other. The $p_\perp$ of a primary hadron is then found as the vectorial sum of constituent quarks $p_\perp$'s. Similarly, the tunneling production mechanism suggests that the production of $u\bar{u}$-, $d\bar{d}$- and $s\bar{s}$-pairs should be in proportions 1 : 1 : 1/3.

Let us for a moment accept these assumptions so that we may consider the longitudinal fragmentation properties without bothering about the two transverse dimensions, except that we everywhere have to use transverse mass $m_\perp$, with $m_\perp^2 = m^2 + p_\perp^2$, rather than just mass m. What remains is then a problem in one time and one space dimension.

For further discussions it is then useful to introduce lightcone variables in space-time $x^\pm = t \pm x$ and in momentum space $p^\pm = E \pm p$. The main advantage of working with these variables is that they transform simply under a longitudinal boost: $x^{\pm\prime} = k^{\pm 1}x^\pm$ and $p^{\pm\prime} = k^{\pm 1}p^\pm$, where $k = ((1+\beta)/(1-\beta))^{1/2}$ for a boost with velocity β. In particular, variables $z^\pm$ introduced here for the energy-momentum fractions taken by the hadrons, i.e. $z^\pm = p^\pm_{\text{hadron}}/p^\pm_{\text{total}}$, will be invariant. Another useful variable, related to the ones above, is rapidity

$$y = \frac{1}{2}\ln\left(\frac{E+p}{E-p}\right) = \frac{1}{2}\ln\left(\frac{p^+}{p^-}\right) \tag{2.1}$$

again with simple transformation properties, $y' = y + \ln k$. Historically, a description of jet fragmentation as a stochastical process was first attempted by Krzywicki and Petersson [4] for meson fragmentation in hadronic collisions. This idea was applied to quark fragmentation by Niedermayer [5]. The process studied is of the type jet → hadron + remainder-jet, where the remainder-jet is assumed to fragment further like a scaled-down version of the original jet. This iterative structure can be treated by means of integral equations for the hadron distributions. This approach seems to imply an "outside-in" cascade, i.e. a cascade where the particles with large energy, near "the endpoints" of the jet system, are the ones to be produced first. Bjorken [6] later argued that Lorentz invariance required the breakup to start in the central region and to spread outwards as an "inside-out" cascade. Consequently, at this point there seems to be a conflict, at least in principle.

Following the historical evolution rather than the logical one, we will in section 2.1 discuss the integral equation approach and in section 2.2 consider a model for an inside-out cascade. In section 2.3 it will be shown that there is, in fact, no contradiction between the two approaches. Some further comments on theoretical issues are given in section 2.4 and in section 2.5 some comparisons with data are presented. The problem of obtaining a scheme that provides the same result whether a two-jet event is generated from one end or the other, i.e. to find a symmetrical stochastical process is considered in section 2.6. Finally the production of heavy particles is discussed in section 2.7.

2.1. Iterative methods for jet fragmentation

Because of colour confinement we never have a single quark jet appearing in isolation. However, in the limit when the energy of a $q_0\bar{q}_0$ jet system becomes very large, it may still make sense to consider the fragmentation of the quark side of the system without bothering about the $\bar{q}_0$. This is then the kind of "infinite energy" single jets we will consider in this subsection.

In the field behind the original, outgoing quark q_0 a new quark pair $q_1\bar{q}_1$ is produced, so that the q_0 may join with $\bar{q}_1$ to form a hadron $q_0\bar{q}_1$, leaving the q_1 unpaired. The production of another pair $q_2\bar{q}_2$ will give a hadron $q_1\bar{q}_2$ etc. To denote this flavour ordering of the hadrons, the concept of rank is introduced [7], $q_0\bar{q}_1$ is the first rank hadron, $q_1\bar{q}_2$ the second rank one, and so on. (For decay products the concept of rank is somewhat less useful, but customarily the decay products inherit the rank of the decaying particle.)

The particle $q_0\bar{q}_1$ will take a fraction z_1 of the energy-momentum available. For a jet with very large energy, whether z_1 is interpreted as the fraction of energy or of (longitudinal) momentum will not matter, but for finite jet energies the proper combination is $z_1 = z_1^+ = p^+_{\text{hadron}}/p^+_{\text{total}}$ for a jet going out along the $+x$-axis, as discussed above. Energy-momentum conservation implies that the remnant-jet carries the remaining fraction $1 - z_1$, so that the particle $q_1\bar{q}_2$ may take a fraction $z_2 = (1 - z_1) \cdot z_2'$, with $0 \leq z_2' \leq 1$, the particle $q_2\bar{q}_3$ a fraction $z_3 = (1 - z_1 - z_2) \cdot z_3' = (1 - z_1')(1 - z_2')z_3'$, etc.

We now assume scaling and an iterative principle, i.e. if the first rank particle $q_0\bar{q}_1$ is taken away, the remnant-jet looks just like a scaled-down version of the original jet, with the obvious exception that the leading flavour is q_1 and not q_0. From these assumptions one may find the resulting particle spectra in a jet, either by writing and solving integral equations or by using Monte Carlo methods. We will start by considering the former approach first.

2.1.1. Integral equations

Consider the quark fragmentation functions $D_q^h(z)$, where $D_q^h(z)\,dz$ expresses the probability to find a hadron h in a quark-jet q, carrying a fraction between z and $z + dz$ of W, or the total $(E + p)$ of the jet. For only one quark and hadron species we may thus write [7, 8]

$$D(z) = f(z) + \int\int dz'\,dz''\,\delta(z - z'z'')\,f(1 - z')\,D(z'') = f(z) + \int_z^1 \frac{dz'}{z'} f(1 - z')\,D\left(\frac{z}{z'}\right). \tag{2.2}$$

The scaling function $f(z)$ here represents the probability to find a hadron containing the original quark q_0 at z (i.e. properly the probability is $f(z)\,dz$ per dz-interval), with the normalization condition $\int_0^1 f(z)\,dz = 1$. In the second term $f(1 - z')$ gives the probability that the remnant-jet has energy $z'W$ and $D(z'' = z/z')$ gives the probability that this remnant-jet produces a particle with energy $z'' \cdot z'W =$

zW. For the simple case

$$f(z) = (1+c)(1-z)^c \tag{2.3}$$

the solution to (2.2) is [7, 8]

$$D(z) = \frac{1}{z}(1+c)\,(1-z)^c\,. \tag{2.4}$$

This gives $1+c$ particles per rapidity unit in the central plateau (since $\mathrm{d}z/z = \mathrm{d}y$ and the central plateau corresponds to $z \to 0$).

When the production of different flavours is taken into account, a set of coupled integral equations is obtained

$$D_{\mathrm{q}}^{\mathrm{h}}(z) = f_{\mathrm{q}}^{\mathrm{h}}(z) + \int_z^1 \frac{\mathrm{d}z'}{z'} \sum_{\mathrm{q}'} f_{\mathrm{q}}^{\mathrm{q}\bar{\mathrm{q}}'}(1-z')\, D_{\mathrm{q}'}^{\mathrm{h}}\left(\frac{z}{z'}\right). \tag{2.5}$$

If the further possibility of having different hadrons with the same quark content is included, $f_{\mathrm{q}}^{\mathrm{q}\bar{\mathrm{q}}'}$ must be considered as a sum over all such different $(\mathrm{q}\bar{\mathrm{q}}')$ hadrons. In any case, the f's are normalized according to

$$\sum_{\mathrm{q}'} \int_0^1 f_{\mathrm{q}}^{\mathrm{q}\bar{\mathrm{q}}'}(z)\,\mathrm{d}z = 1\,. \tag{2.6}$$

2.1.2. Monte Carlo methods

Whereas not only the fragmentation functions, $D_{\mathrm{q}}^{\mathrm{h}}(z)$, but also two-particle correlations etc. can be found by the integral equation techniques, the work involved rapidly becomes prohibitive, the more so when decay chains have to be taken into account. From this point on we will therefore solely rely on Monte Carlo methods, implemented in the form of computer programs, to find the desired distributions. This means that random numbers at each step are used to assign variable values according to given probability distributions, discrete or continuous. Obviously a single jet generated this way is neither more nor less statistically significant than a single jet in nature.

In a program, different quark–antiquark pairs $\mathrm{q}_i\bar{\mathrm{q}}_i$ are then generated according to given probabilities and hadrons $\mathrm{q}_{i-1}\bar{\mathrm{q}}_i$ formed. Each particle may take a fraction z_i', chosen according to the scaling function $f(z_i')$, of the then remaining jet energy, so that the fraction of the total jet energy W is

$$z_i = \left(1 - \sum_{k=1}^{i-1} z_k\right) z_i' = \prod_{k=1}^{i-1} (1-z_k')\, z_i' \tag{2.7}$$

(with $z_1 = z_1'$).

The most widely known Monte Carlo approach is that presented by Field and Feynman [7]. Here a scaling function

$$f(z') = 1 - a + 3a\,(1-z')^2 \tag{2.8}$$

is used, with $a = 0.77$ determined from experiment. New $q_i\bar{q}_i$-pairs are assumed to be produced in the proportions $u\bar{u} : d\bar{d} : s\bar{s} = 2:2:1$ and the hadrons thus formed are assumed to be pseudoscalars or vectors with equal probability. Finally, transverse momentum components for the q_i are introduced according to Gaussian distributions with $\langle p_\perp^2 \rangle = \sigma^2 = (0.35\ \mathrm{GeV}/c)^2$ and with local $\bar{p}_\perp$ compensation within each $q_i\bar{q}_i$ pair. A primary hadron obtains $p_\perp$ from the two constituent quarks and thus will have $\langle p_\perp^2 \rangle = 2\sigma^2$.

2.2. The linear force field

The kind of "cookbook recipes" we have presented in section 2.1 has phenomenologically proven very successful, but they do not provide any dynamical picture of the actual fragmentation process. Our task in this subsection is to present such a picture and show that scaling properties appear naturally in it. To do this, we will assume that not only is the colour field between an outgoing original q and $\bar{q}$ compressed into a flux tube, but also that the tubelike field contains a constant amount of field energy stored per unit length, i.e. that the potential between q and $\bar{q}$ is linearly rising. Support for this picture is provided by Regge phenomenology, "onium" spectroscopy (charmonium, bottomonium), bag model calculations and lattice QCD results. Phenomenologically the string constant κ, i.e. the amount of energy per unit length of the tube, is known to be $\kappa \approx 1\ \mathrm{GeV/fm} \approx 0.2\ \mathrm{GeV}^2$. (Coulombic corrections ($\sim 1/r$) to the potential could correspond to some tapering of the flux tube near the ends, while the cross section is constant otherwise. However, for the typical hadronic distance scales we will be working with, these corrections can be expected to be small.)

2.2.1. The Schwinger model

A simple model for a linear force field is provided by 1 + 1-dimensional massless QED, the Schwinger model [9] defined by the Lagrangian density

$$\mathcal{L} = \bar{\psi}\gamma^\mu (\mathrm{i}\partial_\mu - gA_\mu)\psi - \tfrac{1}{4}F^{\mu\nu}F_{\mu\nu}\,. \tag{2.9}$$

The theory is exactly solvable and the charge of the fermions is a confined quantity in the sense that there exists no asymptotic fermion states. It is convenient to express the fermion current j^μ in terms of a scalar dipole density field ϕ:

$$j^\mu = \varepsilon^{\mu\nu}\,\partial_\nu\phi\,. \tag{2.10}$$

The spectrum of the field ϕ contains a single stable neutral boson with mass $m = g/\sqrt{\pi}$ where g is the coupling constant. It can be shown that the Lagrangian obtained from eq. (2.9) is essentially equivalent to the Lagrangian for a free bosonic field which can be identified with the dipole density ϕ.

An interesting situation discussed in some detail in [10] is the response state which corresponds to a given external current j^μ_{ext} describing two oppositely charged fermions moving with the velocity of light in opposite directions. In this case the final state is a coherent state of the dipole density ϕ, corresponding to a polarization charge which neutralizes the total electric charge and consequently prevents the fermions from appearing as asymptotic free states. The corresponding external dipole density ϕ_{ext} is

$$\phi_{\mathrm{ext}} = -\theta(t+z)\,\theta(t-z) \tag{2.11}$$

and the mean particle density in the coherent state is given by

$$E(p)\frac{dn}{dp}=\frac{dn}{dy}=\frac{1}{(2\pi)^2}\left|\int d^2x\,\exp(ipx)\,g\,\phi_{ext}\right|^2=\frac{g^2}{m^2\pi}=1\,. \tag{2.12}$$

Thus in the mean one boson is produced per unit rapidity interval. This means that the mean field energy per unit length appears in rapidity space as one boson with mass $m = g/\sqrt{\pi}$ per unit rapidity.

From the properties of the coherent state one can also show that the statistical distribution of final state bosons per rapidity interval follows a Poissonian law with density 1. In other words, the probability $P(n, \Delta y)$ to find n bosons in the rapidity interval Δy is given by

$$P(n,\Delta y)=\frac{(\Delta y)^n}{n!}\exp-(\Delta y)\,. \tag{2.13}$$

Whereas the Schwinger model may serve as a useful guide line, it is not directly applicable to colour jet fragmentation. The dressing of the original fermions, which are described by j^{μ}_{ext}, is e.g. not covered by this approach. Also, since there is only one particle species in the Schwinger model, the concept of an ordering (e.g. in rank) of the final particles does not exist.

2.2.2. Bound $q\bar{q}$ *states*

Let us next study the classical motion of two massless particles, e.g. a quark and an antiquark, interacting via a constant force in 1 + 1-dimensional space-time [11, 12, 22]. The Hamiltonian H is given by

$$H = T + V = |p_1| + |p_2| + \kappa|x_1 - x_2| \tag{2.14}$$

where p_1, p_2 are the momenta of the particles and x_1, x_2 their positions. The particles always move with the speed of light and the equation of motion is

$$dp/dt = \pm\kappa \tag{2.15}$$

where the sign depends on whether the other interacting particle is to the right or to the left. We note that the constant force is Lorentz invariant: if in the original frame $x = \pm t$ and $E = \pm p$ (+ and − signs for particles moving to the right and left, respectively), then a Lorentz boost β gives

$$t' = \gamma(t-\beta x) = \gamma(1\mp\beta)t, \qquad p' = \gamma(p-\beta E) = \gamma(1\mp\beta)p \tag{2.16}$$

and thus

$$dp'/dt' = dp/dt\,. \tag{2.17}$$

Actually the system is equivalent to the "yo-yo mode" of the massless relativistic string as described in [12, 22]. In the CM frame a quark and an antiquark will oscillate back and forth as shown in fig. 2.1. For a $q\bar{q}$ system with mass M the maximum relative distance is $L = M/\kappa$ and the time for a full period of motion $T = 2L = 2M/\kappa$. The hatched area spanned by the motion of the quarks is thus proportional to

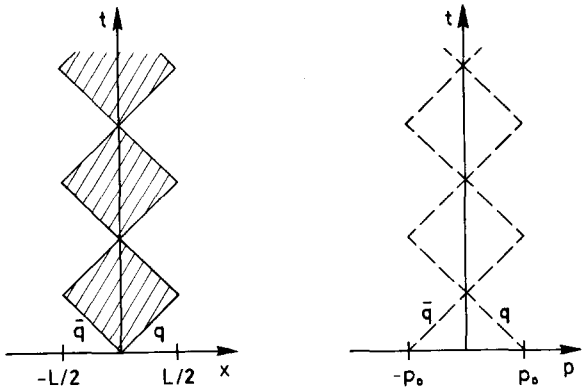

Fig. 2.1. The motion of q and q̄ in the CM frame. The hatched areas show where the field is nonvanishing.

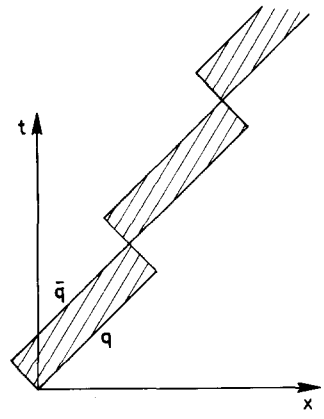

Fig. 2.2. The motion of q and q̄ in a Lorentz frame boosted relative to the CM frame.

M^2. In fig. 2.2 the same motion is shown after a Lorentz boost β. The maximum relative distance has been contracted to $L' = L\gamma(1-\beta) = L\,e^{-y}$ and the time period dilated to $T' = T\gamma = T\cosh(y)$ where y is the rapidity difference between the two frames.

In this model the "field" corresponding to the potential energy carries no momentum, which is a consequence of the fact that in $1+1$ dimensions there is no Poynting vector. Thus all the momentum is carried by the endpoint quarks. This is possible since the turning points, where q and q̄ have zero momentum, are simultaneous only in the CM frame. In fact, for a fast-moving qq̄ system the qq̄-pair will most of the time move forward with a small, constant relative distance (see fig. 2.2).

In the following we will use this kind of yo-yo modes as representations both of our original qq̄ jet system and of the final state hadrons formed when the system breaks up. It is for the subsequent work necessary to know the level spectrum of the yo-yo modes. A precise calculation would need a knowledge of the quantization of the massless relativistic string but for our purposes it is sufficient to use semi-classical considerations well-known from the investigations of Schrödinger operator spectra. We consider the Hamiltonian of eq. (2.14) in the CM frame with $q = x_1 - x_2$

$$H = |p| + \kappa|q| \tag{2.18}$$

and we note that our problem is to find the dependence on n of the nth energy level E_n. If the spatial size of the state is given by δ_n then the momentum size of such a state with $n-1$ nodes is

$$|p| \simeq n/\delta_n \tag{2.19}$$

and the energy eigenvalue E_n corresponds according to variational principles to a minimum of

$$H(\delta_n) = n/\delta_n + \kappa\delta_n \tag{2.20}$$

i.e.

$$E_n \simeq 2\sqrt{\kappa n}\,. \tag{2.21}$$

Consequently the CM energy, i.e. the mass, grows like $\sqrt{n}$ and we conclude that for large excitation masses,

$$dM^2/dn = \text{constant, independent of } n\,. \tag{2.22}$$

2.2.3. Particle production

We now turn to a situation where $q\bar{q}$ pairs are produced at different space-time points (x, t) in which the field is nonvanishing [11]. Energy and momentum will be conserved if the q and $\bar{q}$, still assumed massless, are produced at the same space-time point with zero momentum and afterwards move with increasing momenta in opposite directions with a vanishing force field in between. In a fully quantized theory it should of course also be possible to produce a q and $\bar{q}$ with nonvanishing momenta. However, in 2-dimensional models the density of states is proportional to dp/p and states with low momenta should dominate.

A system may thus originally contain a q_0 and $\bar{q}_0$ moving in opposite directions with large energies. After some time the system will break into two parts by the production of a pair $q_1\bar{q}_1$ at the space-time point (x_1, t_1) (see fig. 2.3). At a later time another pair $q_2\bar{q}_2$ will be produced at (x_2, t_2), so that a hadron can be formed by the pair $\bar{q}_1 q_2$. More $q\bar{q}$ pairs will be produced, giving $q_i\bar{q}_j$ subsystems which either are hadrons or else will fragment further, until only hadrons remain. The energy of the $\bar{q}_1 q_2$ hadron is $\kappa(x_2 - x_1)$ and the momentum $\kappa(t_2 - t_1)$. Thus, in order to obtain the correct hadron mass m, the point (x_2, t_2) must lie on a hyperbola H_1 given by

$$(x_2 - x_1)^2 - (t_2 - t_1)^2 = m^2/\kappa^2 \tag{2.23}$$

which can be parametrized according to

$$(x_2 - x_1,\, t_2 - t_1) = \frac{m}{\kappa}(\cosh y,\, \sinh y)\,. \tag{2.24}$$

Here m/κ is the maximum distance between $\bar{q}_1$ and q_2 in the rest frame of the $\bar{q}_1 q_2$ system and y can be

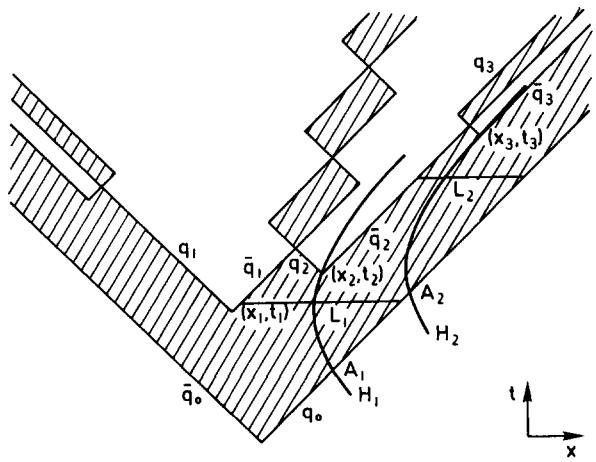

Fig. 2.3. The particles q_0 and $\bar{q}_0$ move with large energies in opposite directions. In the field $q\bar{q}$ pairs are produced at the space-time points (x_1, t_1), (x_2, t_2), (x_3, t_3), etc. Nearby vertices are related by mass constraints (see text). Hadrons are formed by $\bar{q}_1 q_2$, $\bar{q}_2 q_3$, etc.

identified with the rapidity of the hadron in the original frame. The point A_1, where the hyperbola H_1 crosses the world line of q_0, corresponds to the minimal value of y. For the next hadron $\bar{q}_2q_3$ the minimal rapidity corresponds to the point A_2. This rapidity will be larger than the minimum rapidity of $\bar{q}_1q_2$, provided the two hadrons have the same mass, because the length L_2 of the field between q_0 and $\bar{q}_2$ is shorter than the corresponding length L_1 between q_0 and $\bar{q}_1$. Hence the hadrons will, on the average, be ordered in rapidity. The field lengths decrease in a geometric fashion and thus the rapidities increase linearly. The final picture will be like the one in fig. 2.4.

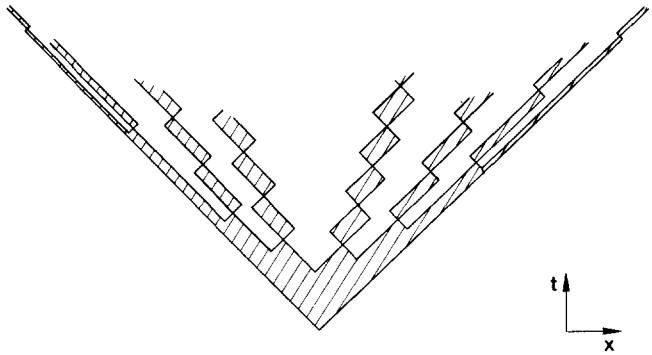

Fig. 2.4. The final picture when q_0 and $\bar{q}_0$ move with large energies in opposite directions. The field has broken at many places by the production of $q\bar{q}$ pairs. Hatched areas indicate nonvanishing field.

It should be emphasized that Lorentz invariant statements can only be made about the production points of $q\bar{q}$ pairs and points where q and $\bar{q}$ world lines cross. Therefore statements about "hadron production points" have no meaning in this model. It is, however, possible to define the first crossing of the q and $\bar{q}$ of a hadron as such a production point. If so, it is evident that, for any Lorentz frame, the particles with low momenta are always produced first in time. The hadrons will emerge around a hyperbola corresponding to a definite proper time, as will be discussed further below. With the usual terminology, this is thus an inside-out cascade in time.

A trivial observation is that all pair production points are causually disconnected. The fact that hadrons nonetheless manage to end up on mass shell cannot be explained in purely classical terms. Quantum mechanically it can be argued that all breakup configurations that give unphysical masses simply cannot be projected onto a physical state.

The time-development properties of our model are further illuminated by the situation shown in fig. 2.5. At the time t_0 the total system can be interpreted as consisting of two jets along the lightcones and an excited state in the center. At a later time the excited state breaks up into two hadrons by the production of another $q\bar{q}$-pair. However, this interpretation depends strongly on the choice of the Lorentz frame. In another Lorentz frame, with coordinate axes x' and t' as indicated in fig. 2.5, the two hadrons seem to be produced one after the other. In fig. 2.5 it is also seen that the hadrons might cross each other. Thus the ordering in rapidity indicated in fig. 2.4 is only true on the average.

From fig. 2.3 it might seem that the fragmentation involves two fundamental subprocesses: in the point (x_1, t_1) the original system breaks into two jets, while in (x_2, t_2) a jet breaks into a hadron and a remainder-jet. However, there cannot be any real difference between these two vertices: it is always possible to make a Lorentz boost to a frame where t_2 occurs before t_1, and in that frame the rôles of (x_1, t_1) and (x_2, t_2) have been interchanged. We therefore only have to study one type of vertex. With a

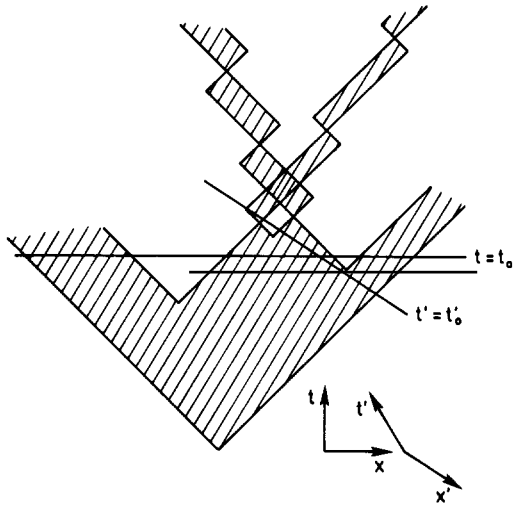

Fig. 2.5. In a Lorentz frame with coordinates x and t an excited state had been formed by time t_0, which later decays into two ground state hadrons. However, in a frame with coordinates x' and t' the hadrons are formed one after the other. It is possible that the hadrons cross. Thus the ordering in rapidity seen in fig. 2.4 is not necessary.

very large boost we come to a frame where the last meson is produced first in time. Thus here also the first break is of the type jet → meson + remainder-jet. This will be further discussed in section 2.3.

We also note that there is no observable difference between the final states obtained by the processes in figs. 2.6a and 2.6b. There is nevertheless only an interpretation in terms of an iterative model in *space-time* for the case in fig. 2.6b. In section 2.4 we exhibit an interpretation of our model in *energy-momentum space* and then only fig. 2.6b is relevant. We therefore subsequently neglect the situation relevant to fig. 2.6a.

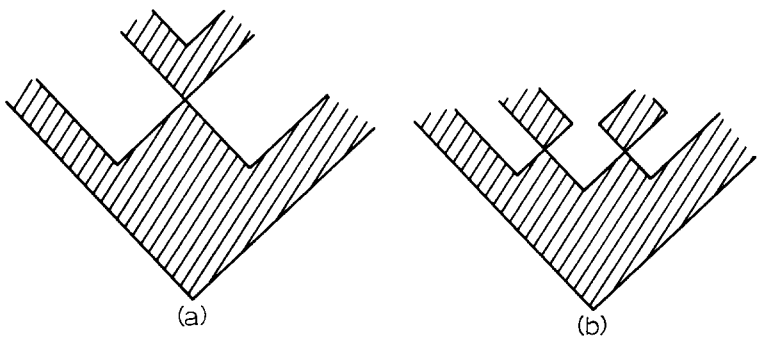

Fig. 2.6. The process (a) is neglected compared to process (b).

2.3. Iterative methods revisited

In every Lorentz frame the slowest hadrons will be produced first, as mentioned above. Thus, if we make a sufficiently large boost, the outermost hadron (containing the original q_0) will be produced first. This situation is shown in fig. 2.7, where the boost for simplicity has been chosen such that the maximum possible rapidity for the hadron in this frame is $y = 0$, corresponding to the hadron taking all the q_0 momentum.

In this frame q_0 starts off with low momentum, $\frac{1}{2}m_1$, whereas the momentum of $\bar{q}_0$ is very large negative. At a point $A = (\frac{1}{2}\lambda, \frac{1}{2}\lambda)$ with $\lambda = m_1/\kappa$, q_0 turns over and follows a worldline parallel to that of $\bar{q}_0$. At some point B on the hyperbola H_1 a pair $q_1\bar{q}_1$ is created and subsequently a hadron $q_0\bar{q}_1$ can be formed. Again, in order to obtain the correct mass $m_1 = m_{q_0\bar{q}_1}$, we may parametrize H_1 according to

$$(x_1, t_1) = \lambda(\tfrac{1}{2} - \cosh y_1, \tfrac{1}{2} - \sinh y_1) \tag{2.25}$$

where $y_1 < 0$ is the rapidity of $q_0\bar{q}_1$ in this frame.

We note that the distance between q_0 and $\bar{q}_0$ (after the q_0 has turned over) is $L_0 = \lambda$ whereas the distance between q_1 and $\bar{q}_0$ is $L_1 = \lambda(1 - e^{y_1})$. If the $p^+ = E + p$ initially carried by q_0 is called W^+, and the initial $p^- = E - p$ of the $\bar{q}_0$ called W^-, then the invariant mass M_0 of the original system $q_0\bar{q}_0$ is $M_0^2 = W^+W^-$. Call the invariant mass of $q_1\bar{q}_0$ M_1. Then

$$M_0^2 = W^-\kappa L_0\,, \qquad M_1^2 \simeq W^-\kappa L_1 \tag{2.26}$$

and thus for the W^+ fraction taken by the particle

$$z_1 = (L_0 - L_1)/L_0 \simeq 1 - M_1^2/M_0^2\,. \tag{2.27}$$

In general we would expect the probability for breakup in a given point to be given by Fermi's Golden rule

$$\mathrm{d}P = |\mathcal{M}|^2\,\mathrm{d}n \tag{2.28}$$

where $\mathcal{M}$ is a quantum mechanical transition matrix element and $\mathrm{d}n$ is the density of states available. For the moment, let us assume [8, 11] that $\mathcal{M}$ is a constant and that $\mathrm{d}n \sim \mathrm{d}M^2$, as shown in section 2.2.2.

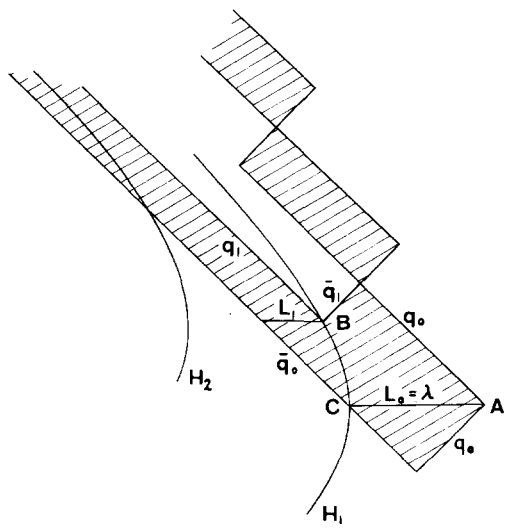

Fig. 2.7. The situation in a Lorentz frame which moves very fast relative to the CM frame. In this frame the original momentum of q_0 is $m_1/2$ and a hadron produced with $z = 1$ is at rest.

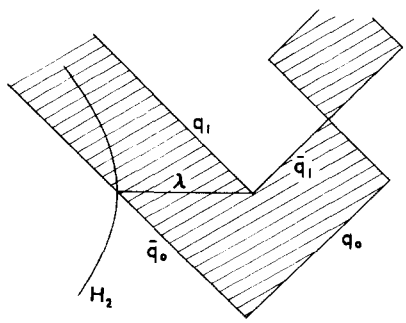

Fig. 2.8. For fixed energy of the first hadron (i.e. z_1 fixed) this figure shows the situation in a Lorentz frame in which the second hadron is at rest if it takes all remaining $E + p_z$, i.e. $z_2' = z_2/(1 - z_1) = 1$.

Then, according to (2.27)

$$\frac{dP}{dz_1} = \text{const}\,\frac{dM_1^2}{dz_1} = \text{const}\,\frac{1}{M_0^2} = 1\,. \tag{2.29}$$

In terms of $y_1 = \ln z_1$, this is $dP/dy_1 = e^{y_1}$.

Let us now turn to the formation of the next hadron $q_1\bar{q}_2$. The new pair $q_2\bar{q}_2$ has to be created at a point along the hyperbola H_2. It is possible to choose a Lorentz frame where the distance between q_1 and $\bar{q}_0$ is $\lambda = m_2/\kappa$, with $m_2 = m_{q_1\bar{q}_2}$, see fig. 2.8. The necessary boost obviously depends on z_1, as well as on the masses. In the new frame the situation for $q_1\bar{q}_2$ is the same as for $q_0\bar{q}_1$, discussed above. Thus we obtain $dP/dy_2 = e^{y_2}$ with $y_2 < 0$ the rapidity of $q_1\bar{q}_2$ in this frame. Defining $z_2' = z_2/(1-z_1)$ we find $z_2' = e^{y_2}$ and $dP/dz_2' = 1$.

We conclude that, when the hadron $q_0\bar{q}_1$ is taken away, the rest looks just like the original system when expressed in the new scaling variable $z' = z/(1-z_1)$, i.e. the total jet energy is lowered by the factor $1-z_1$. This feature immediately implies the integral equation (2.2) with

$$f(z) = dP/dz = 1\,. \tag{2.30}$$

When the production of different flavours is allowed for, the assumption of local conservation of quantum numbers means that each pair $q_i\bar{q}_i$ should be flavourless. Since the shape of $f(z)$ does not depend on the particle produced, eq. (2.5) will in this case read

$$D_q^h(z) = f_q^h + \int_z^1 \frac{dz'}{z'} \sum_{q'} f_q^{q\bar{q}'}\, D_{q'}^h\!\left(\frac{z}{z'}\right) \tag{2.31}$$

where f_q^h now are simple numbers related by

$$\sum_h f_q^h = \sum_{q'} f_q^{q\bar{q}'} = 1 \tag{2.32}$$

giving the probabilities of producing different hadrons.

We thus see how Lorentz invariance implies that a cascade, which in space-time is of the inside-out nature, very well may be described by integral equations of an outside-in nature. This conclusion is not dependent on the choice of $f(z)$ in eq. (2.30): based on other considerations in connection with eq. (2.28) one may arrive at different $f(z)$, e.g. the one used by Field–Feynman, but an iterative outside-in cascade may still be obtained. The particular model described above by eqs. (2.30)–(2.32) will subsequently be referred to as "simple Lund". By suitable (and physically motivated) choices of the numbers $f_q^{q\bar{q}'}$ it provides a surprisingly accurate description of jet fragmentation.

A model of this kind contains a strict ordering of the hadrons in flavour, expressed e.g. by the concept of rank [7]. In our case $q_0\bar{q}_1$ would be the first rank particle, $q_1\bar{q}_2$ the second rank one and $q_{i-1}\bar{q}_i$ the ith rank one. Two adjacent-ranked hadrons thus always share one $q\bar{q}$ pair. However, this ordering need not coincide with the ordering in rapidity space. If two adjacent-ranked hadrons have the same mass, the rapidity difference distribution becomes [11]

$$\frac{dP}{d\Delta y} = \int\int dz_1\, dz_2'\, \delta\left(\Delta y - \ln\left(\frac{z_1}{z_2}\right)\right) = \int\int dz_1\, dz_2'\, \delta\left(\Delta y - \ln\left(\frac{z_1}{z_2'(1-z_1)}\right)\right)$$

$$= \exp -(\Delta y)\left(\ln(1+\exp(\Delta y)) - \frac{1}{1+\exp(-\Delta y)}\right). \tag{2.33}$$

The average value of Δy is 1, but the probability distribution is not vanishing for $\Delta y < 0$, i.e. there is a finite probability that hadron i has smaller rapidity than hadron $i+1$.

Finally we note the similarity between the results of the simple Lund model and the results of exciting the Schwinger model by an external current as in section 2.2.1 [10]. There is in both cases in the mean one particle produced per unit rapidity and the fluctuations in a central rapidity bin is of a Poissonian nature. Actually, in the simple Lund model this result is true for all rapidity bins, not only the central ones.

The basic considerations behind the simple Lund model are, however, not fully satisfactory as we will demonstrate in section 2.6, because the stochastic process defined by the model is not a symmetrical one.

2.4. Momentum space interpretation and details of the underlying stochastic process

The model developed above can be interpreted in momentum space and in terms of a stochastic process as follows [11].

2.4.1. Momentum space interpretation

First we note that for a jet system with q_0 going out in the forward direction and $\bar{q}_0$ in the backward one, all new $q_i\bar{q}_i$-pairs will be pulled apart so that $\bar{q}_i$ moves forwards and q_i backwards (see e.g. fig. 2.9). For hadron i with constituents $(q_{i-1}\bar{q}_i)$ the energy and momentum are given by

$$p_i^0 = E_i = \kappa(x_{i-1} - x_i) \equiv \hat{p}_i^1\,, \qquad p_i^1 = p_i = \kappa(t_{i-1} - t_i) \equiv \hat{p}_i^0 \tag{2.34}$$

where (x_i, t_i) are the space-time coordinates for the pair $(q_i\bar{q}_i)$.

Thus the energy-momentum p^μ of particle i is given by the "step" from the space-time point x_{i-1}^μ to x_i^μ:

$$\hat{p}_i^\mu = \kappa(x_{i-1}^\mu - x_i^\mu) \equiv \kappa\, \Delta x_i^\mu\,. \tag{2.35}$$

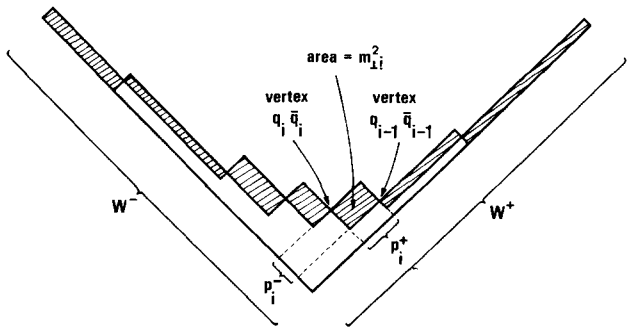

Fig. 2.9. Simple momentum space representation of the breakup of a $q_0\bar{q}_0$ jet system.

The breakup of the system can be represented by a chain of steps, where each step satisfies the condition

$$p_i^\mu p_{i\mu} = -\kappa^2 \Delta x_i^\mu \Delta x_{i\mu} = m_i^2 . \tag{2.36}$$

For meson i the lightcone coordinates $p_i^+ = E_i + p_i$ and $p_i^- = E_i - p_i$ are also given by the distance passed by $\bar{q}_i$ and q_{i-1} respectively, before they meet. Thus the $\bar{q}_i$ can be considered as carrier of the $E+p$ components of the jet while the q_i carry the $E-p$ components.

2.4.2. *Some details of the stochastic process*

In a model of this kind the steps between adjacent production points are actually of a stochastic character, i.e. each step starts from the previous production point and is taken according to a probabilistic rule. The step in the (+)-direction from point $i-1$ to point i is given by the variable z_i' which in the simple Lund model is evenly distributed between 0 and 1

$$\Delta x_i^+ = z_i' x_{i-1}^+ . \tag{2.37}$$

The step in the (−)-direction is then fixed by the meson mass (eq. (2.36))

$$\Delta x_i^- = m_i^2/\kappa^2 \Delta x_i^+ . \tag{2.38}$$

Thus we have the recursion formulae

$$\begin{aligned} x_i^+ &= (1 - z_i')x_{i-1}^+ \\ x_i^- &= x_{i-1}^- + \frac{m_i^2}{\kappa^2}\frac{1-z_i'}{z_i'}\frac{1}{x_i^+} \end{aligned} \tag{2.39}$$

together with the boundary conditions

$$x_0^+ = W^+/\kappa , \qquad x_0^- = 0 . \tag{2.40}$$

There is only one constraint on all the z_i', that the path must end at the turning point of $\bar{q}_0$: $x^+ = 0$, $x^- = W^-/\kappa$. For large energies there will be a large number of steps and the restrictions on each z_i' will not be important.

2.4.3. *Distribution of breakup points in invariant time*

We define a quantity Γ_i proportional to the invariant time-squared at each vertex point [11]

$$\Gamma_i = \kappa^2 x_i^+ x_i^- . \tag{2.41}$$

Thus Γ_i is a measure of the time it takes until the string breaks. Via the relation

$$\Gamma = (M_a^2 + \Gamma)(M_b^2 + \Gamma)/W^2 \simeq M_a^2 M_b^2/W^2 \tag{2.42}$$

(for $\Gamma \ll M_{a,b}^2$) Γ is also connected to the masses M_a and M_b of the two jets created by this break. Equation (2.39) now yields

$$\Gamma_i = (1 - z_i')(\Gamma_{i-1} + m_i^2/z_i') . \tag{2.43}$$

If all m_i are equal and all z_i' equal to their mean value $\frac{1}{2}$, we obtain

$$\Gamma_i = (2 - (\tfrac{1}{2})^{i-1})m^2 . \tag{2.44}$$

For increasing i, Γ_i will rapidly approach an asymptotic value. Thus in the central plateau, away from the ends of the jet system, production points will lie around the hyperbola

$$x^+x^- = t^2 - x^2 = \Gamma/\kappa^2 = 2m^2/\kappa^2 . \tag{2.45}$$

The probability distribution of Γ_i, called $H(\Gamma_i)$ can be determined from the assumption that for sufficiently large values of i we have $H(\Gamma_i) = H(\Gamma_{i-1})$. This gives

$$H(\Gamma) = \int\int \mathrm{d}z'\, \mathrm{d}\Gamma'\, f(z')\, \delta(\Gamma - (1 - z')\,(\Gamma' + m^2/z'))\, H(\Gamma') \tag{2.46}$$

which can be solved analytically [11]. The distribution behaves as

$$\begin{aligned} H(\Gamma) &\to \text{const} \quad \text{for } \Gamma \to 0 \\ &\to \ln(\Gamma)/\Gamma^2 \text{ for } \Gamma \to \infty . \end{aligned} \tag{2.47}$$

2.4.4. Digression on the joining of jets

For a finite jet system, we must satisfy the constraint that the chain of production points ends at $x^+ = 0$, $x^- = W^-/\kappa$ (see section 2.4.2) if we wish to have conservation of energy and momentum. A practical solution adopted in the Lund model is as follows [13]: instead of generating particles from the q_0 end of the system all the way over to the $\bar{q}_0$ end, each new step is with equal probability taken either from the q_0 or the $\bar{q}_0$ end. In the former case the scaling variable $z_i' = z_i'^+$ is used to find p_i^+ and then p_i^- is found from $p_i^+ \cdot p_i^- = m^2$, whereas in the latter case $z_i' = z_i'^-$ gives p_i^- from which p_i^+ is deduced. We keep track of the $W^\pm = E \pm p$ which remains after each step. When the remaining mass-square is below a given value (approximately 5 GeV^2), a final $q\bar{q}$-pair is generated which is used to produce the final two hadrons. The two possible kinematical solutions (if no solution, we start all over again) are weighted with a probability that gives the right average difference in rapidity. In this way at each step we conserve energy, momentum and flavour, and at the same time we obtain a smooth joining prescription in the center, e.g. giving a flat central rapidity distribution at large energies and almost the same mean rapidity difference between any two adjacent-ranked primary hadrons anywhere in the chain.

2.5. Some comparisons with data

A realistic model for jet fragmentation will require a number of further ingredients. So far we have only considered the evolution of the colour flux tube in one space dimension. The very fact of having a

finite transverse cross section of the tube gives a transverse momentum spread due to the uncertainty principle. How this comes about through the tunneling mechanism will be discussed further in section 3. We will here make use of the main results, namely a Gaussian $p_\perp$ spectrum for quarks, with the q and $\bar{q}$ of the pair having opposite and equally large transverse momenta, and a suppression of $s\bar{s}$-pair production.

Further, we will assume that only particles with orbital angular momentum $L = 0$ are produced. The neglect of particles with higher L quantum numbers in fact seems quite reasonable: a classical order-of-magnitude estimate for a hadron of size $d \approx 1$ fm ≈ 0.2 GeV^{-1} with the quarks in the endpoints obtaining $\langle p_\perp \rangle \approx 0.5$ GeV would give an orbital angular momentum $L \sim d \cdot \langle p_\perp \rangle \approx 0.2\,\text{GeV}^{-1} \cdot 0.5\,\text{GeV} \sim 0.1$. Quantum mechanically one could thus expect maybe a 10% admixture of higher states, and these would easily be masked by subsequent decays since these resonances are broad to start with. According to naive counting of spin states we would expect the $L = 0$ pseudoscalar and vector multiplets to be populated in the proportions 1:3.

2.5.1. Simple Lund versus standard Lund

The model for the longitudinal fragmentation presented in sections 2.2–2.4 (based on [8, 11]) coupled with the 1:3 pseudoscalar:vector ratio is then the earliest version of the Lund model, in which effects of the transverse dimensions are neglected except for the Gaussian $p_\perp$ distribution, and this is the reason why we will refer to it as "simple Lund". From a practical point of view there are very large similarities with the parametrization presented by Field and Feynman, even if the latter was never explicitly based on any picture of the space-time evolution as in the Lund case. Essentially only two things are different: instead of having a flat scaling function $f(z) = 1$, Field–Feynman [7] use $f(z) = 0.23 + 2.31(1 - z)^2$, which tends to produce more particles at lower energies, but at the same time an equal production of pseudoscalars and vectors is assumed, which tends in the opposite direction. The resulting particle spectra after decays of unstable particles will be rather similar, as is illustrated in fig. 2.10.

In the following subsections we will discuss corrections to the simple Lund model. The spin–spin forces will be shown to enhance the production of the lighter pseudoscalars, from the naive 1:3 pseudoscalar to vector ratio to something closer to 1:1. We will also discuss how collinear gluon emission may be expected to modify the scaling functions $f(z) = 1$ to $f(z) = (1 + c)(1 - z)^c$, with $c \approx 0.3$–0.5, and how the tunneling mechanism due to finite field lengths will give rise to a further weighting with $\Gamma/(\Gamma + m_{\perp q}^2)$ at each quark pair production vertex, which will further suppress the production of particles at large z. Here Γ is the quantity defined in (2.41) and $m_{\perp q}$ is the transverse mass of the quark produced. Also taking into account baryon production and, if need be, hard gluon emission, we move from the "simple Lund" to the "standard Lund" model. The shapes of the scaling functions are shown in fig. 2.11, where the standard Lund curve gives the average shape, since the $\Gamma/(\Gamma + m_{\perp q}^2)$ factor means that this scaling function is more complicated. In fig. 2.10 some resulting particle spectra are also shown. In particular, note that the ρ^0 spectrum indicates that a P:V ratio of 1:3 is excessive (cf. [14, 15]).

2.5.2. Some dangers in comparisons with data

A comment about the experimental data points may here be in order. Unfortunately comparisons between model predictions and the experimental data are difficult. At low energies, say $W \lesssim 10$ GeV, all kinds of finite energy corrections make themselves felt: resonance production, few-particle (exclusive) states, mass corrections etc. Then it is often a bad approximation to apply iterative schemes

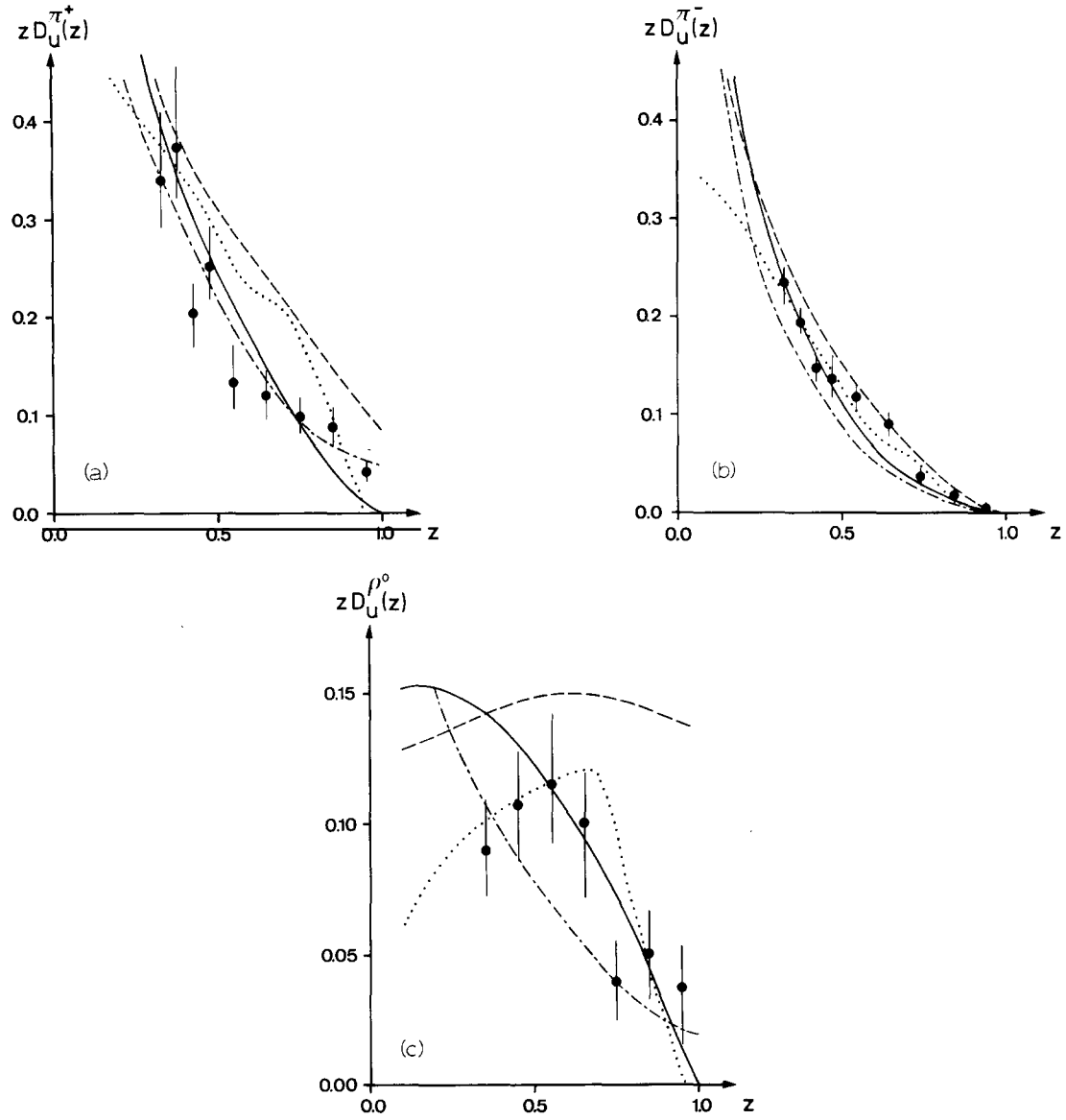

Fig. 2.10. Fragmentation functions for (a) π^+, (b) π^- and (c) ρ^0 in single u quark jets for simple Lund, dashed curve, standard Lund, full line, and Field–Feynman, dash-dotted. Data are from DECO [14], with $3 \leq W \leq 4$, and dotted line standard Lund for jet systems with $W = 4$.

for single jet fragmentation, when actually we have a finite two-jet system, as is shown in fig. 2.10. At higher energies gluon emission starts to become important, to be discussed in section 4. In addition, many experiments do not fully unfold the effects of radiative corrections etc., but rather include those effects in their simulation Monte Carlo programs. We will therefore leave high-precision comparisons to experimentalists (many groups are using our Monte Carlo programs to study e^+e^- annihilation, leptoproduction, hadroproduction, etc.) and mostly use data to illustrate principles.

One comparison of $D^{\pm}(z)$ for incoming ν and $\bar{\nu}$ is presented in fig. 2.12. In particular, note the shift from the dashed to the full line in $D^+_{\nu}(z)$ which represents the effects of detector acceptance etc. The

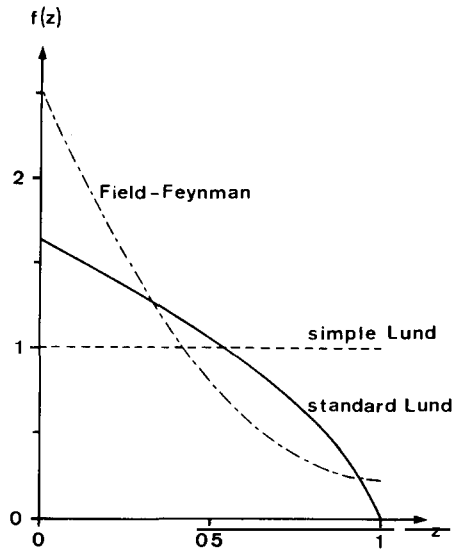

Fig. 2.11. Shape of scaling functions $f(z)$ for simple Lund, dashed, standard Lund (average), full, and Field–Feynman, dash-dotted.

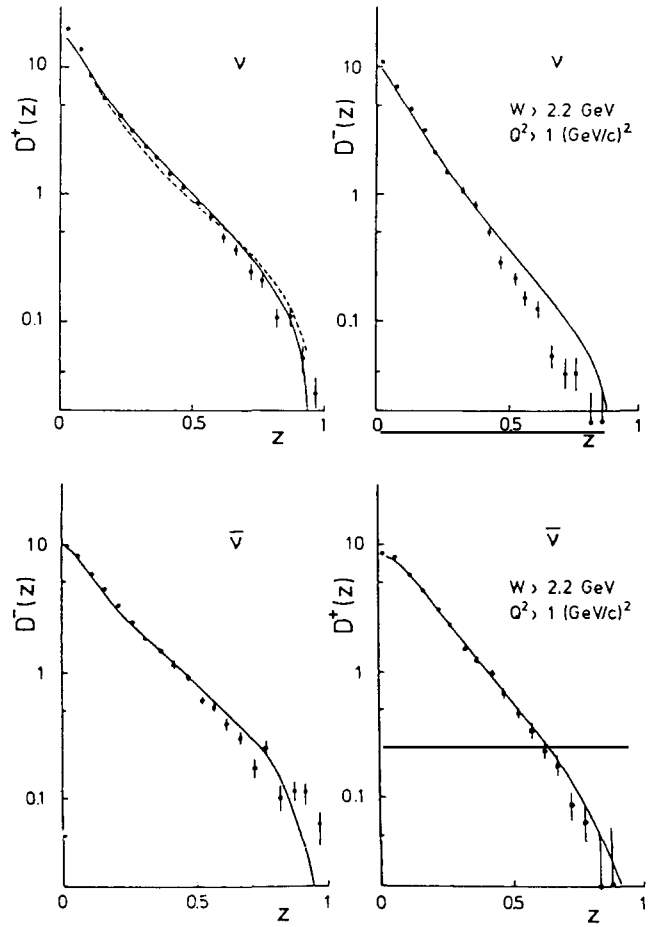

Fig. 2.12. Fragmentation functions for positive and negative particles in ν and $\bar{\nu}$ interactions, data from BEBC [16] compared to standard Lund jet systems, full lines. The dashed curve in one case illustrates the true fragmentation function obtained from the model before detector acceptance effects etc. have been folded in.

amazing thing about figs. 2.10 and 2.12 is not the minor disagreements, but the fact that a jet fragmentation picture works at all for W in the order of 4 GeV.

The development of a rapidity plateau for a simple $u\bar{u}$ jet system is illustrated in fig. 2.13. In fact, the scaling violations are quite significant already for simple $q\bar{q}$ jet systems, fig. 2.14. A minor part of these violations comes from passing the $b\bar{b}$ threshold, but most of the effect is associated with the strong

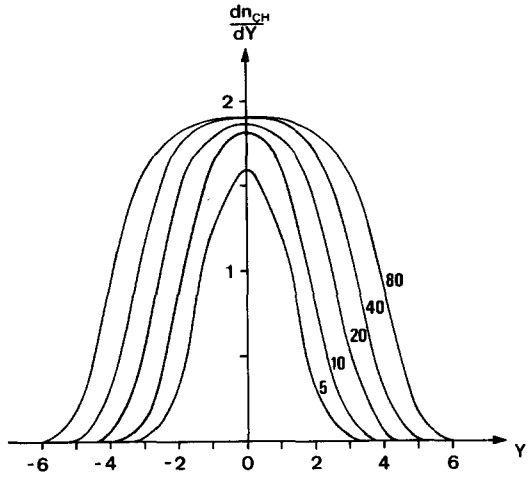

Fig. 2.13. Formation of a rapidity plateau: charged particle rapidity distributions with respect to the true jet axis, in $u\bar{u}$ jet systems at CM energies of 5, 10, 20, 40 and 80 GeV.

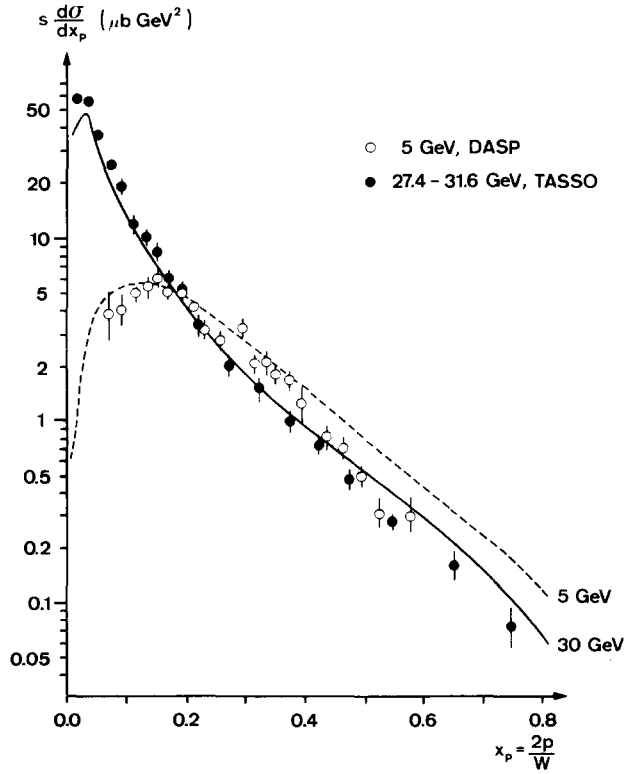

Fig. 2.14. The "scaling" cross section $s\,d\sigma/dx_p$ at 5 GeV, dashed line, compared to DASP data [17], open circles, and at around 30 GeV, full line, compared to TASSO data [18], filled circles. Hard gluon emission is not included.

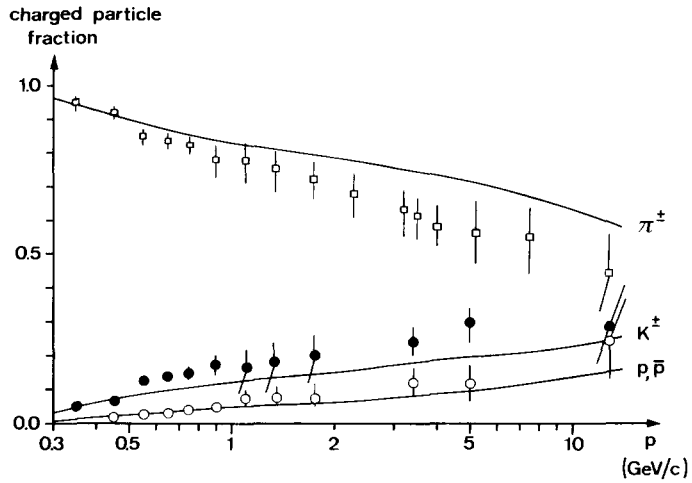

Fig. 2.15. The $\pi^{\pm}$, $K^{\pm}$ and p, $\bar{p}$ fractions of the charged particles compared to TASSO data [19]: open squares $\pi^{\pm}$, filled circles $K^{\pm}$, open circles p, $\bar{p}$.

nonasymptotic corrections below 20 GeV (mass effects etc.). Also for many other measures kinematical effects may well play an important rôle. This is illustrated with the charged particle composition in fig. 2.15 (calculated fractions are for $q\bar{q}$ jet systems alone, inclusion of gluon jets will not significantly change the picture), where the behaviour with momentum comes out qualitatively correct just because of the higher K and p masses and the effects of the profuse particle decays.

2.6. *Left–right symmetry*

We have (e.g. in section 2.4.2) discussed iteration schemes for the fragmentation of a $q_0\bar{q}_0$ jet system, starting at the q_0 end of the system and stepping "left" towards the $\bar{q}_0$ end. Alternatively we could have begun in the $\bar{q}_0$ end and iterated the other way instead. Whatever way we choose to do it, we would wish to obtain the same result on the mean. The use of iteration schemes at all is just a matter of convenience; as we have noted before: all $q\bar{q}$-pair production vertices are causally disconnected from each other. Since our iteration schemes have been derived under the assumption that there is much energy left, an iteration from the q_0 end cannot be taken all the way to $\bar{q}_0$ and vice versa. In the central rapidity plateau of a reasonably large jet system, however, there should be no artefact left to tell the direction of iteration. Unfortunately, for the schemes we have discussed so far, such artefacts exist and are sometimes quite prominent.

The basic reason for an asymmetry is not difficult to understand. In any iterative cascade scheme it is possible to compute a correspondence to the distribution $H(\Gamma)$ for the proper times of the production vertices. The center of the distribution will be along a hyperbola corresponding to a proper time $\tau_0 \approx \bar{m}/\kappa$, where $\bar{m}$ is some median mass in the final state hadronic systems.

If a large mass hadron is produced with a small value z of energy-momentum, the production vertex will in accordance with fig. 2.16 correspond to a proper time far away from this center hyperbola. Unless this is followed by a step with a very large z-value it will take many steps before the proper times of the vertices are back to the hyperbola. Thus the fragmentation process will be asymmetric unless the heavier particles normally take a larger fraction of energy-momentum.

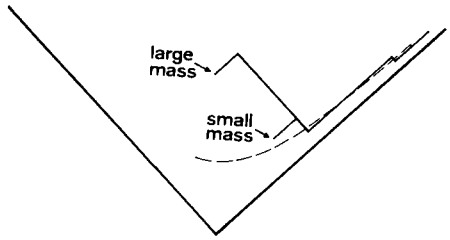

Fig. 2.16. If a large mass hadron is produced with a small value of z, the production vertex will be far away from the hyperbola corresponding to average proper times. It might then take many steps before this hyperbola is reached again.

2.6.1. *Measures for left–right asymmetry*

The left–right asymmetry of a given iterative cascade model can be studied in different ways. As we have noted above, an asymmetry is usually associated with the existence of particles with different masses. Let us therefore consider the rapidity difference $\Delta y_{12} = y_1 - y_2$ of any two hadrons with adjacent rank, where e.g. particle no. 1 is defined as the one generated first of the two if the event is considered to have been generated from the right end of the system. The expected distribution in Δy_{12}, and in particular the mean value $\langle \Delta y_{12} \rangle$, depends on the transverse masses $m_{\perp 1}$ and $m_{\perp 2}$, i.e. $\langle \Delta y_{12} \rangle = \langle \Delta y_{12} \rangle (m_{\perp 1}, m_{\perp 2})$. For a truly symmetric stochastical process the quantity must be independent of the labelling of the particles, i.e.

$$\langle \Delta y_{12} \rangle (m_{\perp 1}, m_{\perp 2}) = \langle \Delta y_{12} \rangle (m_{\perp 2}, m_{\perp 1}) \tag{2.48}$$

since the labelling of particle no. 1 and particle no. 2 would be reversed if the event were instead considered to have been generated from the left end. Actually (2.48) is strongly violated in the Lund and Field–Feynman models, as is shown in fig. 2.17 by plotting $\langle \Delta y_{12} \rangle (m_{\perp 1} - m_{\perp 2})$.

It would be tempting to assume that left–right asymmetries are only associated with different masses, so that if all particles had the same mass, there would be no such asymmetries. This is not true, as we will show using a modification of an argument originally presented by Field and Feynman [7]. This time, consider any three particles adjacent in rank, nos. 1, 2 and 3, where no. 2 is the one with middle rank. For given y_1 and y_3 left–right symmetry implies that y_2 should be symmetrically distributed around $\frac{1}{2}(y_1 + y_3)$, i.e. in particular

$$\langle y_2 - \tfrac{1}{2}(y_1 + y_3) \rangle (y_1 - y_3) \equiv 0 \,. \tag{2.49}$$

Note that $2y_2 - (y_1 + y_3) = (y_2 - y_1) - (y_3 - y_2)$, i.e. (2.49) does not depend on absolute rapidities but only on rapidity differences, just like (2.48). As indicated in fig. 2.18 the relation in (2.49) is violated both in the Lund and in the Field–Feynman cases, if all particles are generated e.g. from the right, even when all masses have been put equal and no transverse momenta are introduced.

We note that these two measures can be used as tests on any model, but that they cannot be directly applied to experimental data, since ranks are not known and since particle decays complicate matters. In principle one could imagine studying e.g. K^+K^--pairs or $K^+\phi K^-$-triplets in events with no other strange particles, and defining the right side of the jet system by the overall direction of motion of the pair or triplet, but this would be a tedious task and would have to depend on comparative Monte Carlo studies for an interpretation.

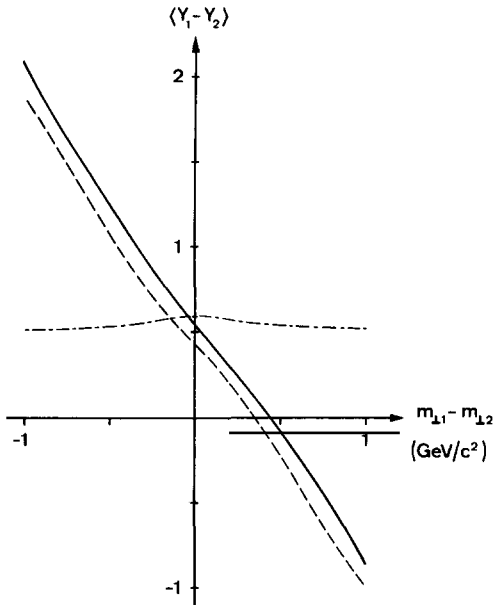

Fig. 2.17. Left–right asymmetry in jet fragmentation: $\langle y_1 - y_2 \rangle$ $(m_{\perp 1} - m_{\perp 2})$, 1, 2 adjacent in rank, for standard Lund, full line, Field–Feynman, dashed and symmetric Lund, dash-dotted.

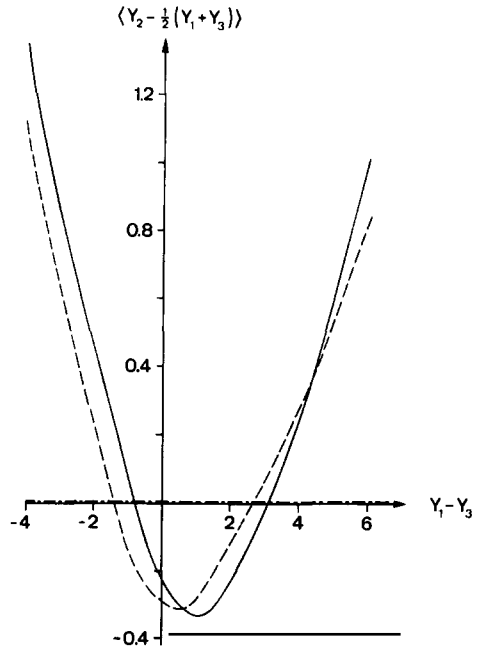

Fig. 2.18. Left–right asymmetry in jet fragmentation: $\langle y_2 - \frac{1}{2}(y_1 + y_3) \rangle$ $(y_1 - y_3)$, 1, 2, 3 adjacent in rank, for standard Lund, full line, Field–Feynman, dashed, and symmetric Lund, dash-dotted.

2.6.2. A symmetric fragmentation scheme

At this point the question arises: is it then possible to have a scaling function which really gives left–right symmetric jets? The answer is yes, it is possible, but only for a very restricted set of fragmentation functions.

Let the scaling function $f_{\alpha\beta}(z, m_\perp^2)$ describe the probability for a quark with flavour α to combine with an antiquark with flavour β to give a meson with transverse mass $m_\perp$ and energy-momentum fraction z. Then, if we require a symmetric fragmentation, $f_{\alpha\beta}$ must have the functional form [20]

$$f_{\alpha\beta}(z) = N_{\alpha\beta} \frac{1}{z} z^{a_\alpha} \left(\frac{1-z}{z}\right)^{a_\beta} \exp -(b m_\perp^2 / z) . \tag{2.50}$$

The indices α and β correspond to the flavours produced at the vertex where we start and end respectively and there is one in principle free parameter a_α and a_β for each flavour. The parameter b is the same for all vertices and $m_\perp^2$ is the transverse mass of the hadron produced. The quantity $N_{\alpha\beta}$ is a normalization constant.

Furthermore the vertices with flavour α are (in the central plateau) distributed in proper time $\tau = \sqrt{\Gamma}/\kappa$ according to

$$H_\alpha(\Gamma)\, \mathrm{d}\Gamma = C_\alpha\, \mathrm{d}\Gamma\, \Gamma^{a_\alpha} \exp -(b\Gamma) . \tag{2.51}$$

Phenomenologically (cf. sections 2.6.3 and 2.7 below) there does not seem to be a necessity to use the freedom of different values of a for different flavours and we will in general assume that all the a-parameters are equal.

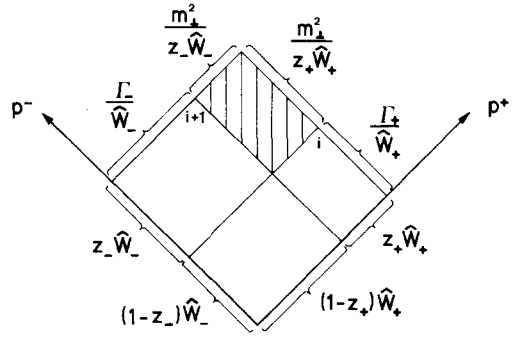

Fig. 2.19. Kinematical variables used for demonstrating left–right symmetry.

We will not here give the complete derivation that (2.50) is the unique solution, but only indicate that f will indeed lead to a symmetric fragmentation. To see that we consider fig. 2.19 where, seen from the right, we start in a point where a $q\bar{q}$ pair with flavour α is produced with momentum space coordinates $p^+ = \hat{W}^+$, $p^- = \Gamma^+/\hat{W}^+$ and take a step z^+ to produce the hadron with transverse mass $m_\perp$, flavour α and antiflavour β. Seen from the left, a step z^- is taken from a point with $p^+ = \Gamma^-/\hat{W}^-$, $p^- = \hat{W}^-$ for the same production process. All of these variables are of course not mutually independent, e.g. $m_\perp^2 = z^+\hat{W}^+z^-\hat{W}^-$. The requirement of left–right symmetry means that in the center of phase space the probability to generate this configuration of variables must be the same whether the fragmentation is done from the right or from the left. Thus we demand

$$H_\alpha(\Gamma^+)\,\mathrm{d}\Gamma^+ f_{\alpha\beta}(z^+)\,\mathrm{d}z^+ = H_\beta(\Gamma^-)\,\mathrm{d}\Gamma^- f_{\beta\alpha}(z^-)\,\mathrm{d}z^- . \tag{2.52}$$

Using the relations

$$\hat{W}^+\hat{W}^- = \Gamma^+ + m_\perp^2/z^+ = \Gamma^- + m_\perp^2/z^- \tag{2.53a}$$

$$(1-z^-)\hat{W}^-(1-z^+)\hat{W}^+ = (1-z^+)\Gamma^+ = (1-z^-)\Gamma^- \tag{2.53b}$$

$$m_\perp^2\,(z^+)^2(z^-)^2\,\mathrm{d}z^+\,\mathrm{d}z^- = \frac{1}{z^+}\,\mathrm{d}z^+\,\mathrm{d}\Gamma^+ = \frac{1}{z^-}\,\mathrm{d}z^-\,\mathrm{d}\Gamma^- \tag{2.53c}$$

it is easy to show that eq. (2.52) is indeed satisfied by the expressions in eqs. (2.50) and (2.51).

We end this subsection with a few remarks on finite mass systems in this model. If we produce a set of n particles adjacent in rank with "flavour powers" $a_0, \ldots, a_n$ it is easily seen, according to the iteration procedure in section 2.1, that in terms of observable lightcone fractions $z_1, \ldots, z_n$ we will obtain the probability

$$\begin{aligned}\mathrm{d}P(z_1, \ldots, z_n) &= \prod_{k=1}^{n} f_{k-1,k}\left(\frac{z_k}{1-\sum_{j=1}^{k-1} z_j}\right)\frac{\mathrm{d}z_k}{1-\sum_{j=1}^{k-1} z_j} \\ &= \left(1-\sum_{k=1}^{n} z_k\right)^{a_n} \exp-(b\,A_n(z_1, \ldots, z_n)) \prod_{k=1}^{n} N_{k-1,k}\,\frac{\mathrm{d}z_k}{z_k}\,z_k^{(a_{k-1}-a_k)} .\end{aligned} \tag{2.54}$$

The quantity A_n is given by

$$A_n = \sum_{k=1}^{n} \frac{m_k^2}{z_k} - \sum_{k=1}^{n} \frac{m_k^2}{z_k} \sum_{j<k} z_j . \tag{2.55}$$

The total lightcone fraction z and the total mass s_n of this n-cluster are

$$z = \sum_{k=1}^{n} z_k \tag{2.56}$$

$$s_n = z \sum_{k=1}^{n} \frac{m_k^2}{z_k} . \tag{2.57}$$

It is useful to define the internal lightcone fractions

$$\begin{aligned} &\breve{z} = z_k/z \\ &\Rightarrow \sum_{k=1}^{n} \breve{z}_k = 1 \end{aligned} \tag{2.58}$$

and we obtain immediately for the probability in eq. (2.54)

$$\mathrm{d}P(\breve{z}_1, \ldots, \breve{z}_n; z, s_n) = \mathrm{d}s_n \frac{\mathrm{d}z}{z} z^{a_0} \left(\frac{1-z}{z}\right)^{a_n} \exp - \left(b s_n \left(\frac{1-z}{z}\right)\right) \mathrm{d}\hat{P}_{s_n}(\breve{z}_1, \ldots, \breve{z}_n) \tag{2.59}$$

with

$$\mathrm{d}\hat{P}_{s_n}(\breve{z}_1, \ldots, \breve{z}_n) = \exp(-b\,\hat{A}_n(\breve{z}_1, \ldots, \breve{z}_n))\, \delta\left(1 - \sum \breve{z}_k\right) \delta\left(s_n - \sum \frac{m_k^2}{\breve{z}_k}\right) \prod_{k=1}^{n} N_{k-1,k} \frac{\mathrm{d}\breve{z}_k}{\breve{z}_k} \breve{z}_k^{a_{k-1}-a_k} \tag{2.60a}$$

$$\hat{A}_n = \sum_{k=1}^{n} \frac{m_k^2}{\breve{z}_k} \sum_{j=k}^{n} \breve{z}_j . \tag{2.60b}$$

Consequently, it is possible to factor out the total z-dependence of the probability distribution and to consider the internal behaviour of an n-particle cluster with a given total mass s_n.

We note that the z-dependence is the same as if we had produced the vertex n (with flavour-power a_n) from the original vertex (with flavour power a_0) in one step with the total mass s_n. The symmetric process therefore implies that any part of a large jet system can be taken out and considered by itself, irrespective of the intermediate steps and flavours. One only needs to know the total mass and the flavours at the beginning and at the end to obtain the distribution.

We also note that if we introduce the quantity

$$\Gamma = s_n(1-z)/z \tag{2.61}$$

which corresponds to the proper time-square of the nth vertex given that the starting vertex is on the lightcone, we obtain the finite mass version of H_{α_n} in eq. (2.51)

$$H_{\alpha_n}^{(s_n)} = \frac{\mathrm{d}P}{\mathrm{d}\Gamma}(\Gamma; s_n) \propto \frac{\Gamma^{a_n}}{(\Gamma + s_n)^{a_0+1}} \exp - (b\Gamma) . \tag{2.62}$$

It is evident that $H_{\alpha_n}^{(s_n)}$ will approach the asymptotic expression in eq. (2.51) as a geometrical progression and a simple estimate tells that the asymptotic distribution will in general be reached after the first four or five particle production steps.

It is useful to note that the quantity $\hat{A}_n$ in eq. (2.60b) is actually equal to the size of the area in the fig. 2.22. We will come back to a discussion of the significance of this in section 2.6.5.

2.6.3. Phenomenology in the symmetric Lund scheme

The parameters a and b in the scaling function $f(z)$ in (2.50) are generally related to the behaviour for z close to 0 and 1. The behaviour as $z \to 0$ is regulated by the factor $(1/z)\exp(-bm_\perp^2/z)$, which peaks at $z = bm_\perp^2$ (for $bm_\perp^2 < 1$) and rapidly vanishes for smaller z values, while the behaviour for $z \to 1$ is determined by the factor $(1-z)^a$.

Experimental data are well reproduced assuming a common value of the parameter a for all flavours, and the results presented below are obtained using this assumption. We comment on the possibility of different values a_i in connection with heavy quark fragmentation in section 2.7.

Experiments then suggest that $0 \leq a \lesssim 2$, since $a < 0$ would have given too many and $a \gtrsim 2$ too few particles at large momenta. Within the region $0 \leq a \lesssim 2$, $b > 0$ there is a rather large freedom for a and b separately, but there is a strong correlation between the two: since the mean step in z decreases and hence the mean multiplicity increases when a is increased or b decreased, only values along a curve in the (a, b) plane will fit the observed particle spectra and multiplicities. Thus for inclusive particle spectra a good agreement can be obtained with $a = 1$, $b = 1/2.25\ \mathrm{GeV}^{-2}$, but a fit with, e.g., $a = 0$, $b = \frac{1}{9}\ \mathrm{GeV}^{-2}$ would also be possible.

For definiteness we will subsequently with "symmetric Lund" refer to a fragmentation scheme à la the standard Lund, but using $f(z)$ according to (2.50) for the longitudinal fragmentation with $a = 1$, $b = 1/2.25\ \mathrm{GeV}^{-2}$ unless otherwise stated. We note that the collinear gluon and finite field length corrections in the standard Lund model have effects very similar to the $(1-z)^a$ term in (2.50), i.e. essentially that of suppressing z values close to 1. Therefore these corrections are not separately implemented in the symmetric Lund scheme The shape of the scaling function $f(z)$ is then given for some different transverse masses in fig. 2.20 (cf. fig. 2.11).

Further restrictions on a and b can be obtained from correlation data. When both a and b are increased (e.g. in such a way that the mean multiplicity stays constant), what happens is that the ordering in rapidity becomes more and more like the one in rank. The extreme case is when a and b are allowed to go towards infinity with the fixed ratio $a/b = \Gamma_0$ for some number Γ_0. Then $H(\Gamma) \to \delta(\Gamma - \Gamma_0)$, i.e. all $q\bar{q}$ pair productions occur at the same invariant time, and the ordering in rapidity agrees completely with that in rank. For more realistic a and b values, the rapidity spread $\sigma(\Delta y_{12}) = \sqrt{\langle \Delta y_{12}^2 \rangle - \langle \Delta y_{12} \rangle^2}$ between two particles adjacent in rank is shown as a function of $m_{\perp 1} + m_{\perp 2}$ in fig. 2.21b (the dependence on $m_{\perp 1} - m_{\perp 2}$ is smaller but not insignificant, with smallest σ for $m_{\perp 1} \approx m_{\perp 2}$). Higher a and b values thus lead e.g. to stronger local charge, strangeness or baryon number compensation. Experimentally this is a difficult subject to study (effects from particle decays are quite substantial, etc.) [21] but eventually such studies could help to fix the a and b values separately.

While the spread $\sigma(\Delta y_{12})$ decreases for heavier particles, the mean value $\langle \Delta y_{12} \rangle$ actually increases, as is seen in fig. 2.21a. This is related to the fact that for small masses $\langle z \rangle \sim m_\perp$, so that the remaining jet energy is not scaled down much with the production of a light particle, whereas a heavy particle will take a large z and therefore does not leave much energy to the subsequent particles.

Thus e.g. kaon and proton spectra should become relatively harder than pion spectra. Numerical calculations show, however, that this effect is very small, and the ratios π/K/p are essentially the same

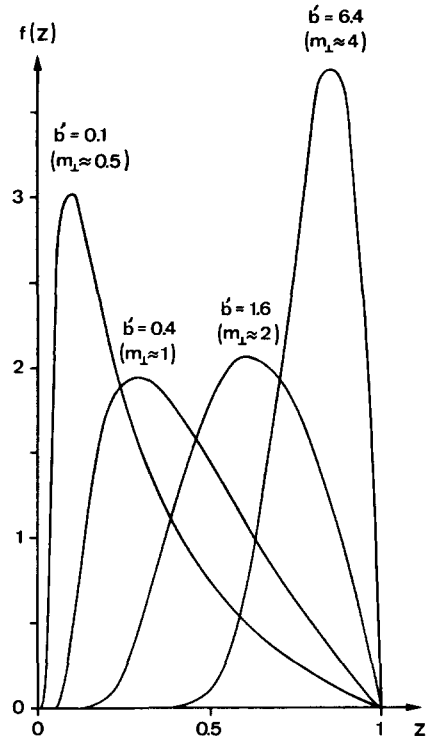

Fig. 2.20. Shape of left–right symmetric scaling function $f(z, m_\perp)$, specifically $(1/z)(1-z)\exp(-b'/z)$ with $b' = 0.1$, 0.4, 1.6 and 6.4, corresponding to $m_\perp \sim 0.5$, 1, 2 and 4 GeV, respectively.

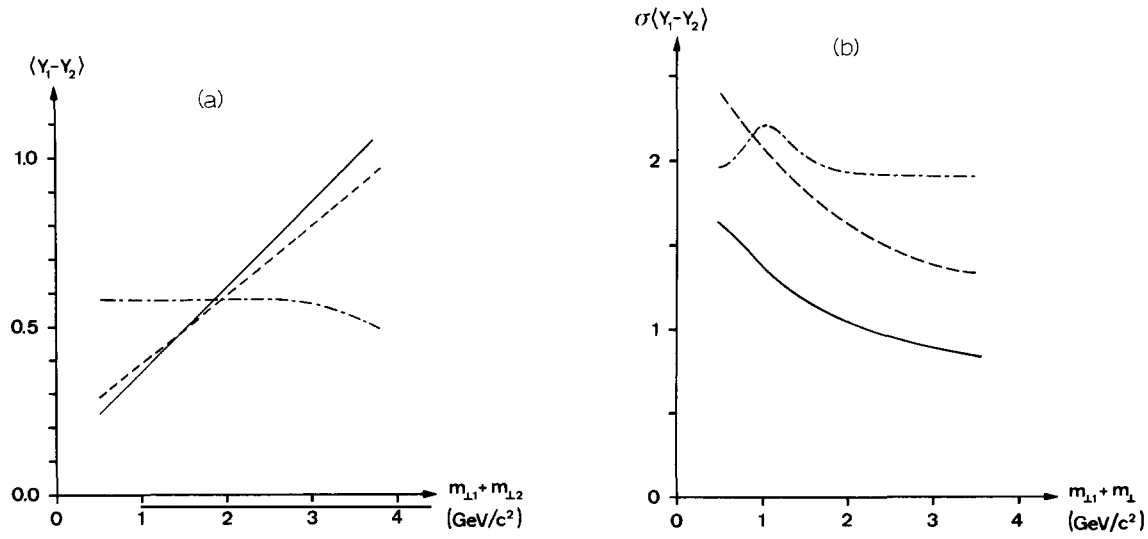

Fig. 2.21. (a) Rapidity difference $\langle y_1 - y_2 \rangle$ and (b) rapidity spread $\sigma(y_1 - y_2) = \sqrt{\langle (y_1 - y_2)^2 \rangle - \langle y_1 - y_2 \rangle^2}$; both as functions of $m_{\perp 1} + m_{\perp 2}$; for 1 and 2 of adjacent rank. Full line $f(z) = (1/z)(1-z)\exp(-m_\perp^2/2.25z)$, dashed $f(z) = (1/z)\exp(-m_\perp^2/9z)$ and dash-dotted standard Lund.

as in the standard Lund model. The differences in transverse mass simply are not large enough, in particular since many pions stem from vector meson decays.

In the symmetric Lund scheme, transverse and longitudinal properties do not completely decouple: since $m_\perp^2 = m^2 + p_\perp^2$ and not just m^2 enters in (2.50) the average z will rise with $p_\perp$. The effect is small, however, and experimentally hidden, e.g., by particle decay effects.

2.6.4. The Artru–Mennessier model

The symmetric Lund scheme has similarities with the Artru–Mennessier model [22]. This model was conceived very early, before the use of iterative fragmentation jets became popular.

The breakup properties of the string in the A-M model is based upon classical probability arguments. It is assumed that there is a constant probability P_0 per unit time and length that the string breaks by the production of a $q\bar{q}$-pair. No further breaks can occur in the forward lightcone with respect to a given vertex point since the field is vanishing there (cf. e.g. fig. 2.4). This approach then leads to an exponential decay law, i.e.

$$dP/d\Gamma = b \exp(-b\Gamma) \tag{2.63}$$

with $b = P_0/2\kappa^2$.

With this basic probability argument the different vertex points will appear completely independent of each other so that the mass of the final state hadrons will not be fixed numbers but instead be given by a mass distribution. If one considers the breakup closest to the q_0 end, i.e. the one with the smallest $x^- = t - x$ coordinate one obtains [22, 23]:

$$\begin{aligned} dP &= \exp -(bW^+ z^- W^-)\, bW^+ \, dz^+ \, W^- \, dz^- \\ &= \exp -(bm^2/z^+) \frac{b}{z^+} dz^+ \, dm^2 \end{aligned} \tag{2.64a}$$

$$\frac{dP}{dm^2} = \int_0^1 \exp -(bm^2/z^+) \frac{b}{z^+} dz^+ = b\, E_1(bm^2)\,. \tag{2.64b}$$

This expression is singular for $m^2 \to 0$, corresponding to a large probability for the string to go on breaking into very small pieces unless some lower cutoff is imposed on the mass spectrum. Such a cutoff is difficult to introduce in a consistent way if one wants to keep the classical probability interpretation mentioned above. Nevertheless it is possible to interpret the mass spectrum in a way similar to the well-known Hagedorn model (which however has a linear dependence upon the masses in the exponent [24]) as corresponding to resonances etc. which may decay in later steps to the ordinary hadrons. The Artru–Mennessier model, which is explicitly left–right symmetric, was conceived independently of any iterative framework, but can actually be given an iterative structure using (2.64).

It would thus be natural to assume that our model presented in section 2.6.2 is just a specialization of the Artru–Mennessier model to a physical mass spectrum, but this is not true. A classical probability argument would not in the case of fixed masses lead to an exponential decay law. To see that we start to assume that inside a finite width δm^2 around the mass hyperbolae we will allow for the breakup just as in the A-M model. Then we calculate the z^+ value for which the first (in time) breakup occurs if the production probability is a constant per unit length and time within the band of

allowed breakup points

$$f(z^+)\,dz^+ = \frac{P_0}{2\kappa^2}\,W^+W^-\,\delta z^-\,dz^+ \exp-\Big(\int_{z^+}^{1}\frac{P_0}{2\kappa^2}\,W^+W^-\,\delta z^-\,dz^{+\prime}\Big)$$

$$= \frac{P_0\,\delta m^2}{2\kappa^2}\frac{1}{z^+}\,dz^+ \exp-\frac{P_0\,\delta m^2}{2\kappa^2}\Big(\int_{z^+}^{1}\frac{dz^{+\prime}}{z^{+\prime}}\Big) = \frac{P_0\,\delta m^2}{2\kappa^2}\,z^{+(P_0\,\delta m^2/2\kappa^2-1)}. \tag{2.65}$$

We may now let $\delta m^2 \to 0$ if at the same time $P_0 \to \infty$. Note that for $P_0\,\delta m^2/2\kappa^2 = 1$ we recover $f(z) = 1$, i.e. the simple Lund result that does not give a symmetric fragmentation process.

2.6.5. A possible interpretation of the symmetric model

There is another interesting and rather suggestive interpretation of the fragmentation distributions in eqs. (2.50) and (2.60) [20]. The expression in the exponent does, as explained in connection with eq. (2.60), have the interpretation of the area of a space-time surface. At this point it is useful to consider the detailed fig. 2.22 in which the string system breaks up at a set of vertices labelled $V_1, \ldots, V_{n-1}$. The original pair $q_0\bar{q}_0$ starts out at the space-time point O and in QCD language they correspond to a colour singlet. At the point O_1, q_0 (which has turned around at D_0) and $\bar{q}_1$ (produced at V_1) will meet "for the first time" to form a colour singlet final state hadron. The surface in question is given by $OD_0O_1C_1$ where C_1 is the point along the $\bar{q}_0$ lightcone marked out in the figure.

Inside this surface there must evidently be a "memory" of the $q_0\bar{q}_0$ colour properties as compared to the $q_0\bar{q}_1$ properties, and we will call it a "colour coherence region". The fragmentation distribution for the final state hadron composed of $q_1\bar{q}_2$ (produced in the vertices V_1 and V_2 respectively) is similarly related to the colour coherence region $C_1V_1O_2C_2$ and so on, so that the hadron $q_{n-1}\bar{q}_0$ is related to $C_{n-1}V_{n-1}O_nC_n$ with C_n the turning point of $\bar{q}_0$.

We may, however, evidently just as well consider the fragmentation process from the antiquark end in which case we will have the corresponding fragmentation distributions related to the colour coherence surfaces $OC_nO_nD_{n-1}$, $D_{n-1}V_{n-1}O_{n-1}D_{n-2}$ etc. until $D_1V_1O_1D_0$. We may also split up the surface in any way taking steps either from the right or from the left as shown in fig. 2.23. The area of the total surface is always equal to $\hat{A}_n$ in eq. (2.60b).

This freedom of considering the process "in any direction" corresponds in a suggestive way to the

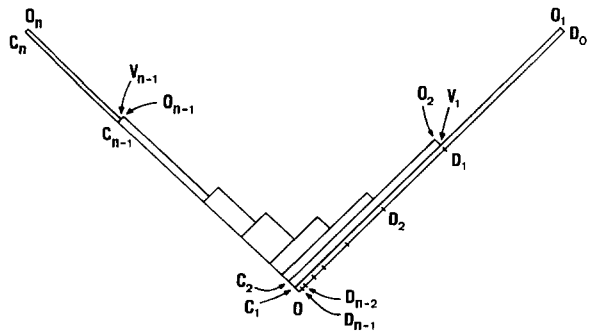

Fig. 2.22. "Colour coherence regions" in a gauge where $A^a_- = 0$ and all gluons are emitted along the positive lightcone.

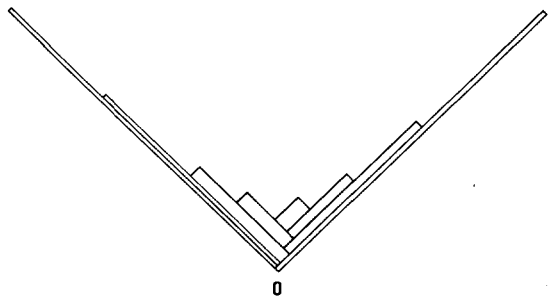

Fig. 2.23. "Colour coherence regions" when gluons can be emitted randomly.

gauge freedom in 1 + 1-dimensional QCD where we may, e.g., choose the lightcone gauge $A^a_- = 0$ (with a a colour index) corresponding to "emission of gluons" only along the positive lightcone etc. When we consider the results for producing an n-particle cluster with total mass s_n in accordance with eq. (2.60), we note that the probability is governed by an area law [25], corresponding to $\exp(-bA)$ and a product of factors $z_j^{a_{j+1}-a_j}$ corresponding to "the distances" travelled along the lightcones of a q-particle (positive power) and a $\bar{q}$-particle which, moving along the opposite lightcone, should and does exhibit a negative power. The two powers $z_1^{a_0}$ and $z_n^{-a_n}$ correspond similarly to the motion of the original pair along D_0O_1 and C_nO_n respectively. Evidently the whole setup is very suggestive of the expected expression for Wilson loop integrals with the well-known dominating area law and the corresponding perimeter dependence [25].

The differentials are Lorentz invariant phase-space factors:

$$\mathrm{d}\gamma_i/\gamma_i = \mathrm{d}y_i = \mathrm{d}^2p\,\delta(p^2 - m^2)\,. \tag{2.66}$$

In the light of this interpretation the generality of the parameter b is evident; it corresponds to the area law parameter. The parameters a_j are similarly together with the normalization constants $N_{\alpha\beta}$ the perimenter law parameters and the existence of different possible values for different flavours is rather easy to understand.

2.7. Heavy particle production

2.7.1. Motion of massive constituents

In section 2.2.2 we studied the "yo-yo modes", when massless q and $\bar{q}$ oscillate back and forth. Very similar results are obtained for massive constituents, but it is necessary to make use of a different set of particle orbits. For massive constituents (mass μ) the motion is no longer along light-rays but along the hyperbolae [11]

$$(x - x_1)^2 - (t - t_1)^2 = \mu^2/\kappa^2\,. \tag{2.67}$$

These hyperbolae have, however, the straight lines corresponding to the motion of massless constituents as asymptotes. A q and a $\bar{q}$ which move along the hyperbolae with centers (x_1, t_1) and (x_2, t_2), respectively, can form a hadron with mass m if (x_1, t_1) and (x_2, t_2) satisfy the same condition as for massless quarks, i.e. if

$$(x_1 - x_2, t_1 - t_2) = \pm\frac{m}{\kappa}(\cosh y, \sinh y)\,. \tag{2.68}$$

Here y is the rapidity of the hadron as before. In particular, only the hadron mass m occurs in this expression (but it is evidently necessary that m is larger than the sum of the masses of the constituents). This motion is shown in fig. 2.24, which thus is the generalization of fig. 2.2. We note that the oscillation time not only depends on m but also on μ. However, this influences only the internal motion of the hadron after the formation, and not the jet structure.

There is a conceptual difference with respect to massless constituents when a massive $q\bar{q}$-pair is created in the field. From the point of view of classical dynamics the production cannot take place at a single space-time point if energy and momentum are to be conserved in the system. The classical motion

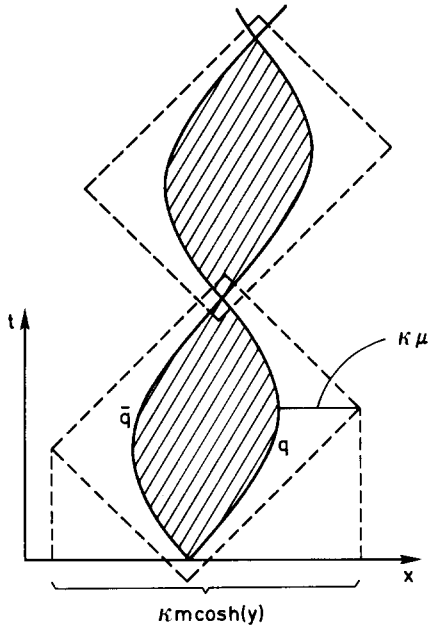

Fig. 2.24. The motion of a massive q and q̄ in a system.

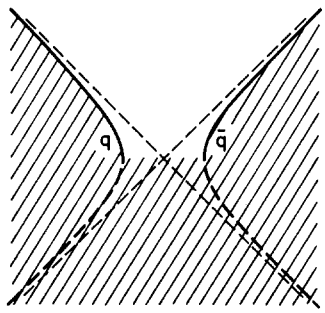

Fig. 2.25. A pair qq̄ of massive quarks is produced in the field and move apart on different branches of the same hyperbola.

of the qq̄-pair is along the opposite branches of the same hyperbola, as shown in fig. 2.25. The production of such a pair can be treated as a quantum mechanical tunneling phenomenon, as will be described in section 3.

The only Lorentz invariant statement of the production is then related to the center of the hyperbola. Thus with the centers of the hyperbolae taking the rôle of the production points and the turning points for the massless case (i.e. where massless constituents have zero energy), the situation is very similar for massive constituents. The model can be developed in exactly the same way as before, with the only difference that the straight lines in the figures should be interpreted as asymptotes for the hyperbolic worldlines of massive quarks.

In the symmetric Lund scheme heavier particles take more energy; the particles are ordered in rapidity rather than in momentum. As mentioned above, this effect is hardly noticeable in the π/K/p ratios. However, for particles with heavy c-, b- or t-quarks the effect is important.

2.7.2. Heavy quark fragmentation

If the production in the colour field of quarks with mass and transverse momentum can be treated as a tunneling phenomenon, which well describes the suppression of strange quarks and $p_\perp$ (see section 3), then the probability to produce a $c\bar{c}$ pair is extremely small ($\sim 10^{-11}$). Thus, if heavy quarks only can be produced in the initial hard process (in e.g. e^+e^- annihilation), and be at the ends of the stretched colour field, then there is no compelling reason to demand a symmetric scheme for the fragmentation of heavy flavours. However, if we anyway pursue the idea that a c-quark produced in the field with very small probability behaves as a c-quark produced directly by the virtual photon, we would assume that also heavy quark fragmentation is described by the scaling function f in eq. (2.50).

If we consider the fragmentation of some heavy flavour quark q_0, then fig. 2.26 shows the formation

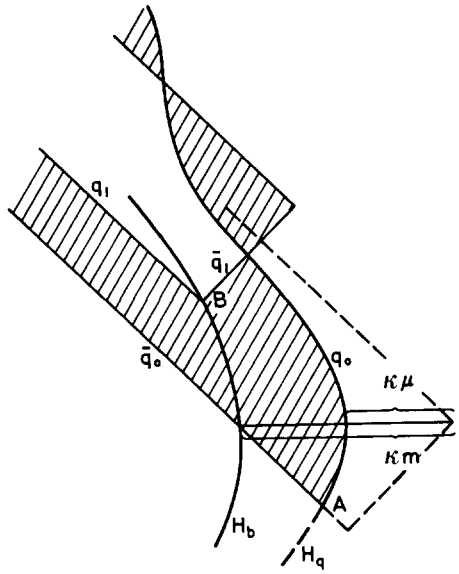

Fig. 2.26. The generalization of fig. 2.7 to the case when the original quark q_0 is massive.

of the first hadron $q_0\bar{q}_1$. Here q_1 and $\bar{q}_1$ are assumed massless for simplicity. The point A is the starting point of the pair $q_0\bar{q}_0$. The rapidity of the hadron only depends on the point B on the hyperbola H_b, and thus only on the mass m of the hadron. It is independent of the mass μ of q_0, which however determines the hyperbola H_q.

According to the considerations in the simple Lund scheme, we would obtain a flat scaling function, $f(z) = 1$. The further corrections from collinear gluons and finite field sizes will tend to die away with higher masses, but these corrections are anyhow small, also for light particles. Thus in the standard Lund scheme the mean value of z, $\langle z \rangle$, should be close to

$$\langle z \rangle \simeq \tfrac{1}{2} \tag{2.69}$$

for charm and bottom fragmentation. This means that light particles produced behind the heavy one will often obtain a larger rapidity.

This may seem unphysical, and actually Bjorken [26] has argued that asymptotically, i.e. for very large masses M,

$$\langle z \rangle \simeq 1 - (1\ \text{GeV})/M. \tag{2.70}$$

This result can be derived from the assumption that all primary hadrons on the average are equally spaced in rapidity. A similar result was also obtained by Bowler [23] from a generalization of the model by Artru and Mennessier [22].

Our symmetric fragmentation scheme will predict an even harder heavy quark fragmentation. For very large meson masses M we obtain asymptotically, due to the increased rapidity gap for heavier particles

$$\langle z \rangle \simeq 1 - (a+1)/bM^2. \tag{2.71}$$

Numerically we obtain for $a = 1$ and $b = 1/2.25\,\mathrm{GeV}^{-2}$ that the first rank hadron in a u-quark jet will in our scheme on the average be 0.28 rapidity units ahead of any other hadron, in a c-quark jet 0.65 units and in a b-quark jet 1.24 units ahead (if compared to the second rank particle only, the differences are 0.55, 0.94 and 1.50, respectively).

If fig. 2.27 we show charm spectra for leptoproduction and e^+e^- annihilation (in the latter case we also include charm from bottom decays). The experimental data favour a harder fragmentation spectrum but the actual difference in $\langle z \rangle$ between the two models is not all that large. Only with bottom are we in the asymptotic region where (2.71) applies. Since B mesons are hard to observe, one may look at muons (and electrons) coming from semileptonic decays, either by the one-particle muon spectra, with contributions both from charm and bottom, fig. 2.28, by same side $\mu^+\mu^-$-pairs, dominated by bottom, fig. 2.29, or by using the transverse muon spectrum with respect to the jet axis to enrich the bottom contribution in the one-particle spectrum. Mark II has looked at the latter quantity and concludes that the B meson spectrum indeed is harder than the D meson one [29].

We have here assumed that all the a-parameters are equal. The finite field length correction in the standard Lund model arises from the fact that the field must not be too short for the energy to suffice for the quark pair creation. As mentioned above this has an effect similar to the Γ^a factor in eq. (2.51), suppressing small Γ-values (and large z-values). As this effect becomes stronger for larger (transverse) quark masses, it is tempting to assume that the a-parameter should be larger for larger quark masses. This would make the fragmentation of a u-quark into a kaon or a proton (by production of a more massive $\bar{s}$-quark or diquark) softer and the fragmentation of a c- or b-quark into a D- or B-meson even

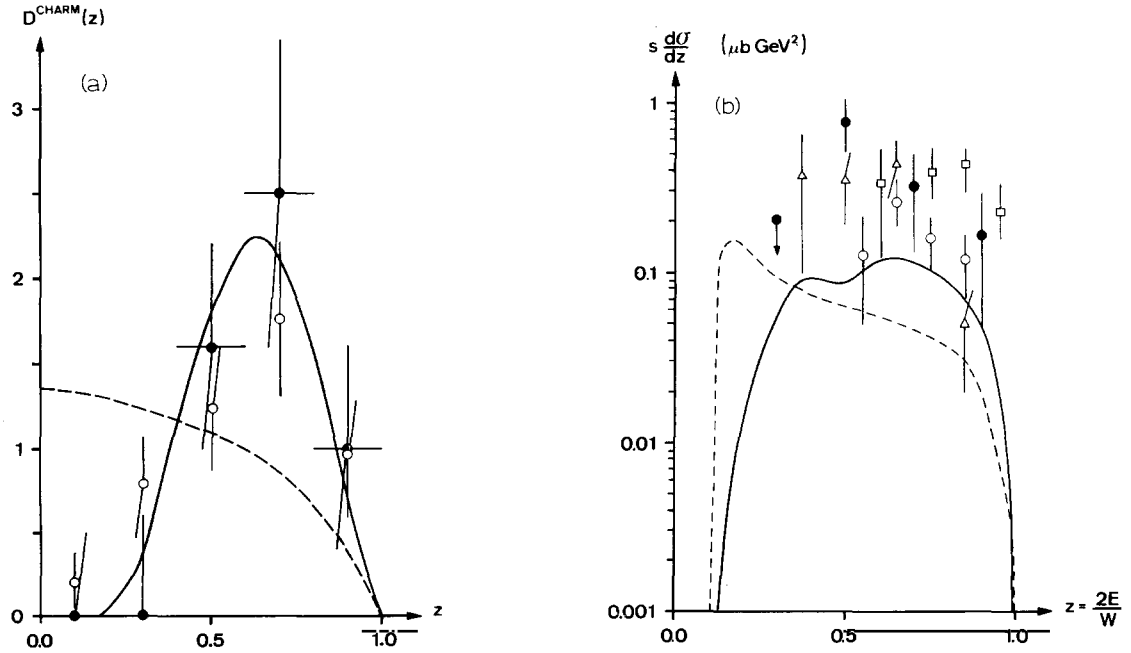

Fig. 2.27. Charm fragmentation spectra for symmetric Lund, full line, and standard Lund, dashed, (a) in leptoproduction, data from CDHS [27] (filled circles) and E531 [28] (preliminary) (open circles), (b) in e^+e^- annihilation, filled circles Mark II [29], open circles TASSO [30], triangles DELCO [31], open squares CLEO [32]. The former three data sets are around 30 GeV, as are the Lund model curves, while CLEO data are at 10.4 GeV, so that $z_{\min} = 0.39$. Large systematic normalization errors may be present due to uncertainties e.g. in the $D^0 \to K^-\pi^+$ branching ratio. Contributions from B meson decays are included in the model calculations (and give rise to the peaks at low z).

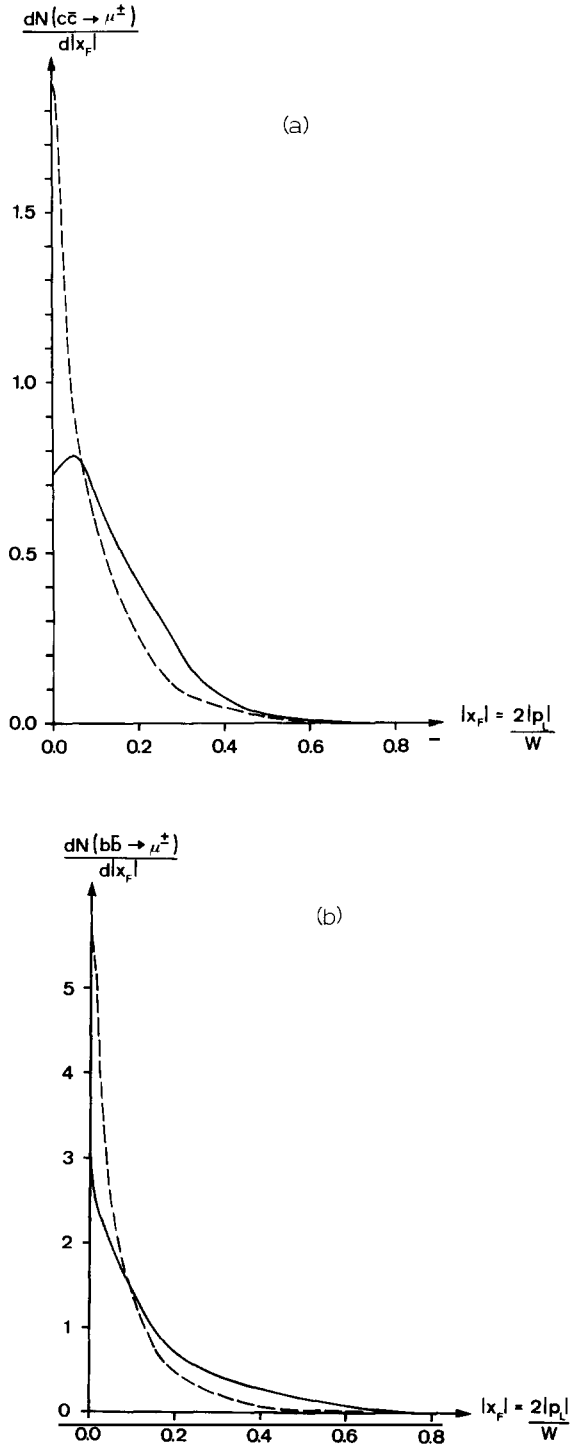

Fig. 2.28. Muons in (a) $c\bar{c}$ and (b) $b\bar{b}$ events ($W = 32$ GeV) as a function of $|x_F| = 2|p_L|/W$. Full line symmetric Lund, dashed standard Lund. In e^+e^--annihilations $c\bar{c}$ events are 4/11 of the total cross section and $b\bar{b}$ events 1/11, while $u\bar{u}$, $d\bar{d}$ and $s\bar{s}$ events give no contribution to the prompt muon spectrum.

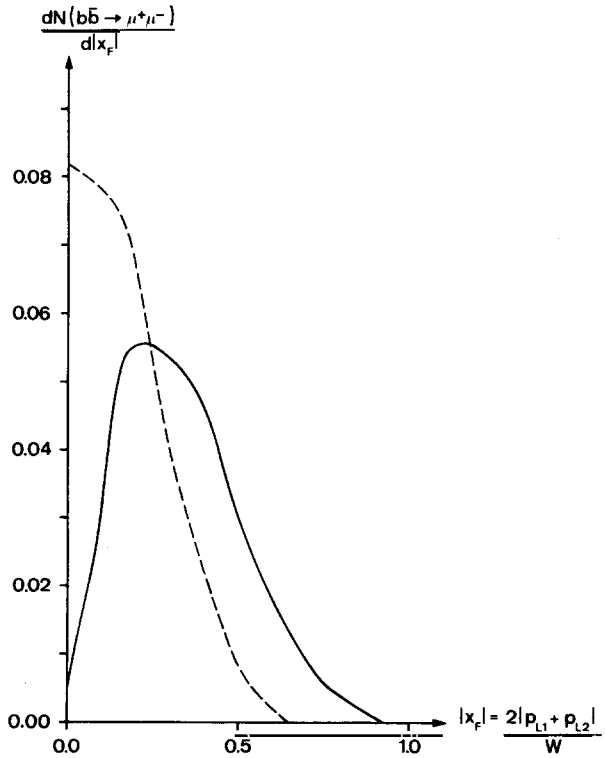

Fig. 2.29. The total $|x_F| = 2|p_{L1} + p_{L2}|/W$ of opposite sign, same side muon pairs in $b\bar{b}$ events ($W = 32$ GeV). Full line symmetric Lund, dashed standard Lund. Contributions from $c\bar{c}$ events are small. Note the vertical scale; only one $b\bar{b}$ event in 40 contains a same side $\mu^+\mu^-$ pair (if electrons also may be identified, this rate can be quadrupled). With only one event in 11 being $b\bar{b}$, the rate is too small for detailed studies at present energies, but at LEP it will be of interest.

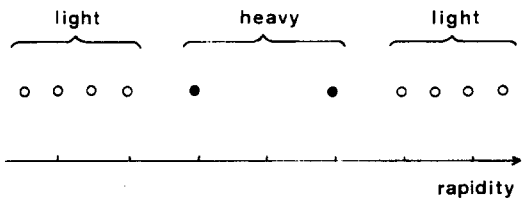

Fig. 2.30. When all the a-parameters are equal, the rapidity difference between two heavy particles is larger than that between one heavy and one light, which in turn is larger than that between two adjacent light particles.

harder than the result presented above (eq. (2.71) and figs. 2.27–2.29). Although this cannot be excluded it has presently no support in the experimental data.

We note that if a pair of heavy quarks would be produced in the field, the distribution in rapidity will be as shown in fig. 2.30 in case all a-parameters are equal. The rapidity difference between the two heavy particles is larger than that between one heavy and one light, which in turn is larger than that between two adjacent light particles. If the a-value for the heavy quark is larger, the two heavy mesons will come closer in rapidity and farther away from the light particles. Similarly a smaller a-value for the heavy quark would push the heavy mesons away from each other. This would increase the invariant mass of the heavy meson pair and decrease the number of produced light particles.

3. The tunneling process for local massive $q\bar{q}$ production

3.1. Preliminaries

In this section we will consider the local production of colour $(3\bar{3})$ pairs with mass and transverse momentum in a uniform force field. We will show that the production process, which we for obvious reasons will call "the tunneling process", is governed by the strength of the colour electric force κ

acting on a colour (3) charge. For the particular case of an infinitely thin colour flux line – a vortex line – this quantity corresponds to the tension in this stringlike force field. Most of our results are, however, independent of the transverse size of the colour electric flux tube. It is sometimes useful to picture the ensuing Gaussian transverse momentum fluctuations as an indication that the mean square radius of the flux tube is

$$\langle \vec{r}^2 \rangle \simeq \pi/2\kappa \,. \tag{3.1}$$

The assumption of a uniformity in the force field will, except for the constancy of κ, also include the property that there are no concentrations of energy, transverse momentum or angular momentum along the field. We note that with such field properties massive $(3\bar{3})$ pairs (mass μ) cannot be produced in a single space-time point. Classically they must be produced at a distance $2l$ apart so that the field energy in between can be used for the mass production:

$$2\kappa \cdot l = 2\mu \,. \tag{3.2}$$

Thus the production process is basically a quantum mechanical phenomenon.

The assumption above on the uniformity of the field implies strong similarities to a time-honoured dynamical mechanism firstly invoked by Heisenberg and Euler [33] in the thirties, later by Schwinger [33] in the fifties and recently by several authors [35, 36] in this context. (For a pedagogical treatment in a QCD field theoretical setting cf. [34].) In the presence of an external, constant electromagnetic field the no-particle state in QED is unstable. Its rate of decay may be interpreted as the production rate of electron–positron pairs.

A simpler but equivalent formulation which is more useful for our purposes is to consider the production as a tunneling process in a linear potential. With a knowledge of the wavefunction ψ_C of the particle at the classical turningpoint $(x = +l)$ (and the wavefunction $\psi_{\bar{q}C}$ for the antiparticle similarly at $(x = -l)$) we may interpolate the wavefunctions into the classically forbidden regions $|x| < l$ by WKB-methods. Such a calculation would in its simplest form give

$$\psi(x) \simeq \psi_C \exp \mathrm{i} \int_l^x p(x)\, \mathrm{d}x \tag{3.3}$$

with

$$p(x) = \sqrt{(E + \kappa x)^2 - \mu^2} \,. \tag{3.4}$$

In this way (cf. fig. 3.1) a particle with total energy $E = 0$ would inside the classically allowed region $x > l$ be described by an oscillating wavefunction. For $x < l$ the wavefunction will be damped and in particular the integral in eq. (3.3) is readily found to be

$$\psi(0) = \psi_C \exp -(\pi\mu^2/4\kappa) \,. \tag{3.5}$$

We obtain the same result for the antiparticle wavefunction $\psi_{\bar{q}}(x) \equiv \psi(-x)$. If we take as a model for the production matrix element $\mathcal{M}$ the overlap between the initial flat field (uniform wavefunction = 1)

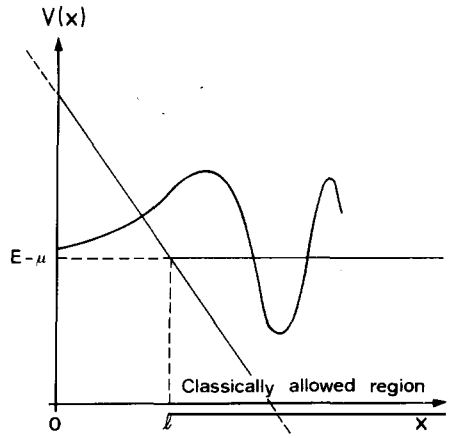

Fig. 3.1. A particle moving in a linear potential. For a given energy value E (which may be chosen as zero for a suitable choice of the origin in a linear potential) the wavefunction is oscillating in the classically allowed region and exponentially damped outside it.

and the final state particle–antiparticle wavefunctions we expect

$$|\mathcal{M}|^2 \propto \exp -(\pi\mu^2/\kappa) \tag{3.6}$$

which is just the results of refs. [34–36] with κ corresponding to the electric force.

It is for our purposes necessary to make a more precise calculation in order to take into account finite size field corrections, but the basic tunneling result in eq. (3.6) will be the same. With the use of a κ-value determined as in section 2 ($\kappa \simeq 0.2\,(\mathrm{GeV}/c)^2$) we obtain a suppression of the heavier strange (s) and charm (c) quark pair production as compared to u- and d-quark pair production which may be estimated as

$$\mathrm{u:d:s:c} \simeq 1:1:\tfrac{1}{3}:10^{-11}. \tag{3.7}$$

This means in particular that charmed pair production essentially never occurs during a soft hadronization process.

With the mass in eq. (3.6) exchanged for the transverse mass it is also possible to show that one obtains a Gaussian suppression of transverse momentum [35, 36] and this has already been used in the discussion in section 2.

We will in section 3.2 consider a simple model for the production of massive $q\bar{q}$-pairs which we will later extend to the case of pairs with transverse momentum. After that we will show that the size of the wavefunction (ψ_C) in eq. (3.5) at the classical turingpoint is not necessarily the same for all hadrons. In particular we show by means of a simple model in section 3.3 that this effect will imply a suppression of the vector to pseudoscalar ratio below the expected spin-counting result 3:1. Finally in section 3.4 we consider a simple model for baryon–antibaryon production based upon diquark–antiquark production in the field. We note in passing that in a process in which one of the participating original particles is a baryon, there will evidently also be a baryon in the final state. This baryon fragmentation process is considered in section 5.

3.2. A simple model for the production of $q\bar{q}$-pairs in a constant force field

In order to investigate the space-time properties of the tunneling production process we will consider a simple dynamical model in which most of the mathematics can be done analytically.

We will describe the motion of a $q\bar{q}$-pair attached to the endpoints of a flat string in accordance with the space-time description in fig. 2.25. The Hamiltonian for a q-particle is given by

$$H = -\kappa x + \sqrt{p^2 + \mu^2} \tag{3.8}$$

and we obtain for the energy $E = 0$ the classical trajectory for the q-particle which is at rest at the time $t = 0$

$$p(t) = \kappa t, \qquad x(t) = \frac{1}{\kappa}\sqrt{(\kappa t)^2 + \mu^2}\,. \tag{3.9}$$

For the corresponding $\bar{q}$-particle we obtain the same result with $\kappa \to -\kappa$. The coordinate-space trajectories are then the branches of the hyperbola H_q in fig. 2.25.

The quantum mechanical wavefunction for the q-particle in momentum space with energy eigenvalue E is

$$\psi_q(p) = A \exp\left(i\frac{Ep}{\kappa}\right) \varphi_q(p) \tag{3.10}$$

$$\varphi_q(p) = \exp -\frac{i}{2\kappa}\left[p\sqrt{p^2+\mu^2} + \mu^2 \ln\left(\frac{p+\sqrt{p^2+\mu^2}}{\mu}\right)\right]. \tag{3.11}$$

To localize the particle in time we study a wavepacket by letting A depend on E. The motion in time is then given by

$$\psi_q(p, t) = \tilde{A}_q(p/\kappa - t)\, \varphi_q(p) \tag{3.12}$$

with $\tilde{A}$ the Fourier transform of A. The localization of the wavepacket is as usual the better the wider the energy packet is; in particular for a constant A the wavefunction is $\delta(p - \kappa t)$. We expect that the width of the wavepacket should be of the order m/κ so that the wavefunction of the produced $q\bar{q}$-pair should be localizable inside a final state meson with mass m. The wavefunction $\psi_{\bar{q}}(p, t)$ is obtained by changing $\kappa \to -\kappa$ in eq. (3.12). The wavefunctions $\psi_q(x, t)(\psi_{\bar{q}}(x, t))$ in coordinate space:

$$\psi_q(x, t) = \int \tilde{A}_q\left(\frac{p}{\kappa} - t\right) \mathrm{d}p \exp(ipx)\, \varphi_q(p) \tag{3.13}$$

can however not be expressed in terms of elementary functions.

As a model for the production matrix element $\mathcal{M}(\mu, S)$ of a pair with the vertex situated in the origin we take the overlap between the product wavefunctions $(\psi_q(x, t) \cdot \psi_{\bar{q}}(x, t))$ and a constant corresponding to the flat field integrated over the space-time region S where the field is nonvanishing:

$$\mathcal{M}(\mu, \mathrm{S}) = \int_{\mathrm{S}} \mathrm{d}x\, \mathrm{d}t\, \psi_{\mathrm{q}}(x, t)\, \psi_{\bar{\mathrm{q}}}(x, t) \cdot 1 \,. \tag{3.14}$$

It is then easily shown from eqs. (3.10)–(3.13) above that for the case when S corresponds to all of space-time

$$\mathcal{M}(\mu, \infty) = \exp - \left(\frac{\mu^2 \pi}{2\kappa}\right) \mu f\left(\frac{\mu^2}{2\kappa}\right) 2\pi \int \mathrm{d}z\, A_{\bar{\mathrm{q}}}(z)\, A_{\mathrm{q}}(z) \tag{3.15}$$

with μf a slowly varying function of its arguments

$$\mu f = \mathrm{Im} \int_{\mu}^{\infty} \mathrm{d}\lambda \exp\left(\mathrm{i} \frac{2}{\kappa} \int_{\mu}^{\lambda} \mathrm{d}\lambda' \sqrt{\lambda'^2 - \mu^2}\right). \tag{3.16}$$

With proper normalization of the wavefunctions this essentially coincides with the results of refs. [34–36].

It is also rather easy to convince oneself that, almost independently of the properties of the wavepackets A_{q} and $A_{\bar{\mathrm{q}}}$ the integral in eq. (3.14) obtains its principal contributions from the space-time region

$$|x| \lesssim \mu/\kappa \,, \qquad |t| \lesssim \mu/\kappa \tag{3.17}$$

and that the overlap-wavefunction $\psi_{\mathrm{q}} \psi_{\bar{\mathrm{q}}}$ is exponentially decreasing in all directions outside this region. We therefore expect the result of eq. (3.15) to be essentially unchanged for the production-matrix element $\mathcal{M}(\mu, \mathrm{S})$ as long as the space-time region S includes the region in eq. (3.17).

There are, however, physically interesting situations when the available field region is smaller than the region described in eq. (3.17). We note from the considerations of section 2 that in order to produce a very high-energetic meson (having z close to 1), the field will have to break very early. On the other hand, in order to produce a heavy mass pair $\mathrm{q\bar{q}}$ the field must be sufficiently long, i.e. we have to wait until the original pair $\mathrm{q_0\bar{q}_0}$ has come sufficiently far apart.

In fig. 3.2 we show a situation where this conflict is very obvious. In this case the heavy mass (μ)

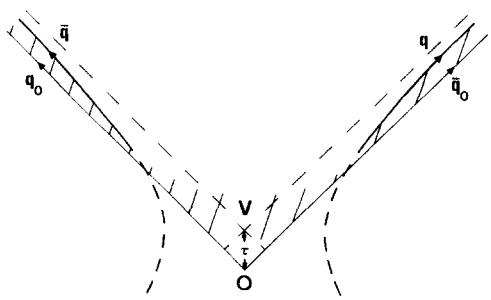

Fig. 3.2. The production of a heavy mass (μ) $\mathrm{q\bar{q}}$ pair in the force-field from the original $\mathrm{q_0\bar{q}_0}$ pair which starts out in the space-time point O. The invariant space-time distance τ from O to the production vertex V is smaller than μ/κ, and the $\mathrm{q\bar{q}}$ pair cannot classically be produced at rest inside the field.

$q\bar{q}$-pair cannot (classically) be produced at rest inside the field. In particular the proper time τ for the production vertex is too small as compared to the quantity μ/κ. The Lorentz frame has been chosen such that the difference vector OV (corresponding to the proper time τ) has no space-component. It is obvious that the pair cannot be produced at rest in any other frame.

The available space-time region S is then much smaller than the region in eq. (3.17), in particular the parameter

$$\varepsilon = \kappa\tau/\mu \tag{3.18}$$

will for the situation in fig. 3.2 fulfil $\varepsilon \ll 1$. We are then interested in the ratio $g(\mu, \varepsilon)$

$$g(\mu, \varepsilon) = \mathcal{M}(\mu, \tau)/\mathcal{M}(\mu, \infty) \tag{3.19}$$

with $\mathcal{M}(\mu, \mathrm{S}) \equiv \mathcal{M}(\mu, \tau)$.

It is rather easy to show for $g(\mu, \varepsilon)$ that it
1. is small for small ε
2. rapidly approaches 1 for $\varepsilon \gg 1$
3. is smoothly varying in between.

The precise behaviour is, however, not independent of the details of the model (the behaviour of A, i.e. the boundary conditions etc.). Fortunately, for the applications we have in mind the detailed properties of the ratio g are irrelevant. As a matter of fact, *we find that different functions g with the properties* 1–3 *give almost identical results when used for the production of* $q\bar{q}$*-pairs in quark and gluon jets.*

Actually, if we use a parametrization which incorporates the properties 1–3 above, either as a linear effect in ε^2 or as an exponential effect, i.e. we define vertex production factors $|g_1|^2$ and $|g_2|^2$:

$$|g_1|^2 = \frac{\varepsilon^2}{\varepsilon^2 + 1} = \frac{(\kappa\tau)^2}{(\kappa\tau)^2 + \mu^2} \equiv \frac{\Gamma}{\Gamma + \mu^2} \tag{3.20}$$

$$|g_2|^2 = \mathrm{erf}\left(\frac{\varepsilon}{2}\right) = \frac{2}{\sqrt{\pi}} \int_0^{\varepsilon/2} \exp(-x^2)\,\mathrm{d}x \tag{3.21}$$

then the results for the final state distributions will differ only on the percentage level (for details cf. ref. [36]).

This production vertex factor generally implies a suppression of the production of mesons with z close to 1. In particular for values of z inside the region $1 > z \gtrsim 1 - \langle \mu_\perp^2/m_\perp^2 \rangle$ ($m_\perp$ is here the transverse mass of the meson), the earlier constant probability (in z) from the simple Lund scheme is changed to an effective behaviour $\sim(1-z)$.

As an interesting consequence of this suppression for $z \sim 1$ we find that the single particle spectra for π- and K-particles for $z > 0.1$ turn out to be rather insensitive to the ratio of vectors to pseudoscalars produced in the jet. The size of this ratio is discussed below in section 3.3.

We note that the extension of the above-mentioned considerations to the production of transverse mass in the field is straight-forward. Our assumption of no excited transverse degrees of freedom for the force field implies that a $q\bar{q}$-pair is formed with total transverse momentum equal to zero, i.e. with

transverse components $\boldsymbol{k}_\perp$ and $-\boldsymbol{k}_\perp$, respectively. The production amplitude for such a pair in the field is given by eq. (3.15) with $\mu \to \mu_\perp$, i.e. the transverse mass $\mu_\perp = \sqrt{\mu^2 + k_\perp^2}$. (Although the classical trajectory for an endpoint of a string carrying transverse momentum with respect to the string direction is not a hyperbola (for a discussion cf. refs. [12, 36]), the hyperbola is the locus for the "effective" longitudinal coordinate describing the endpoint and a small adjoining piece of the string (the part which is "bent").)

We note that this result provides a justification for the method of generating transverse momentum in quark jets that was first suggested by Feynman and Field as an easily implemented phenomenological recipe. Then the quark-pairs are assumed to be produced with compensating transverse momentum $\boldsymbol{k}_\perp$ weighted by the distribution $\sim \mathrm{d}^2 k_\perp \exp(-\boldsymbol{k}_\perp^2/(0.35\ \mathrm{GeV}/c)^2)$. There are in that case further no correlations between the transverse and longitudinal dimensions.

In our situation there are such correlations, however, because of the vertex production factors $|g|^2$ discussed above. It is physically evident that for large values of z when the available field length is small and the parameter ε in eq. (3.18) is small, then the production of large transverse momenta will be suppressed in the same way as large masses. The effect is, however, difficult to disentangle experimentally, in particular when one also takes into account the transverse mass-dependence of the symmetric Lund model in section 2.6 and the soft gluon emission effects in section 4.

3.3. The production ratio of vector to pseudoscalar mesons

In phenomenological models for jet fragmentation the relative production of vector mesons and pseudoscalar mesons is usually determined by an adjustable parameter. This ratio is commonly set to about 1:1, which is very different from the ratio 3:1 which would be obtained if the spins of quarks and antiquarks, which combine to mesons, are randomly distributed. In this section we want to discuss the reason for this relative suppression of the vector mesons.

Up to now, when we have considered the tunneling mechanism we have been satisfied to normalize the wavefunction of the quark and antiquark to a fixed value at the classical turningpoint, where the tunneling particle comes on shell. Implicitly, this assumes that the probability that the particle will fit into the wavefunction of a final state hadron, is independent of the hadron. This is evidently only an approximate relationship and we will here show that the spin–spin interaction implies a different normalization of the quark or antiquark wavefunction at the classical boundary for final state singlet or triplet spin states, i.e. for pseudoscalar or vector mesons. This will imply that the sizes of the wavefunctions are different also in the classically forbidden tunneling region.

In order to exhibit these ideas in more detail we consider a very simplified model of the wavefunctions involved. We begin with the production of a quark–antiquark pair in the neighbourhood of the origin $x = 0$. We study first a nonrelativistic wavefunction ψ for a quark q_0 moving in the potential $V = -\kappa x$, which is given by a solution to the equation

$$H\psi = 0 \tag{3.22}$$

$$H = \frac{1}{2\mu} p^2 + \mu - \kappa x\,. \tag{3.23}$$

The wavefunction ψ will be exponentially damped to the left of the classical turningpoint $x_c = \mu/\kappa$ and will be oscillating to the right of this point, just as for the relativistic situation in section 3.2. A

corresponding wavefunction for an antiquark $\bar{q}_0$ (which is pulled in the opposite direction by the constant force) is given by $\psi_{\bar{q}}$

$$\psi_{\bar{q}}(x) = \psi(-x)\,. \tag{3.24}$$

A model for the production amplitude of the $q_0\bar{q}_0$-pair will contain the overlap of their wavefunctions $\psi_{\bar{q}}(x)\cdot\psi(x)$. As before this overlap essentially vanishes except for a small neighbourhood around $x = 0$.

In a confined theory neither the quark nor the antiquark will however move away towards large positive and negative values of x respectively. The quark in particular will end up in a meson state together with a corresponding antiquark $\bar{q}_1$ produced somewhere along the positive x-axis. Therefore the Hamiltonian for the quark q_0 in eq. (3.23) should actually be replaced by

$$H' = \frac{1}{2\mu}p^2 + \kappa|x-\xi| + \mu + \alpha\bar{S}_1\cdot\bar{S}_2\,\delta(x-\xi)\,. \tag{3.25}$$

Here $2(x-\xi)$ is the relative coordinate for q_0 and $\bar{q}_1$ and we have normalized the potential so that $V = 0$ when this relative coordinate equals zero.

We have introduced a local spin–spin interaction for the pair $q_0\bar{q}_1$ with a coefficient α. We note that H' in eq. (3.25) is functionally identical to H in eq. (3.23) for $x < \xi$ with the exception of an added constant $\kappa\xi$. This constant therefore plays the rôle of the energy of the state if we demand that the classical turningpoint is still at $x = x_c = \mu/\kappa$.

When $\alpha \neq 0$ there are two states fulfilling the differential equation:

$$H'\phi_i = E_i\phi_i \tag{3.26}$$

$$E_i = \kappa\xi_i \tag{3.27}$$

with the index i denoting either a triplet or a singlet spin state.

From the relationship between H and H' noted above we conclude that the wavefunctions ϕ_i are identical to ψ (apart from normalization) for $x < \xi_i$ while for $x > \xi_i$, ϕ_i is given by the mirror image:

$$\phi_i(x) = N_i\,\psi(x)\,, \qquad x < \xi_i \tag{3.28}$$

$$\phi_i(x) = \pm N_i\,\psi(2\xi_i - x)\,, \qquad x > \xi_i\,. \tag{3.29}$$

For the case with no spin–spin interaction ($\alpha = 0$) the energy and the value of ξ for the ground state are determined from the condition that the wavefunction ϕ_0 and its derivative must be continuous for $x = \xi_0$. Thus

$$\phi_0'(\xi_0) = \psi'(\xi_0) = 0\,. \tag{3.30}$$

For $\alpha \neq 0$ the derivative is not continuous but satisfies the condition

$$\lim_{\varepsilon\to 0}\frac{1}{2\mu}\left(\phi_i'(\xi_i+\varepsilon) - \phi_i'(\xi_i-\varepsilon)\right) = \alpha\boldsymbol{S}_1\boldsymbol{S}_2\,\phi_i(\xi_i) \tag{3.31}$$

or

$$-\frac{1}{\mu}\frac{\psi'(\xi_i)}{\psi(\xi_i)} = \alpha \boldsymbol{S}_1 \cdot \boldsymbol{S}_2 = \begin{cases} -\frac{3}{4}\alpha & \text{singlet} \\ \frac{1}{4}\alpha & \text{triplet} \end{cases}. \tag{3.32}$$

According to the discussion above, the production amplitude is related to $\phi(0) = N\psi(0)$ and thus proportional to the normalization constant N. To estimate N we note that the normalization integral obtains its main contribution from the classically allowed region

$$\mu/\kappa < x < 2\xi - \mu/\kappa \tag{3.33}$$

which implies

$$N^2\, 2\left(\xi - \frac{\mu}{\kappa}\right) = N^2 \cdot \underline{2\frac{E-\mu}{\kappa}} \sim \text{const}. \tag{3.34}$$

Thus the production probability, which is proportional to N^2 is $\simeq E^{-1}$.

This general result, that N^2 has a power-dependence on the energy, i.e. the mass of the final state hadron, and not e.g. an exponential dependence, is also borne out by a more quantitative analysis in our simple Hamiltonian system. In particular, for a Gaussian approximation of the wavefunction, as described in ref. [37], one obtains that

$$N_t^2/N_s^2 \simeq (E_s - \mu)/(E_t - \mu) \equiv \rho \qquad (\text{for } \rho \geq 0.2) \tag{3.35}$$

with the indices t and s for triplet and single spin states. For values of ρ below 0.2 the ratio N_t^2/N_s^2 will level off and always stay positive (for e.g. $\rho = 0$, $N_t^2/N_s^2 = 0.12$ in the Gaussian approximation).

We have begun our discussion with the nonrelativistic Schrödinger equation. However, also for a relativistic Hamiltonian like

$$H = \sqrt{p^2 + \mu^2} + \kappa|x| + \alpha\, \boldsymbol{S}_1 \cdot \boldsymbol{S}_2\, \delta(x) \tag{3.36}$$

the results are approximately the same, even if the operator $\sqrt{p^2+\mu^2}$ is not a local operator.

We conclude that under very general conditions the spin–spin interaction term will make the triplet wavefunction more spread out than the singlet one, as in fig. 3.3. We note in particular that with a *local* spin–spin interaction the wavefunction in the classically forbidden tunneling region will have (almost) the same shape for vector mesons and for pseudoscalar mesons. In a linear potential the width of the classically allowed region, where the wavefunction is large, is proportional to E. Therefore the normalization condition implies that the height of the wavefunction is roughly proportional to $E^{-1/2}$.

We now turn to the question how this normalization constant affects the tunneling probability. The magnitude of the wavefunction at the classical limit, as well as in the classically forbidden tunneling region, is proportional to N. Thus the probability for a quark to tunnel out into a meson is proportional to N^2. If the tunneling of the antiquark provides a similar factor, we expect a relative production factor N^4. However, in the basic fragmentation mechanism as described in section 2, the hadronization has an iterative structure with a series of incoherent steps. The initial excited state decays into one meson plus one less excited state, which in turn decays into one meson plus an excited state, etc. Each decay is

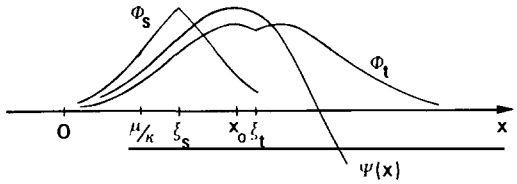

Fig. 3.3. The shape of the wavefunctions for a particle tunneling out into a final triplet or singlet spin state is for a local spin–spin interaction essentially the same outside the classically allowed region, while the size of the classically allowed region is larger for a triplet state than for a singlet state.

determined by the tunneling probability and the density of states for the produced excited system. In this picture we obviously obtain one factor N^2 for the quark (or antiquark) which goes into the meson. However the accompanying antiquark (or quark) will be part of a highly excited quark–antiquark system for which we do not expect the spin–spin interaction to be important. Thus if the hadronization can be treated in this way as a series of incoherent steps, where in each step one meson is produced, then we only get one factor of N^2, determining the relative production of a meson with spin 1 or 0.

Under these circumstances we expect that the production probability for vector mesons as compared to pseudoscalar mesons should be in accordance with eq. (3.35), i.e. smaller than the spin counting result 3.

Although the ratio in eq. (3.35) is difficult to evaluate quantitatively as it contains the quark masses, we expect for K* and K a smaller relative suppression than for ρ and π. In this case both the spin–spin interaction and the mass difference is smaller. For D* and D the suppression is even smaller.

Further the discussion is only related to the relative spin-directions of the quark and antiquark in the vector-meson. It is not dependent on the direction of the initial colour field (i.e. the jet direction). Thus the phenomenological result that $\rho : \pi \sim 1:1$ is not caused by a strong suppression of certain helicity states for the ρ-mesons, and we will not expect any sizeable polarization effects. This is consistent with the results of the DECO Collaboration [38] for electro production of ρ-mesons. Their result for the density matrix element ρ_{00} is $\rho_{00} = 0.41 \pm 0.08$. Admittedly the energy in this experiment is not very high and it would be interesting to see polarization measurements performed at higher energies as a test of our simple model.

3.4. Baryon–antibaryon production

One of the findings in e^+e^- annihilation is a surprisingly large yield of baryon–antibaryon pair production [40]. Similarly fast protons and antiprotons have been observed in inelastic muon scattering [39]. This implies the existence of a mechanism for production of several quark–antiquark pairs locally in phase-space and the combination of three quarks to a colour singlet baryon. A deeper knowledge of this process is of essential value for our understanding of the confining forces.

Several different production mechanisms have been suggested. The baryons may be produced in a stepwise manner, i.e. in e.g. an originally red–antired colour field, a blue–antiblue pair is firstly produced and afterwards a green–antigreen pair [35]. It is also possible that a diquark in a colour antitriplet state may be produced more or less as a unit together with a corresponding antidiquark [41, 42]. Further, one may imagine that baryons are usually produced at the end of the colour fields so that they contain the quark produced originally at the virtual photon vertex or that baryon production is associated with the production of heavy flavours like c- and b-quarks.

The experimental data from inclusive spectra indicate that baryons are produced evenly over the

whole allowed rapidity range. This seems to exclude the last two possibilities. The increase of the p/π ratio with the Feynman x_F-variable can be understood as kinematical effects due to the larger mass of the proton (cf. section 2). There is a recent, excellent review [43] of the baryon–antibaryon mechanisms presently in the market, and we will therefore subsequently discuss only the Lund model mechanism in detail, with due remarks on the pros and cons of the model when compared to present experimental data.

Only a small amount of experimental results on baryon–antibaryon correlations is available although the TASSO Collaboration at DESY has excluded the possibility that they are uncorrelated [40]. Further correlation studies will be essential in order to pinpoint the dynamical details.

Baryon production can also give valuable information about the topology of the colour field. As will be described in section 4 hard gluon emission in the string picture implies that the colour field is pulled along by the gluon. The transverse velocity of the field is transferred to the hadrons, and since the baryons are heavy they will also get a relatively large extra momentum due to this velocity.

To be able to draw conclusions about the dynamics from the experimental data it is necessary to take into account kinematical effects from resonance decays and from different particle masses.

It is also necessary to take into account the fact that a baryon is a *symmetric* state of three quarks (with regard to flavour and spin). This implies that it is *not* possible to produce quarks according to a classical probabilistic rule and let a combination of three quarks give a baryon with the same flavour. As an example, neglect SU(3)-breaking and assume that u-, d- and s-quarks are equally probable. Then if we take three quarks with parallel spins, the probability to get a uuu-system (Δ^{++}) will be $(\frac{1}{3})^3 = 1/27$. The probability to get a uds-system (Y^{*0}), disregarding the order of the quarks, will be $1 \cdot \frac{2}{3} \cdot \frac{1}{3} = 2/9$, i.e. much larger. If we project out on symmetric states we would instead (neglecting SU(6)-breaking effects) obtain equal probabilities for all states in the ground state 56-multiplet. Thus, neglect of the baryon symmetry would evidently give e.g. an overestimate of strange baryons.

We have developed a model in which diquark–antiquark pairs (colour $\bar{3}$–3) can be produced in a colour field in a way similar to the production of a quark–antiquark pair [41]. This has the advantage that it gives well-defined predictions with as few free parameters as possible. It is also an extreme model in the sense that it gives very strong correlations between baryons and antibaryons. If the quarks are e.g. produced in a stepwise manner [35] we may expect smaller correlations.

3.4.1. Description of the model

The diquark colour $\bar{3}$ is in our model treated as one unit and the suppression of baryon–antibaryon production, as compared to meson production, is determined by a larger diquark mass compared to the quark mass. We do not expect such a diquark, although equipped with certain quantum numbers like spin etc., to correspond to a pointlike object, e.g. to be a single elementary excitation of a local quantum field. For the small momentum transfers involved in the soft hadronization process we feel, however, that also an extended object may have an effective coupling to the (constant) chromo-electric field. Implicitly we expect that the density of virtual quarks along the field is high enough so that the probability to find a partner quark in a colour antitriplet diquark state is effectively one. Then the production probability for the diquark–antidiquark pairs can be treated by means of the tunneling formula obtained above, i.e. it is

$$\mathrm{d}^2 p_\perp \exp(-\pi \boldsymbol{p}_\perp^2/\kappa) \cdot \exp(-\pi \mu^2/\kappa)\,. \tag{3.37}$$

In that way we obtain the following predictions:

(i) A common Gaussian $p_\perp$ spectrum is obtained for all primary mesons and baryons. It should be remembered, however, that further $p_\perp$ contributions come from hard and soft gluons (cf. section 4) and that decays of resonances modify the spectra differently for baryons and mesons.

(ii) A baryon and an antibaryon will be neighbours in rank and thus close in rapidity.

(iii) Equation (3.37) implies that for $\mu > \sqrt{\kappa/\pi} \approx 250$ MeV a small increase in μ will give a large change in the probability. Thus strange diquarks will be much suppressed compared to nonstrange diquarks. Therefore, e.g. a Λ is more often produced together with a K and an $\bar{\mathrm{N}}$ than together with a $\bar{\Lambda}$. It also implies that production of Ξ and Ω is strongly suppressed.

Due to the large uncertainty in the determination of diquark masses eq. (3.37) cannot be directly used for predicting the absolute size of baryon–antibaryon production. We have, therefore, in the Lund model used expected diquark masses to fix the relative probability between the different diquarks but fitted the overall ratio between diquark–antidiquark and quark–antiquark production to the result of the low energy Spear Mark II-data [44]. From the 4 GeV-region we find for the overall diquark to quark ratio (summing over all spin and flavour states):

$$p(\mathrm{qq})/p(\mathrm{q}) = 0.065\,. \tag{3.38}$$

This corresponds to (nonstrange) diquark masses around 450 MeV which is clearly very reasonable, showing that the scheme is consistent. The errors in the determination of the ratio in eq. (3.38) are about 25% due to the systematic experimental uncertainties.

To fix the relative diquark probabilities we make the following assumptions about the masses:

$$\begin{aligned} &m(\mathrm{ud}_0) = 420\ \mathrm{MeV}\,, \qquad m(\mathrm{uu}_1) = m(\mathrm{ud}_1) = 490\ \mathrm{MeV}\,,\\ &m(\mathrm{us}_0) = 590\ \mathrm{MeV}\,, \qquad\qquad m(\mathrm{us}_1) = 640\ \mathrm{MeV}\,,\\ &\qquad\qquad\qquad\qquad\quad m(\mathrm{ss}_1) = 790\ \mathrm{MeV}\,. \end{aligned} \tag{3.39}$$

This gives the following probabilities

$$p((\mathrm{ud})_0) : p((\mathrm{ud})_1) : p(\mathrm{uu}) : p((\mathrm{us})_0) : p((\mathrm{us})_1) : p(\mathrm{ss}) = 1 : 0.35 : 0.35 : 0.06 : 0.02 : 0.007\,. \tag{3.40}$$

Note, however, that the spin-1 diquarks will get an extra factor of 3 from counting the different spin states.

As stated before, the numbers in eq. (3.40) are very uncertain. A ud_0-diquark (which has $S = I = 0$) is expected to have a smaller mass than a uu- or ud_1-diquark (both with $S = I = 1$). This difference, coming from chromomagnetic spin–spin interactions is related to the Λ–Σ mass difference, but to extract it the quotient of strange to nonstrange quark masses has to be known. The figures above represent the use of current algebra masses, whereas constituent masses would lead to a ud_1–ud_0 mass difference around 200 MeV. This corresponds to a spin 1 to spin 0 diquark suppression of 0.05 rather than 0.35. It is interesting to note the stability of this simple model even with respect to such large changes. In particular the spectra and total amounts of p, n and Λ are not sensitive to such variations of the mass parameters. The increase in direct Λ production is, e.g., compensated by a decrease in production via Σ^0 and Σ^*. Decuplet production is reduced, for Δ :s by a factor 2.5. Again this is less than what naively could be expected, but enough to make a determination from data meaningful in the future.

As mentioned above, a baryon is a *symmetric* system of three quarks. A basic property of the Lund jet model is the assumption that the production of a certain $q\bar{q}$-pair is determined by the density of available final states. When a diquark joins a quark to form a baryon, we therefore weight the different flavour and spin states by the probability that they form a symmetric 3-quark system. As for mesons we neglect the orbital angular momentum and consider only baryons in the ground state 56-multiplet.

In the same way as vector mesons are suppressed (cf. section 3.3) we expect a suppression of the decuplet relative to the octet states, in addition to the suppression implied by the diquark mass differences. However, once again the spectra of p, n and Λ are insensitive to such a change.

3.4.2. Properties of the model

A. Even production in rapidity

In this model baryons are obviously produced evenly in the whole available rapidity range, and we note that this reproduces both the increase in the production rate between 4 and 30 GeV in e^+e^--annihilation data and the x_F-spectra observed in e^+e^- annihilation and in μp-scattering (cf. figs. 2.15, 3.4). The proton data from TASSO at 34 GeV are fitted with a diquark ratio: $P(qq)/P(q) = 0.085$ [43] which is within the region allowed by the errors in the SPEAR data at 4 GeV. The p/π ratio increases with x_F as a result of the larger proton mass. Even if this increase is somewhat less than in the experimental data, this does not allow for an important production of protons at the end of the jet (cf. ref. [43]).

There are, however, indications that the model somewhat underestimates the Λ production relative to the proton production [43]. As mentioned above this Λ/p ratio is rather stable against changes of the

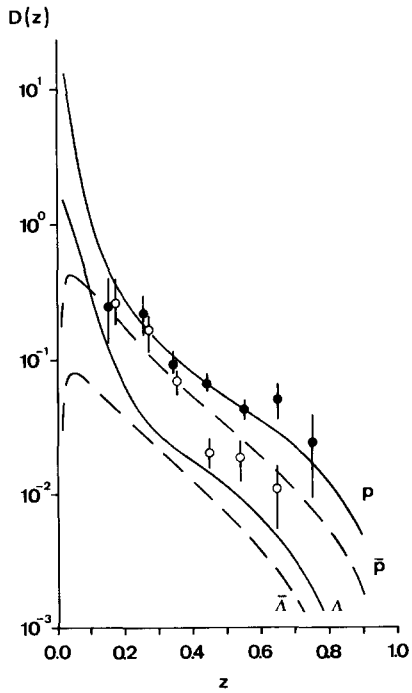

Fig. 3.4. Production of p, $\bar{p}$, Λ and $\bar{\Lambda}$ versus $z = E_h/\nu$. The data points are results for p (●) and $\bar{p}$ (○) at 120 and 280 GeV from the EMC Collaboration [39]. The agreement with data is somewhat improved (in particular at small z) if the experimental momentum range for proton identification is taken into account.

parameters, e.g. the decuplet suppression relative to the octet. This might indicate that the suppression of strange diquarks is overestimated by the tunneling formula (3.37) which assumes that the diquark tunnels out as one unit. This can only be checked by studies of whether a Λ is usually produced together with $K\bar{N}$ rather than with $\bar{\Lambda}$ and of the production of Ξ-particles. (We here repeat the warning that neglect of the symmetry properties of the baryon state could give erroneous estimates of the strange baryon production.)

B. Baryon production in gluon jets

We note that if this baryon production model is combined with our model for gluon fragmentation, described in section 4, where a gluon acts as a kink on a stringlike colour field, then we obtain a somewhat higher fraction of baryons and antibaryons in a gluon jet than in a quark jet (cf. section 4.2). Also the transverse velocity of the colour field between the gluon and the quark will give a larger extra transverse momentum to baryons because of their large masses. Thus while in 2-jet events at 30 GeV in e^+e^- annihilation the baryons will have a $\langle p_\perp^2 \rangle$ with respect to the sphericity axis of 0.23 $(\mathrm{GeV}/c)^2$ (corresponding to 0.15 $(\mathrm{GeV}/c)^2$ for pions) in 3-jet events it is changed to 0.35 $(\mathrm{GeV}/c)^2$ (compared to 0.21). The 3-jet event asymmetry discussion in section 4.3 is also much larger when studied for baryon production. In section 4.5 we consider the effects of soft gluon emission which give extra $p_\perp$-contributions and discuss how baryon–antibaryon pairs can be used to investigate these effects.

C. Correlations

Because a baryon and an antibaryon in this model always share a diquark–antidiquark pair, we obtain very strong correlations both in transverse momentum and rapidity. (Note however that these correlations are somewhat distorted by resonance decays.) With respect to $p_\perp$-correlations we obtain for an observed $p\bar{p}$-pair for the two cases when only 2-jets and when also 3-jet events are taken into account:

$$\frac{\langle \boldsymbol{p}_{\perp p} \cdot \boldsymbol{p}_{\perp \bar{p}} \rangle}{\langle \bar{p}_\perp^2 \rangle} = \begin{cases} -0.30 \pm 0.08 & \text{(2-jets only)} \\ -0.14 \pm 0.92 & \text{(including 3-jets)}. \end{cases} \tag{3.41}$$

The results for rapidity correlations are discussed in section 2.6.3 (cf. fig. 2.21a).

D. Polarization properties

As we will discuss in section 5.6 we expect strong polarization properties in the fragmentation of stringlike colour fields. A Λ-particle is in our model usually produced from an s-quark and a (ud_0)-diquark, and the spin of the Λ is given by the spin of the s-quark. The polarization of the s-quark depends on the direction of the colour field, i.e. which is the quark end and which is the antiquark end. In a leptoproduction event with sufficiently large x_B we know that there is a (valence) quark at the current end of the field. Thus, according to the arguments in section 5.6 we expect Λ-particles to be polarized along $\bar{Q} \times \bar{P}_\Lambda$ (with $\bar{Q}$ the current direction).

Due to the suppression of strange diquarks a $\Lambda(\bar{\Lambda})$ is in our model mostly produced together with a $K\bar{N}(\bar{K}N)$ state. However, when a $\Lambda\bar{\Lambda}$ pair is found it usually shares the same ud_0–$\overline{ud_0}$ pair. Because these diquarks are spinless we expect no correlation between the polarization of the Λ and the $\bar{\Lambda}$. However if the Λ and $\bar{\Lambda}$ share the s- and $\bar{s}$-quark from the same $s\bar{s}$-pair, then one expects a positive correlation i.e.

$$\boldsymbol{p}_\Lambda \cdot \boldsymbol{p}_{\bar{\Lambda}} > 0\,. \tag{3.42}$$

This might be expected if the diquarks are not produced as entities but in a stepwise manner as in ref. [35].

4. Gluon fragmentation

This section deals with various hadronization effects related to gluons. In the first subsection we discuss, in general terms, some models for the fragmentation of jet systems including gluons. The confinement of colour force flux lines leads to essentially two possible structures of the force field in a quark–antiquark–gluon jet system, which both can be described within the string model. In section 4.2 one of these cases, the possibility to have a localized excitation ("kink") on the massless relativistic string, is used to construct the Lund model for a gluon in the string picture. The dynamics of such a string system and its subsequent fragmentation into hadrons are discussed. The general three-jet event structure arising in different models is discussed in section 4.3, where in particular an interesting asymmetry in the particle distribution is compared with data from the JADE group at PETRA.

Details of how a jet system including a gluon can arise due to perturbative QCD are given in section 4.4, and the problem with divergences in matrix elements is discussed as well as their treatment using cuts in a Monte Carlo program. In section 4.5 effects due to the emission of soft and collinear gluons are derived and the resulting physical observables are indicated. A comparison of the predictions of the model with experimental findings in both e^+e^- annihilation and deep inelastic lepton–nucleon scattering is made in section 4.6. Some characteristic features of perturbative QCD at the parton level are seen to be well observable also at the hadron level (e.g. planar three-jet structure) but others (like angular energy flow asymmetry in leptoproduction) are shown to be washed out in the hadronization process. The recent debate about the influence of the hadronization scheme on the determination of α_s in e^+e^- annihilation is also discussed in that subsection. Finally, in section 4.7, the decays of heavy onium states into gluons and the resulting string structure are briefly mentioned.

4.1. Models for gluon jets

Since free colour charges do not seem to appear in nature, a gluon is always part of an overall colour neutral system, and a high energy gluon should produce a jet of hadrons just like a quark does. The problem of gluon fragmentation then contains two basic questions:

A. How is the confining colour field stretched between the gluon and the other colour charges in a colour neutral system?

This question is mainly important for low energy particles. For fast hadrons in a high energy gluon jet, the other quarks and gluons can be treated as if emerging in the direction opposite to the gluon. Thus the second question is:

B. What are the longitudinal and transverse distributions and the flavours of the fast hadrons in a high energy gluon jet?

The simplest colour neutral system including a gluon is a quark–antiquark–gluon state in an e^+e^- annihilation event, and we choose this system to begin with as an illustration. A basic assumption is then that there are two space-time scales involved. On the short scale, characterized by the QCD parameter $1/\Lambda \simeq 0.4$ fm, the coloured objects behave as essentially free particles and perturbative QCD is applicable. In particular the quark (or the antiquark) can radiate hard gluon bremsstrahlung at a rate determined by the strong coupling constant α_s. The longer scale starts when the partons have begun to move apart and feel the confining colour forces. The energy is now transformed into hadrons and in this phase perturbative QCD is no longer useful.

When one studies properties which are less sensitive to low energy particles (e.g. inclusive x_F and p_t spectra, thrust distributions etc.) it may be possible to neglect the first question, about the colour-field

structure in the system, and treat the three jets as independent jets emerging from the origin in the CM frame. This is the usual extension of the Field–Feynman model [7] for the fragmentation of a quark-jet to a system of jets. Models of this kind do not always conserve energy, momentum and flavour exactly but rather as properties on the mean. Neither are they manifestly Lorentz invariant, since a specific point in a certain Lorentz frame is chosen to join the jets. At high enough energies one would, however, expect the errors to be small when the interest lies mainly on the fast particles so that the joining in the center is less important. This is essentially the line followed in the Hoyer et al. [45] and Ali et al. [46] Monte Carlo programs, but with the addition of special routines that ensure energy, momentum and flavour conservation by suitable adjustments of the jets "post facto".

For studies of quantities constructed to be as independent of hadronization as possible (e.g. angular energy flow and thrust) it may also be possible to neglect the second question and treat the gluon as a quark jet, giving a random flavour to the leading quark (and possibly also using a softer fragmentation function) as is done by Hoyer et al. [45]. However, we will see below (sections 4.3 and 4.6) that such measures are often more sensitive to the hadronization than originally expected.

These approximations may be sufficient when investigating effects of perturbative QCD, e.g. hard gluon bremsstrahlung. However, to gain understanding of the confinement mechanism we have to answer the two basic questions above.

The general property that colour force-fields do not spread out in space but are confined to thin flux tubes allows essentially only two ways to connect the three colour charges ($q\bar{q}g$) by colour fields. The simplest possibility (case I), is to connect the gluon directly with the quark and the antiquark as in fig. 4.1. These flux tubes then contain colour triplet fields of the same kind as between a quark and an antiquark in an ordinary 2-jet event as discussed in the previous sections. This is also the assumption in the Lund model [108].

A second possibility (case II), discussed by Montvay [47], is that each parton stretches a colour flux tube, which is connected to the other two in a junction as shown in fig. 4.2. The colour field between the gluon and the junction is here of a different nature, with colour octets at each end. (The third possibility that one of these cases is complemented with a flux tube also directly between the quark and the antiquark seems very artificial.)

Due to causality and relativity the potential energy from a confined field cannot depend only on the distance between a quark and an antiquark. Fig. 4.3a shows a quark and an antiquark connected by a confined colour field. If the quark gets a kick it will move and pull the field along with it. The antiquark, however, cannot notice anything until it is reached by a signal travelling with the velocity of light. Thus we expect the field to move as in fig. 4.3b–d. A bend moves, with the velocity of light, along the field

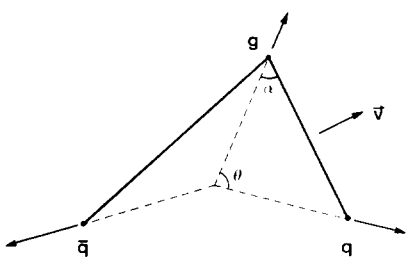

Fig. 4.1. The simplest possibility to connect the three colour charges in a $q\bar{q}g$ jet system is with an ordinary colour triplet field (with string tension κ) stretched via the colour octet gluon. The velocity of a string piece is $v = \cos\theta/2$.

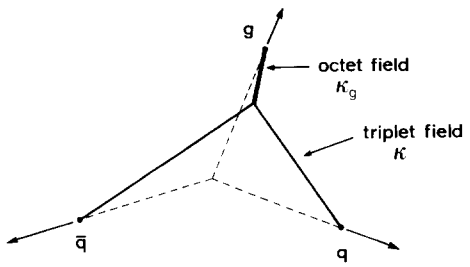

Fig. 4.2. The gluon stretches an octet field (with string tension κ_g) which joins the two triplet fields (tension κ) in a junction.

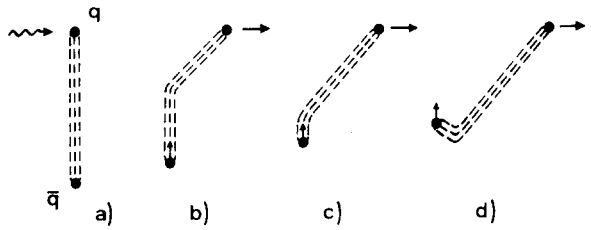

Fig. 4.3. The motion of the colour field when the quark gets a kick illustrates that the antiquark cannot notice anything until it is reached by the disturbance of the field which moves with the velocity of light.

towards the antiquark. When the quark is retarded its lost transverse momentum must be carried by the field.

We note that when an electric field is boosted transversely one also gets a magnetic field and a momentum density in accordance with the Lorentz transformation of energy-momentum. If the transverse dimensions of the field can be neglected, a very strong electric field in a very thin tube behaves as the massless relativistic string discussed extensively by Artru in [12].

In this string approximation, where the transverse dimensions of the field are neglected, we note that for the first colour-field configuration (case I shown in fig. 4.1) the gluon acts as a kink on a string stretched between the quark and the antiquark. In the second case (fig. 4.2) there is a colour octet string with a different tension, κ_g, between the gluon and the junction. The position of the junction depends on the relative sizes of the tensions in the colour octet and colour triplet strings. We note that for $\kappa_g \geq 2\kappa$ (where κ is the tension in the colour triplet string) it will cost too much energy to stretch the colour octet string and it will collapse to zero length and case II will go over into case I. As we will discuss further below, experiments seem to favour either case I (fig. 4.1) or case II (fig. 4.2) with a rather large value of κ_g such that the octet field becomes short.

Turning now to question B above (concerning the fragmentation properties of a gluon jet), we first note that the gluon fragmentation function is, at present, not at all well determined experimentally. Further experimental studies are important to distinguish between different models.

With the Lund model recipe for the question about the colour-field topology (question A) we also get directly an answer to question B. If the gluon acts like a kink, or a transverse excitation on the colour field between the quark and the antiquark, we can use the method for breaking this field as developed in previous sections. This will be further discussed in the next subsection. We note that treating the gluon as a kink on a string is easily generalized to situations where more than one gluon has been emitted. The string will then be stretched from the quark (colour triplet) via each gluon (colour octet) in turn and finally end up on the antiquark (colour antitriplet). The field will be a simple colour triplet field all the way and after the formation of the leading hadron at each hard gluon kink has been considered, what remains is a number of simple string pieces that fragment in the usual way. We also note that this scheme is infrared stable in the following sense. Many soft gluons will correspond to many small bends on the string. The string can, however, break into pieces in much the same way even if it is not completely straight and one obtains a smooth transition between hard and soft gluon emission. We will discuss this point further in section 4.5.

In the Monte Carlo program by Ali et al. [46] it is assumed that the gluon splits into a quark and an antiquark which share the total gluon energy according to the Altarelli–Parisi splitting function for $g \to q\bar{q}$. This quark and antiquark could then (although this is not done in [46]) naturally be connected to the original antiquark and quark respectively to form two colour singlet systems, giving a field structure

as in case I. However, such a scheme for gluon fragmentation is not automatically infrared stable in the sense discussed above; some cuts have to be introduced to prevent small invariant masses for the two $q\bar{q}$ systems.

If the colour field topology is as in the second case with a colour octet field at the gluon, we have to study how this field fragments. The octet field cannot break simply by the production of $q\bar{q}$-pairs. Instead it could break by gluon pair production. Thus we could expect the production of glueballs and SU(3) singlets, as suggested by Peterson and Walsh [48], which would give more η'-, ω- and ϕ-particles.

4.2. The Lund gluon model

In the Lund model a gluon is treated as a kink, or a transverse excitation, on a stringlike colour force field between a quark and an antiquark. This is in a sense an extreme model because it contains no new elements or parameters. Quark–antiquark pairs are produced in exactly the same way as discussed in section 2. The only complication is the corner of the string at the gluon, which is handled by letting the string break at both sides of the kink in the usual way, but with the constraint that the hadron thus formed (and which also contains the gluon-kink) has the correct physical mass. Thus, an important assumption of the model is that it does not matter whether the string piece is straight or has a bend when projecting it onto a physical hadron state.

As discussed by Artru [12] a one-dimensional linear force-field can be generalized, in a relativistically invariant way, to three dimensions by the dynamics of the massless relativistic string. On such a string it is possible for a pointlike part (away from the endpoints) to carry energy and momentum. Such a localized excitation, a kink, moves with the velocity of light and is pulled back by the string by a force which is twice as strong as the one acting on an endpoint quark. The kink thus acts much like a gluon, since in QCD with N colours it has been suggested that the ratio between the forces on a gluon and a quark is $2/(1-1/N^2)$, i.e. 9/4 for three colours and 2 for infinitely many colours. The dynamical mechanism for creating such a kink on the string can e.g. be hard gluon emission in perturbative QCD to be discussed below, but we will in this subsection concentrate on the motion and subsequent decay of such a string system once it is formed.

We will start by considering an originally straight string segment L with a $q\bar{q}$-pair (q_0 and $\bar{q}_0$) at the endpoints in the previously described yo-yo mode. At the initial time a large momentum $\boldsymbol{Q}$ is suddenly transferred to the point C on the string, fig. 4.4a. In the subsequent motion, fig. 4.4b, two straight string segments L_1 and L_2, which connect C to the original string L at the corners D and E, will start to move outwards. The points C, D and E all travel at the velocity of light. Energy and momentum is all the time flowing away from C and the energy-momentum lost by C is stored in the string segments L_1 and L_2. The gluon-kink loses its energy equally rapidly to both string segments attached to it, independently of their angle α (see fig. 4.1) to the gluon momentum, as can be realized in the following way. The string piece actually drawn out by the gluon per unit time is proportional to $\cos\alpha$, but this piece also moves with a transverse velocity $\beta = \sin\alpha$ and thus has an energy density per unit length which is a factor $1/\cos\alpha$ higher than for a string at rest. The net effect is that the gluon loses the same amount of energy to each string segment and in total twice the amount lost by a quark stretching a single string. The retarding force acting on the kink C is therefore opposite to $\boldsymbol{Q}$ and equals 2κ, where κ is the tension in a colour triplet string as discussed before (numerically $\kappa \simeq 1$ GeV/fm $\simeq 0.2$ GeV^2). We note, as shown in [12, 108] that also for a (massless) quark stretching a string at some angle α, the retarding force equals κ and is directed opposite to the quark motion independently of α.

After some time the string field will obviously break along the two segments L_1 and L_2, see fig. 4.4b.

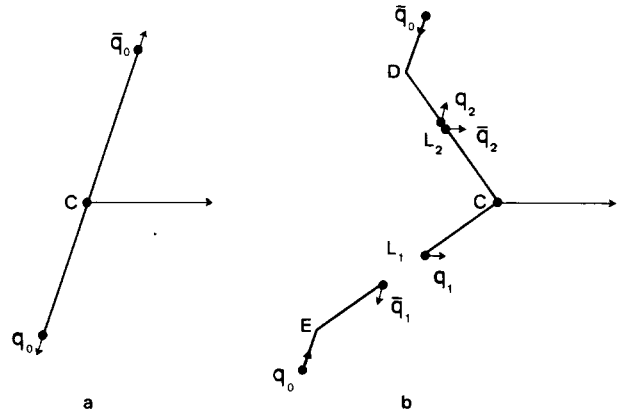

Fig. 4.4. (a) The initial state when a large momentum Q is transferred to a point C along the string in a yo-yo mode. (b) The momentum-carrying kink-singularity C moves away along Q and $q\bar{q}$ pairs are produced along the string segments L_1 and L_2.

The reason is that the systems $\bar{q}_1 q_0$ and $q_2 \bar{q}_0$ will contain sufficiently much energy and momentum to form meson states. The remainder of the "kink-jet" will in the lab frame move as a rigid body. At some later time the string will break again producing a new hadron and so on.

To study the particles in the gluon-kink fragmentation region, that is the mesons with large energies in the lab frame, it is convenient to transform to a Lorentz frame moving very fast along Q with respect to the lab frame so that these mesons are slow in this frame. In this new coordinate system the whole gluon jet will look like a thin "hair pin" jet, i.e. the string segments L_1 and L_2 will have a very small relative angle. Actually the whole original string piece L will be seen moving away with large velocity. The motion in space-time has some similarities to the motion of a soft q-particle as discussed in connection with fig. 2.7. The difference is that there are two adjoining fields, i.e. the kink is spanning a "folded" space-time sheet with two surfaces adjoining along the space-time orbit of the kink as illustrated in fig. 4.5. In the points A_1 and A_2 $q\bar{q}$-pairs are formed in the two field sheets and the $\bar{q}_1$-particle is accelerated along the field in L_1 while the q_2-particle is accelerated in the field in L_2. As mentioned above, we make the important assumption that the remaining pair $q_1\bar{q}_2$ can form a bound state together with the kink C if the total energy-momentum of the system corresponds to a bound state meson.

Defining the variables z_1 and z_2 from

$$z_i = l_i/2L\,, \qquad 0 < z_i < \tfrac{1}{2}\,, \qquad i = 1, 2 \tag{4.1}$$

where l_i and L are the distances as indicated in fig. 4.5, we find that the light cone variable $z = (E+p)/(E+p)_{\text{tot}}$ for the meson $q_1\bar{q}_2C$ is given by $z = z_1 + z_2$. The masses M_1 and M_2 of the remainder systems $q_0\bar{q}_1$ and $\bar{q}_0 q_2$ are given by

$$M_i^2 \propto (\tfrac{1}{2} - z_i) W^2\,. \tag{4.2}$$

(The proportionality constant is determined by the original position of the kink on the string.)

The leading meson $q_1\bar{q}_2C$ is a folded string in one dimension whose state of motion depends on the positions of the points A_1 and A_2. The only restriction for these points is the condition that the meson

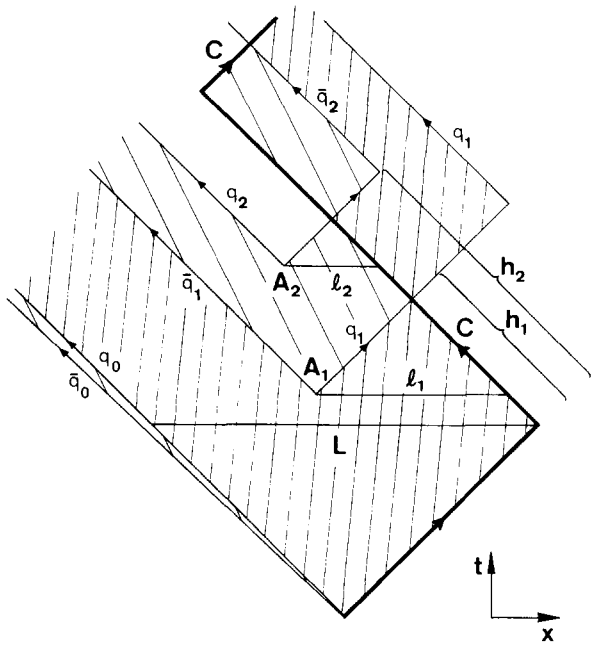

Fig. 4.5. The space-time motion of a kink C and the two adjoining string-fields ending in q_0 and $\bar{q}_0$.

has mass m which implies

$$\kappa^2(l_1 + l_2)(h_1 + h_2) = m^2\sqrt{2} \tag{4.3}$$

where h_1 and h_2 are the distances as shown in fig. 4.5. Different points A_1 and A_2, which satisfy this condition give different relative momenta for the q_1, $\bar{q}_2$ and the kink C in the string. Since we have assumed that all these states have the same projection on a physical meson state we conclude that the relative probability for different z_i-values is determined by the density of states in the remaining systems, i.e. in accordance with the "simple Lund" prescription (see section 2.4) we obtain:

$$\mathrm{d}P \propto \mathrm{d}n_1\,\mathrm{d}n_2 \propto \mathrm{d}M_1^2\,\mathrm{d}M_2^2 \propto \mathrm{d}z_1\,\mathrm{d}z_2\,. \tag{4.4}$$

Thus normalization gives

$$\mathrm{d}P/\mathrm{d}z_1\,\mathrm{d}z_2 = 4\,, \qquad 0 < z_i < \tfrac{1}{2}\,. \tag{4.5}$$

The total number density of mesons with a fraction z of the gluon-jet energy is then given by

$$\frac{\mathrm{d}n}{\mathrm{d}z} \equiv D_{\mathrm{gluon}}(z) = \int_0^{1/2} \mathrm{d}z_1 \int_0^{1/2} \mathrm{d}z_2 \frac{\mathrm{d}P}{\mathrm{d}z_1\,\mathrm{d}z_2} \left\{ \frac{\theta(\frac{1}{2} - z_1 - z)}{\frac{1}{2} - z_1} D\left(\frac{z}{\frac{1}{2} - z_1}\right) + \frac{\theta(\frac{1}{2} - z_2 - z)}{\frac{1}{2} - z_2} D\left(\frac{z}{\frac{1}{2} - z_2}\right) + \delta(z - z_1 - z_2) \right\} \tag{4.6}$$

where $D(z) = 1/z$ is the fragmentation function for a quark jet. The first two terms in eq. (4.6)

correspond to the two "ordinary" quark jets along L_1 and L_2 while the third contribution corresponds to the state $q_1\bar{q}_2C$.

The integrals are trivial and one obtains

$$z\,D_{\text{gluon}}(z) = \begin{cases} 2+4z+4z^2 & z \le 1/2 \\ 4z(1-z) & z \ge 1/2\,. \end{cases} \tag{4.7}$$

We note that although D_{gluon} is twice as large as D_{quark} $(=1/z)$ for $z \to 0$ and has an extra power of $(1-z)$ for $z \to 1$ it is *not* just $2(1-z)\,D_{\text{quark}}$. In case there are several different flavours of the $q\bar{q}$-particles and several different mesons produced in the jet, we must supplement the relative

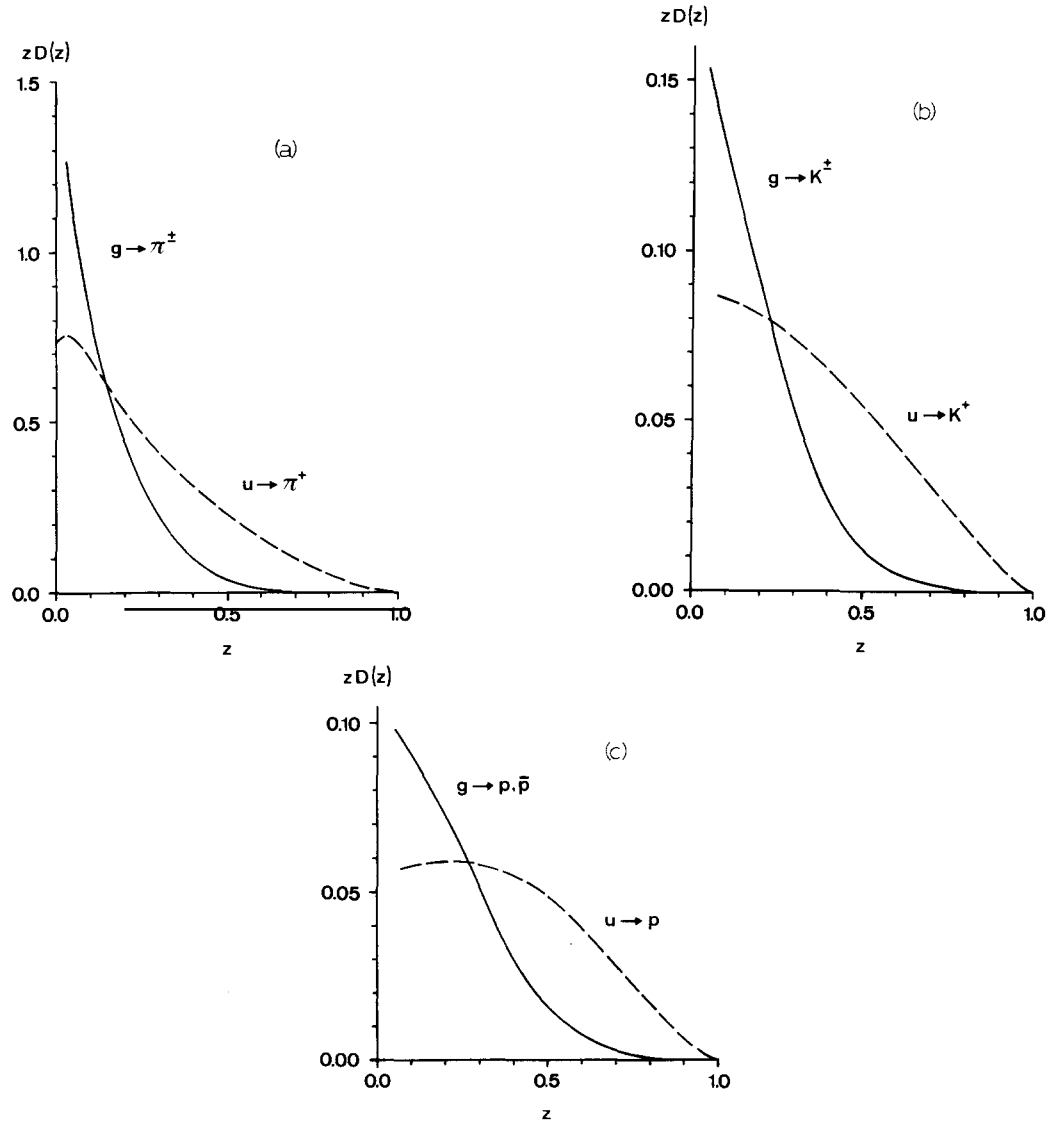

Fig. 4.6. The gluon fragmentation functions $D_g(z)$ (full lines) into pions (a), kaons (b) and protons (c) compared with the corresponding u-quark fragmentation functions (dashed lines). The "standard Lund" model has been used.

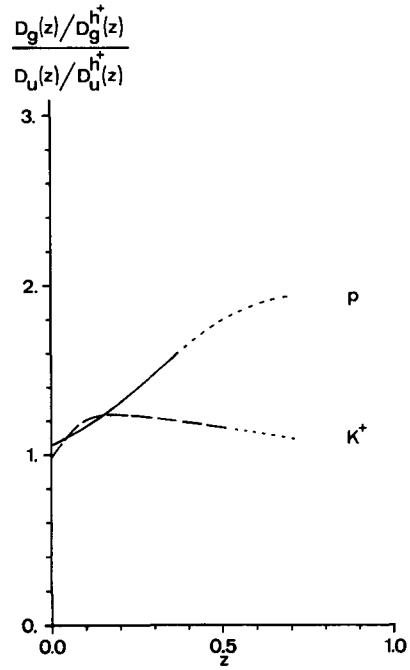

Fig. 4.7. The z dependence for ratio of the fractions of protons and K^+ in a gluon jet to a u-quark jet.

probabilities in the same way as was done for quark jets. In a similar way as for quark jets, when going from "simple Lund" to "standard Lund" (section 2.6), there are also corrections to the gluon fragmentation function eq. (4.7) due to effects from soft gluon emission (section 4.5.1) and finite field lengths (similarly as in section 3.2). For details of this last point and also more detailed formulae for the gluon fragmentation, in particular for more general string configurations, we refer to [13].

For all studies in this section we have used the "standard Lund" model, i.e. the newly developed left–right symmetric fragmentation (discussed in section 2.6) has not been used.

As an example of the resulting distributions we show in figs. 4.6a and 4.6b the π- and K-spectra. For comparison we have also indicated the quark fragmentation functions as obtained in section 2.6.

As described in section 3.4 baryon–antibaryon pairs can be produced via diquark–antidiquark pair production in the breakup of the colour force-field. This leads to the gluon fragmentation function into protons as given in fig. 4.6c. We note, see fig. 4.7, that the fraction of baryons increases more with z in a gluon jet than in a quark jet. This reflects the simple fact that when producing a first rank particle in a quark jet only one breakup of the field takes place and there is consequently only one chance to produce a diquark pair. For a higher rank particle in a quark jet and also the first rank particle in a gluon jet, two breakups occur and there are two chances to produce a diquark pair since that probability is the same in each breakup. Therefore, a leading particle in a gluon jet (including the kink and quarks/diquarks from two breakups) has roughly twice the probability to be a baryon or antibaryon as compared to the leading particle in a quark jet.

4.3. Event structure for 3-jet events

The simplest system with a gluon is a $q\bar{q}g$ state in e^+e^- annihilation. In the Lund model this is represented by a string with a kink, which is stretched and breaks into pieces as illustrated in fig. 4.8.

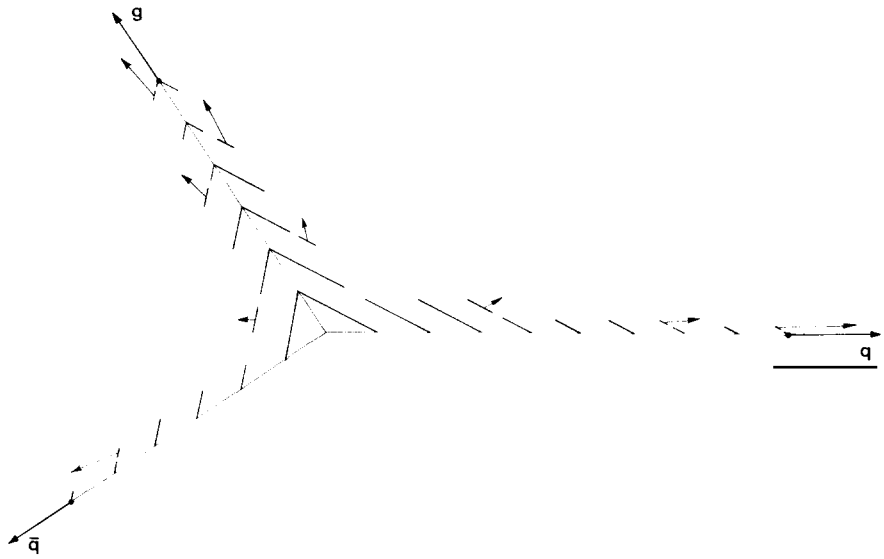

Fig. 4.8. The space-time development of a quark–antiquark–gluon event. The quark and antiquark move along the directions marked q and $\bar{q}$ and are at the endpoints of a string field. The gluon is a pointlike energy-momentum carrying piece of the string moving along the direction g, thereby causing a triangular shape of the outmoving string-field. The field breaks by the production of $q\bar{q}$ pairs and the directions of the final state mesons are marked by arrows when they become independent entities. (Note that the slowest mesons in the cms are the first ones to emerge, and also take the largest pieces of the string.)

The relativistic invariance of the model implies that we avoid the selection of a fixed point in a particular Lorentz frame (e.g. the origin in the CM frame) to connect the jets. A very essential feature is that the force field is stretched from the quark to the antiquark *via* the gluon. The kink on the string is handled by letting the string break at both sides of the kink in the usual way, but with the constraint that the hadron thus formed has its correct physical mass. Then two separate pieces of string remain which are each one a one-dimensional quark–antiquark system, moving with a velocity $v = \cos(\theta/2)$ transverse to their longitudinal direction (see fig. 4.1). These systems can then fragment in their own rest systems in exactly the way described in section 2, and then be boosted back to the overall CM frame of the original $q\bar{q}g$ system. The hadrons produced in each such subsystem appear as back-to-back jets in the CM frame of the subsystem, but when boosted back to the overall CM frame they will be distributed along two hyperbolae in momentum space as illustrated in fig. 4.9. The typical distance from the hyperbolae to the origin is around 300 MeV for primary particles, i.e. of the same order of

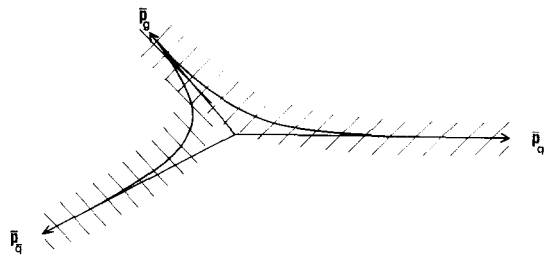

Fig. 4.9. The momentum space distribution of the final state particles which appear in the mean along two hyperbolae. The size of the strokes indicates the size of the transverse momentum fluctuations in a string field without excited transverse degrees of freedom.

magnitude as the typical fragmentation p_t in a jet. It has been pointed out in [49] that this leads to characteristic correlations between multiplicity and angular distribution, namely fewer particles in the angular region opposite to the gluon jet. An asymmetry of this type has been observed by the JADE Collaboration at PETRA in the following way.

In a selected sample of events showing a 3-jet planar structure they studied [50] the angular distribution of particles in the three different regions between the three reconstructed jet axes, which are ordered in decreasing jet energy. The result, see fig. 4.10, shows that there are more particles in the angular region between the softest jet (according to perturbative QCD usually the gluon jet) and the two harder jets and fewer particles between the two harder jets (usually the q- and $\bar{q}$-jet). These results are in good agreement with our model having a string stretched via the gluon; the absence of a string in the angular region between the quark and the antiquark explains why there are fewer particles in that region. The effect is partly of a kinematical origin since the angular regions are different, but a model where the three jets fragment independently of each other and are joined at the origin in the CM frame (dashed lines in fig. 4.10) cannot reproduce this experimental fact equally well. The fragmentation parameters for quark- and gluon-jets were here separately chosen to give the best possible agreement with the data for the particle flow within the jets ($g \neq q$ model, with a softer fragmentation function and a higher $\langle p_\perp \rangle$ for the gluon jet), but the result is essentially the same if the gluon jet is just assumed to fragment like an ordinary quark jet ($g = q$ model). Note that the effect inherent in the Lund model is very much larger than the one visible in the figure, but since the gluon jet is misidentified in a large fraction of the events, only a remnant of the "true" effect survives.

Since, in the string model, these phenomena are associated with the boost from the subsystem of each string piece to the overall CM frame, they should be more pronounced for particles with larger mass or larger momentum out of the event plane, i.e. transverse to the boost direction. We thus expect a larger effect from particles with high p_{out}, as well as for kaons (and even more for protons). This seems validated by the data in fig. 4.11 and in table 4.1, which shows the ratio of the number of particles in a central angular range between jet no. 1 and no. 3 to the number between jet no. 1 and no. 2. Also note that the effect is even larger in energy flow than in particle number flow.

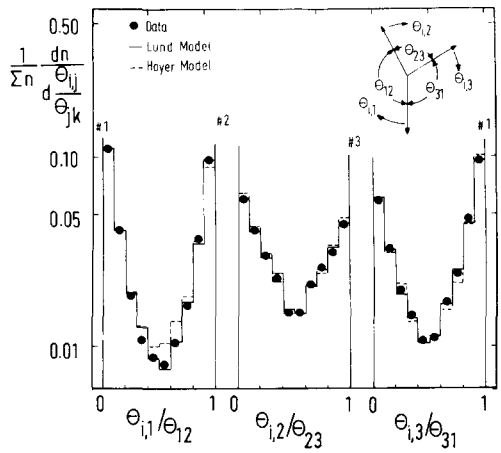

Fig. 4.10. The average number of particles between the indicated jet-axes versus the normalized angle projected onto the event plane. Jets are ordered so that #1 is most energetic and #3 least energetic, see insert. The data from the JADE Collaboration [50] are shown together with model results.

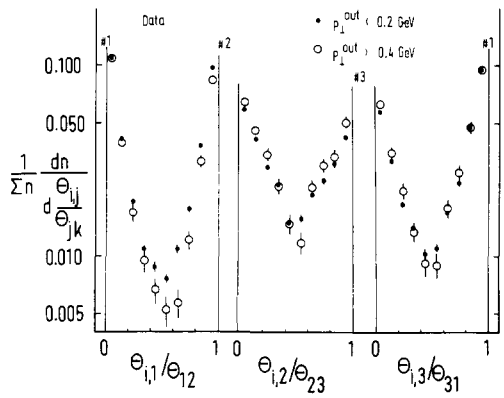

Fig. 4.11. The distribution of particles with $p_\perp^{out} < 0.2\,\text{GeV}/c$ and $p_\perp^{out} > 0.4\,\text{GeV}/c$ in the three-jet regions, normalized to 1 separately for each region [50]. The data from the JADE Collaboration show that the effects are larger for particles with larger $p_\perp^{out}$, as expected in the Lund model.

Table 4.1
The ratio of the number of particles (or energy) within $0.3 \leq \theta_{ij}/\theta_{ik} \leq 0.7$ between jets #3 and #1 to the corresponding number between jets #1 and #2 together with the statistical uncertainties [50]

				Hoyer model	
	Particles	Data	Lund model	$g \neq q$	$g = q$
ratio of	all	1.39 ± 0.04	1.33 ± 0.03	1.09 ± 0.03	1.03 ± 0.03
number of	$p_\perp^{out} < 0.2$ GeV	1.36 ± 0.05	1.27 ± 0.04	1.09 ± 0.04	1.05 ± 0.04
particles	$p_\perp^{out} > 0.4$ GeV	1.8 ± 0.2	1.61 ± 0.12	1.18 ± 0.12	1.12 ± 0.11
	K	1.9 ± 0.2	1.70 ± 0.16	1.14 ± 0.1	1.0 ± 0.2
ratio of energy	all	1.56 ± 0.04	1.50 ± 0.03	1.20 ± 0.03	1.09 ± 0.03

In this sample of 3-jet events it has also been observed [51] that the mean $p_\perp$ in the lowest energy jet (usually the gluon) is somewhat larger than the corresponding values for the other two jets, fig. 4.12. Such an effect is expected in a string model since the gluon stretches two strings at some relative angle. However, if the gluon has a softer fragmentation its jet axis will be less well determined experimentally, which leads to a somewhat increased $\langle p_\perp \rangle$ in the jet. It also matters whether the leading quark is given a p_t with respect to the jet-axis, as in Field–Feynman, or not, as in our model. From second order QCD one would also expect, due to the possibility for the gluon to split up into two gluons, a somewhat broader gluon jet. Without using the string scheme or second order effects, the fragmentation $p_\perp$ in the gluon jet would have to be ~50% higher than that in a quark jet.

It is interesting to note that the Montvay scheme with the colour octet field from the gluon to the

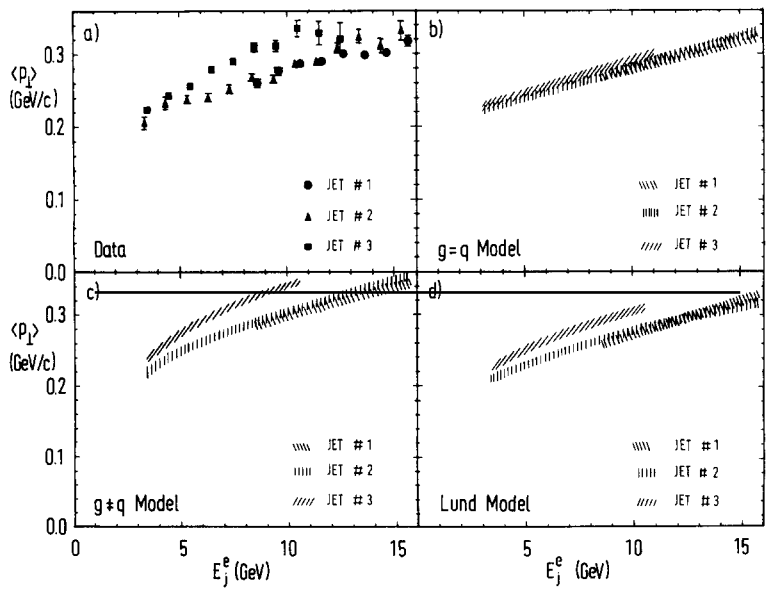

Fig. 4.12. The mean transverse momentum of the hadrons in the three different jets, with jet energies arranged so that $E(\#1) > E(\#2) > E(\#3)$. In (a) the experimental data from the JADE Collaboration [51] are shown, in (b) the results in a model where jets fragment independently in the CM frame and the gluon fragments like a quark, in (c) the same when the gluon jet is assumed to have a fragmentation $p_\perp$ 50% higher than that of a quark jet, and in (d) the Lund model results.

junction (case II in section 4.1), in a sense interpolates between the event structure obtained in our string model and the one obtained in models with independently fragmenting jets. If the junction is close to the gluon our model will be obtained as a limiting case. If, on the other hand, the junction is not close to the gluon, an event structure may be obtained (depending on how the octet "slip" fragments) which resembles the one resulting from independent jets. We note, however, that the junction will be at rest at the origin in the CM frame only for very special jet configurations, namely when the forces on the junction from the three string pieces exactly balance.

4.4. Gluon emission in electron–positron annihilation

After presenting this model for the fragmentation of a gluon jet we need to be more specific about how the initial state of partons is obtained. It is given by the initial interaction as described by the parton model and quantum flavour dynamics and gluon emission due to perturbative QCD. To be more specific the lowest order process $e^+e^- \to q\bar{q}$ ($q\bar{q}$ event) is in first order QCD modified by the probability for gluon emission, i.e. by the process $e^+e^- \to q\bar{q}g$ ($q\bar{q}g$ event). The matrix element for this is conveniently given in terms of scaled energy variables in the CM frame, $x_1 = 2E_q/W$, $x_2 = 2E_{\bar{q}}/W$ and $x_3 = 2E_g/W$, where W is the total energy in the CM frame (i.e. $\Sigma x_i = 2$). For massless quarks the cross section reads [52]

$$\frac{d\sigma_{q\bar{q}g}}{dx_1\,dx_2} = \sigma_0 \frac{\alpha_s(Q^2)}{\pi} \frac{2}{3} \frac{x_1^2 + x_2^2}{(1-x_1)(1-x_2)} \tag{4.8}$$

where σ_0 is the well-known 0th order cross section and $\alpha_s(Q^2)$ is the running strong coupling constant

$$\alpha_s(Q^2) = \frac{12\pi}{(33 - 2n_f)\ln(Q^2/\Lambda^2)} \tag{4.9}$$

with n_f being the number of active quark flavours and Λ the parameter in QCD.

The kinematically allowed region is $0 \le x_i \le 1$, $i = 1, 2, 3$. The cross section diverges for x_1 or $x_2 \to 1$, but when the first order vertex and propagator corrections also are included, a singularity with the opposite sign appears in the $q\bar{q}$ cross section, so that the total first order cross section becomes finite

$$\sigma_1 = \sigma_0(1 + \alpha_s(Q^2)/\pi)\,. \tag{4.10}$$

Physically, this cancellation corresponds to the difficulty to distinguish a single quark from a quark accompanied by a soft or collinear gluon. Specifically for QCD, where the experimentally observable entities are not quarks and gluons but hadrons, we expect the general properties of a $q\bar{q}g$ event to approach those of a $q\bar{q}$ event when the gluon becomes soft or collinear. As will be shown below this is indeed the case in the Lund model.

In a Monte Carlo program the problem of divergences may be solved by imposing cuts, so that events with hard gluons are generated according to the matrix element in eq. (4.8), but events with a soft or collinear gluon are lumped together with the two-jet events. The Lund string model provides a natural cutoff for these divergences.

For a collinear gluon the energy in the field between the gluon and the quark (or antiquark) is so small that it cannot break to produce a meson at the end. The first break will then be on the other side

of the kink and the leading (first rank) particle will contain the whole string piece between the quark and the kink. The gluon and the quark will then look just like a single quark jet. We thus find a smooth transition between the 3-jet and 2-jet events. For a rather small angle between the quark and the gluon, the distribution of particles in momentum space will be as indicated by the shaded area in fig. 4.13. Note that the hadron which includes both the quark and the gluon can in this way obtain an energy which is larger than each one of the initial quark- or gluon-jet energies.

In case of a soft gluon we also obtain an effective 2-jet event if the energy of the gluon is so small that it stops before the string starts to break. The effect of the gluon will then essentially be a small $p_\perp$ broadening of a 2-jet system as illustrated in fig. 4.14.

Fig. 4.13. The momentum space distribution of final state hadrons in the case of almost collinear gluon and quark momenta. The size of the hatched area indicates the size of the transverse momentum fluctuations in a string field without excited transverse degrees of freedom.

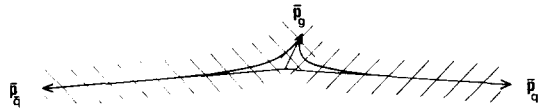

Fig. 4.14. The momentum space distribution of the final state particles in the case of a soft gluon. The same notation as in fig. 4.13.

The singularities encountered in the gluon emission probability are thus regularized in a natural way by the soft fragmentation process. In order for a description of the strong interaction in terms of quarks and gluons to be meaningful, a necessary requirement is *infrared stability*. By this we mean that the effects of soft or collinear gluon emission on the observable hadron momenta should vanish when one approaches the singularity. (We note that, in contrast, a model in which the jets are assumed to fragment independently and then joined in the CM frame is not explicitly infrared stable.)

The cutoffs we use for soft and collinear gluons are expressed in terms of requirements on the invariant masses M_{qg}, $M_{\bar{q}g}$ and $M_{q\bar{q}}$, where M_{qg} is the invariant mass of the quark–gluon subsystem etc. Note that the cutoffs are in this way explicitly Lorentz invariant as opposed to e.g. a requirement of a certain energy fraction outside a specified Sterman–Weinberg cone. The exact numerical value of the cutoff can, within some reasonable limits, be chosen arbitrarily since a change merely corresponds to a theoretical reshuffling of (2-jet like) events between the classes of 2-jet and 3-jet events. The values actually used in our model are those given in [13], i.e.

$$M_{qg},\, M_{\bar{q}g} \geq 4\,\text{GeV}\,, \qquad M_{qg}M_{\bar{q}g}/M_{q\bar{q}} \geq 2.8\,\text{GeV} \tag{4.11}$$

(for massless quarks).

4.5. Effects due to emission of soft and collinear gluons

The soft and collinear gluons avoided with cuts in a Monte Carlo program can, however, not be totally neglected since they do in fact produce observable effects. In order to get a better understanding of these effects we first study the situation in the particular coordinate system where the gluon is moving transversely to the direction of the back-to-back motion of the $q\bar{q}$ pair, fig. 4.15. The gluon transverse momentum is during the classical motion of the string system transferred to two string segments which, after the gluon is stopped, will move one in each direction. As will be discussed in more detail in section

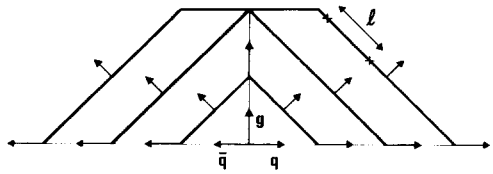

Fig. 4.15. The space-time motion of a soft kink-gluon, which is stopped before the string breaks up, in a Lorentz frame where its momentum is transverse to the (back-to-back) motion of the endpoint q- and q̄-particles. The transverse momentum of the kink-gluon is transferred to two straight string segments, which after the stopping moves in opposite directions. The transverse momentum carried by a string piece, like the one marked out in the figure, is proportional to its length.

5.3.1 the transverse momentum carried by a string piece, like the one marked out in the figure, is independent of the size of the gluon $k_\perp$ and only depends on the length of the string segment, i.e. in particular is proportional to the longitudinal (projection on the $q\bar{q}$ direction) size.

The longitudinal size of a string piece corresponding to a meson, with mass m, is Lorentz contracted, i.e. proportional to $m_\perp/E$ with E being the meson energy. Therefore a gluonic disturbance will only affect mesons with rapidities y close to the gluon rapidity y_g and we conclude that any such disturbance will fall like $\exp(-|y - y_g|)$ for $|y - y_g| \geq 1$. A rapidity range of about 2 units is also the typical one in the Lund model for hard gluon emission. If one would plot the multiplicity as a function of rapidity, the multiplicity will increase above the general background (related to the q- and q̄-jets) inside a range of typically 1 unit in rapidity on each side of the gluon rapidity. The central value will increase and the half-width of the "bump" will decrease with increasing gluon energy but the "range of disturbance" is independent of energy.

For soft central gluons we obtain essentially that a gluon with transverse momentum $\boldsymbol{k}_{\perp g}$ and rapidity y_g will affect mesons in the rapidity range $(y, y + dy)$ like

$$\boldsymbol{k}_{\perp g} \frac{N}{\cosh(y - y_g)} dy \tag{4.12}$$

with N a normalization constant.

The arguments above and also the fact (derived in [11]) that the median production time at rest for a meson of rest size l is given by l/c, implies that gluons emitted at rapidities more than about a unit apart will not interfere. If there are several (soft) gluons emitted into a certain angular range, the effect will be very similar, although the straight string segments of fig. 4.15 will be modified into several broken segments, i.e. for many soft gluons be "rounded off".

There is a further effect on the final state particle distributions which is not noticeable in fig. 4.15 due to the particular coordinate system chosen. There will be an obvious recoil effect on the q- and q̄-particles from the gluon emission. This recoil will be distributed among the fast particles along the q- and q̄-directions in accordance with the fractional energy-momentum, i.e. for the gluon emission discussed above as

$$-\boldsymbol{k}_{\perp g}\, dz \approx -\boldsymbol{k}_{\perp g}\, dy \exp\{|y| - y_m\} \tag{4.13}$$

with y_m the maximum rapidity of a meson

$$y_m = \ln(W/m)\,. \tag{4.14}$$

Thus the particles in the fragmentation region $|y| \simeq y_m$ are affected by the soft central gluon emission.

4.5.1. Collinear gluons

It is obvious that the combined effects from (4.12) and (4.13) will imply that the collinear gluon emission, i.e. $y_g \simeq y_m$ will give only minor contributions to the transverse momentum spectra. A Monte Carlo study has in fact shown that the combined effect of collinear gluon emission and the corresponding recoil of the quark is compensating and the resulting effect so small that it can be neglected given the general zero-point Gaussian $p_\perp$-fluctuations in the fragmentation process. This can easily be understood since, as argued above, both the quark and the collinear gluon will end up in the same hadron.

The longitudinal distributions are, however, affected by the emission of collinear gluons since they disturb the formation of fast (i.e. large z) particles and therefore lead to a softening of the z spectra. The reason for this is that, in our model, large z particles are produced by an early breakup of the force-field which are suppressed until the energy concentration in the collinear gluon is delivered to the field and becomes available for particle production.

To see this in more detail we consider fig. 4.15 in which the quark (with momentum p) and antiquark go apart in opposite directions and the gluon (with momentum $2k$) is moving transversely to this direction. We note that in case $4kp < m_0^2$ with m_0 a (transverse) meson mass, then both the quark and the gluon will end up in this same final state meson. There will be no disturbance for such a collinear gluon emission, i.e. expressed in terms of the scaled CM frame variables in eq. (4.8) for

$$x_2 > 1 - m_0^2/W^2 \tag{4.15}$$

there can be no difference between a 3-jet event and a 2-jet event with only the single quark moving away.

On the other hand, in case $m_0^2 < 4kp$, then we will have to wait some time to form a meson with mass m_0 from the original quark and an antiquark from a pair produced along the string. To see that, we note that after the time t the quark carries energy and momentum $(p - \kappa t)$, the string between the quark and the gluon carries the energy $(2\kappa t)$ and momentum along the quark direction (κt) and along the gluon direction (transverse) (κt). The gluon carries energy and momentum $(2(k - \kappa t))$. Thus the mass square of the quark and the quark-gluon segment is $2p\kappa t$ and if we also include the gluon, the mass square will be $2p(2k - \kappa t)$. Therefore for small values of t the mass in the quark and the quark-gluon segment of the string is too small, and if we also include the gluon the mass of that system will be too large to form the meson. It is not difficult to convince oneself that the largest value of $z = z_{\max}$ for a meson of mass m_0 will in that way not be 1 but

$$z_{\max} = 1 - \frac{4pk - m_0^2}{4p^2 + 4pk}. \tag{4.16}$$

Thus, in order to produce a meson with mass m_0 and an invariant energy-momentum fraction z, no gluon such that

$$(1 - x_1)(1 - x_2) > \hat{\beta}(1 - x_1) + \gamma(1 - x_2), \qquad \gamma = 1 - z, \quad \hat{\beta} = m_0^2/W^2 \tag{4.17}$$

should be emitted.

The mean number $\bar{n}$ of such gluons can be computed from eq. (4.8). At this point it may be necessary to take into account the running coupling constant $\alpha_s(Q^2)$ and in particular to determine the value of Q^2

to be used. If we for simplicity assume some effective value of $\bar{\alpha}_s$ in the calculation we obtain to leading order in $(1-z)$

$$\bar{n} \simeq -\frac{4}{3\pi}\bar{\alpha}_s \ln\left(\frac{M_1^2}{m_0^2}\right)\ln(1-z)\,. \tag{4.18}$$

If on the other hand we use $\alpha_s(Q^2)$ with

$$Q^2 = 4pk = W^2(1-x_2) \tag{4.19}$$

we obtain

$$\bar{n} \simeq -\frac{4}{3\pi}\alpha_s(M_1^2)\ln(M_1^2/\Lambda^2)\ln\left(\frac{\ln(M_1^2/\Lambda^2)}{\ln(m_0^2/\Lambda^2)}\right)\ln(1-z)\,. \tag{4.20}$$

In both cases M_1 is some mass corresponding to a cutoff for hard gluon emission (cf. the next subsection or ref. [13]). We note that eq. (4.18) is more cutoff-dependent than eq. (4.20) which exhibits a *very* slow dependence upon M_1. In any case we note that if collinear gluons are emitted in a Poissonian way, then the main result will be

$$P \simeq \exp -\bar{n} \simeq (1-z)^{\beta} \tag{4.21}$$

where P is the probability that no soft gluon is emitted such that eq. (4.17) is fulfilled and β can be read off from eq. (4.18) or (4.20). Rather independently of whichever of the two indicated treatments of the remaining coupling constant that we choose, we obtain for the ordinary vector and pseudoscalar mesons a value of

$$\beta \approx 0.3\text{–}0.5 \tag{4.22}$$

in the present energy-regime. We note that, although the physical interpretation differs, the numerical result obtained here is similar to the one obtained e.g. in jet calculus [116].

4.5.2. Soft central gluons

In this subsection we will discuss how all soft gluons emitted in a unit rapidity interval can be summed to give an effective gluon with a finite $\boldsymbol{p}_\perp$. It is then assumed that the soft gluon emission is of a Poissonian nature and that the probability to emit a certain number of gluons as well as their individual $\boldsymbol{k}_\perp$ are given by first order perturbative QCD. This $\boldsymbol{p}_\perp$ of the effective gluon gives a bump on the 2-jet colour-field structure and there is also a corresponding recoil for the quark which emitted the soft gluons.

For the 3-jet events the $p_\perp$ distribution for the leading quark is a smooth function above a certain cutoff value P, where P is essentially half the invariant mass M_{qg} discussed in section 4.4. Without the soft gluons the 2-jet events would correspond to a δ-function at $p_\perp = 0$. The inclusion of the soft gluon effects implies that the leading quark in a 2-jet event will get a $p_\perp$ so that the hole in the distribution between 0 and P is filled up. When summing 2- and 3-jet events the $p_\perp$ distribution for the leading quark is now a smooth function from 0 upwards. The result for the final state hadrons is insensitive to a

change in the cutoff P. Such a change will only imply that some events are moved from the class of 3-jet events to the class of 2-jet events, or vice versa. We again note that by using different cuts one can get somewhat different fractions of 3-jet events, although the fraction of events with a visible 3-jet structure is the same.

To obtain a quantitative treatment of the $p_\perp$ effects due to soft gluon emission we first have to make a precise division of soft and hard gluons. Using the scaled energy variables, defined in connection with the cross section formula eq. (4.8), it can be shown [13] that the situations when there is at least one meson related to the emitted gluon (i.e. true hard gluon emission) can be disentangled by the requirements

$$x_i \leq 1-2\gamma, \qquad i=1,2 \tag{4.23a}$$

$$(1-x_1)(1-x_2) > \gamma\,(x_1+x_2-1) \tag{4.23b}$$

with γ defined by

$$\gamma = (M_0/W)^2, \qquad M_0 \approx 2.5\ \text{GeV}. \tag{4.24}$$

The requirements in (4.23a) are usually referred to as "thrust-cuts" on collinear gluons while (4.23b) defines a situation in which a centrally (in phase-space) emitted gluon is hard enough to permit related particle production. It should be understood that the requirements in (4.23) are "theoretical" conditions based on properties of the Lund model. Many of the events which in that way are classified as 3-jet events are experimentally indistinguishable from 2-jet events. The experimentally observable rate of 3-jet events (which correspond to a scale $M_0 \geq 5\ \text{GeV}/c^2$) on the 10–20% level at 30 GeV [50, 53] is, however, the same.

Let us introduce the variables

$$k = W\sqrt{\frac{(1-x_1)(1-x_2)}{x_1+x_2-1}}, \qquad y = \frac{1}{2}\ln\left(\frac{1-x_1}{1-x_2}\right) \tag{4.25}$$

where k is the transverse momentum of the gluon in the Lorentz frame shown in fig. 4.15. For soft central gluons (with $x_1 \simeq 1$, $x_2 \simeq 1$) k and y are also the transverse momentum and rapidity of the gluon in the CM frame with regard to the direction defined by the quark and the antiquark. Expressed in these variables the cross section (4.8) takes the form

$$\frac{1}{\sigma_0}\frac{\mathrm{d}^2\sigma}{\mathrm{d}k^2\,\mathrm{d}y} = \frac{4}{3}\frac{\alpha_s}{\pi}\frac{1}{k^2}\frac{x_1^2+x_2^2}{x_1+x_2}(1-x_3) \approx \frac{4}{3}\frac{\alpha_s}{\pi}\frac{1}{k^2}; \qquad \begin{matrix} x_1 \approx 1 \\ x_2 \approx 1 \end{matrix}. \tag{4.26}$$

True hard gluons have $k > M_0$ and collinear gluons correspond to

$$k^2 < M_0^2\frac{4\gamma\,\mathrm{e}^{2y}}{1-2\gamma-2\gamma\,\mathrm{e}^{2y}}. \tag{4.27}$$

The remaining region consists of soft central gluons as illustrated in fig. 4.16. An effective maximum rapidity for soft gluons is given by $k^2 = M_0^2$ in (4.27). Hence the soft gluon region is approximately

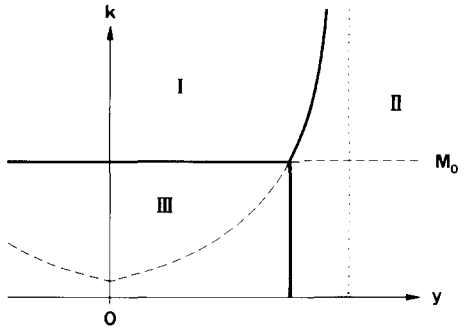

Fig. 4.16. The phase-space boundary curves separating true hard gluon emission (I), collinear gluon emission (II) and soft central gluon emission (III). The exponentiallike curve is given by (4.27) with an asymptote represented by the dotted line.

described by

$$|y| \lesssim \frac{1}{2}\ln\left(\frac{1-2\gamma}{6\gamma}\right) \approx \frac{1}{2}\ln\left(\frac{W^2}{6M_0^2}\right), \qquad k < M_0 . \tag{4.28}$$

The QCD result in (4.26) for soft central gluons can then be formulated as

$$\frac{\mathrm{d}\bar{n}}{\mathrm{d}k_{\perp g}\,\mathrm{d}y_g\,\mathrm{d}\varphi} = \frac{2}{3}\frac{\alpha_s}{\pi^2}\frac{1}{k_{\perp g}^2} \tag{4.29}$$

with φ the azimuthal angle. The quantity $\mathrm{d}\bar{n}$ in (4.29) corresponds to the mean number of gluons emitted. Since the quark hardly loses any energy when a soft gluon is radiated, the probability for this bremsstrahlung is independent of if one or more soft gluons has already been emitted. This makes it reasonable to assume, in accordance with [54], that this can be considered as a Poissonian process. Then the probability to obtain a resulting $\boldsymbol{p}_\perp$ from many increments $\boldsymbol{k}_\perp$ each determined by a Poissonian emission governed by $\mathrm{d}\bar{n}$ is given by [54, 55]

$$\frac{\mathrm{d}P}{\mathrm{d}^2p_\perp} = \frac{N}{(2\pi)^2}\int \mathrm{d}^2b\,\exp\{\mathrm{i}\boldsymbol{b}\cdot\boldsymbol{p}_\perp\}\exp\left\{-\int \mathrm{d}\bar{n}\,(1-\exp(\mathrm{i}\boldsymbol{k}_\perp\cdot\boldsymbol{b}))\right\} \tag{4.30}$$

where N is a normalization constant, depending upon the allowed $k_\perp$ and y-range.

As noted above the $p_\perp$ effects from collinear gluon emission on the final state particles can be neglected. For soft central gluon emission, where the available phase-space is defined by eq. (4.28), the effect is twofold. According to eqs. (4.12) and (4.13) we expect a $p_\perp$-bump in the rapidity neighbourhood of the gluon and a corresponding recoil in the fragmentation region with negligible interference. As discussed above, however, it is reasonable that neighbouring soft gluons will interfere to give a combined effect which, given the size of the rapidity neighbourhood, can be computed from eq. (4.30).

Because a gluon gives a transverse momentum to a piece of the linear colour-field, which is localized within about one unit of rapidity, all gluons within a rapidity range $\Delta y \simeq 1$ can be summed to one effective gluon. The $\boldsymbol{p}_\perp$ of this effective gluon is shared among the hadrons in the rapidity neighbourhood according to eq. (4.12). We obtain for the mean number of soft gluons emitted inside the range Δy

$$\frac{\mathrm{d}\bar{n}}{\mathrm{d}^2k_{\perp g}} = \frac{2\alpha_s}{3\pi^2}\Delta y \frac{1}{k_{\perp g}^2}\theta(M_0^2 - k_{\perp g}^2). \tag{4.31}$$

The upper limits on the $k_{\perp g}$-integrals imply that a good approximation for the combined effect according to the integral in (4.30) is

$$\frac{\mathrm{d}P}{\mathrm{d}^2p_\perp} = \frac{1}{2\pi}\frac{a}{p_\perp^{2-a}M^a}\theta(M^2 - p_\perp^2); \qquad a = \frac{4}{3\pi}\bar{\alpha}_s\Delta y. \tag{4.32}$$

The quantity M is a mass with the size of order M_0, representing the boundary for soft central gluons, at which the cross section should join smoothly to the hard gluon cross section. The normalization

$$\int_0^M \frac{\mathrm{d}P}{\mathrm{d}^2p_\perp}\mathrm{d}^2p_\perp = 1 \tag{4.33}$$

implies that the soft gluons emitted within a rapidity range Δy of the order of 1 unit have been summed up to one effective gluon with a combined $p_\perp$ such that $p_\perp^2 < M^2$. The exact value used for M is not critical. A change in M will essentially only correspond to a reshuffling between gluons considered as hard and as soft.

The validity of the approximation (4.32) to the expression (4.30) has been checked numerically [56]. In fig. 4.17 we show the behaviour of (4.30) normalized to (4.32) without the θ function. For relevant $\alpha_s \cdot \Delta y \simeq 0.2$ the deviation from (4.32) is noticeable only for $0.9 < p_\perp/M < 1.1$.

For the recoils given to the leading quark and antiquark we have to sum the effects of all the effective gluons corresponding to different rapidity bins. This can also be obtained from eq. (4.30) by treating the whole rapidity range. The rapidity range to include in the calculation depends on the specific process being studied. We note here a difference between e^+e^- annihilation and leptoproduction on the one hand and Drell–Yan production on the other hand. In the latter process the recoil from the gluon emission is taken by the muon pair which is unaffected by the confining force. Thus, in that case one has to add the effects from gluons in the whole kinematically allowed rapidity range. For Drell–Yan this will give results [54, 55] for the integral in eq. (4.30) which differ rather essentially from ours due to the phase-space considerations discussed above. If, as in the Drell–Yan process, the integral in eq. (4.30) is performed over the whole kinematically allowed rapidity range of the gluons, similarly as in connection with the infrared problems in QED, one obtains results like

$$\frac{\mathrm{d}\bar{n}}{\mathrm{d}^2k_{\perp g}} = \frac{2\alpha_s}{3\pi^2}\frac{1}{k_{\perp g}^2}\ln\left(\frac{W^2}{k_{\perp g}^2}\right). \tag{4.34}$$

In QED the resolution of the infrared problems is related to the experimental resolving power (soft photon emission is in principle always detectable by a sufficiently fine-grained and distant detector), but due to confinement they are in QCD related to a nonvanishing hadronic mass scale. So the treatment of soft emission should be rather different in the two theories.

As we have shown above the size of the rapidity phase-space, inside which gluon emission gives transverse momentum effects noticeable from the zero-point fluctuations, is in our model (and for the processes we consider)

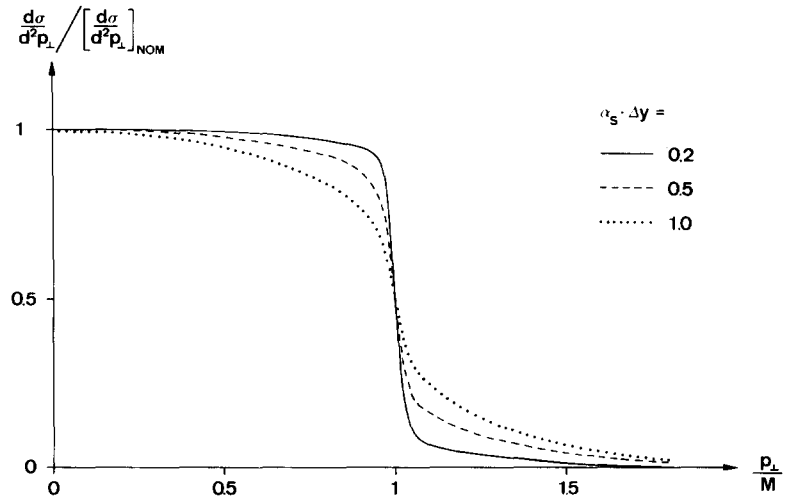

Fig. 4.17. The $p_\perp$ spectrum obtained in one Δy interval from (4.30) with upper $k_\perp$ cutoff M, normalized to the expression in (4.32) (neglecting the θ function). The resulting functions are shown for three values of $\alpha_s \cdot \Delta y$: 0.2 (full) 0.5 (dashed) and 1 (dotted).

$$\Delta y_{\max} \approx \ln(W^2/6M_0^2) \tag{4.35}$$

independently of $k_{\perp g} \leq M_0$.

The treatment of soft gluon emission can then be summarized as follows: the emitted soft gluons, given by first order perturbative QCD, are in each rapidity bin summed to give an effective gluon with a finite $\boldsymbol{p}_\perp$. This gives a bump on the 2-jet colour flux tube in such a way that the $\boldsymbol{p}_\perp$ is shared by the hadrons in the rapidity neighbourhood of the effective gluon according to eq. (4.12). The corresponding recoil is taken up by the leading quark (or antiquark). Hence, one obtains a distribution of hadrons with $p_\perp$-bumps in the central region and a corresponding recoil in the fragmentation region.

In a study of the effects of soft gluon emission on the event structure in e^+e^- annihilation it was found [56] that for central (in rapidity) hadrons the main result is an increase in the effective Gaussian width in $p_\perp$ from $\simeq 0.35$ to $\simeq 0.42$ GeV/c. The non-Gaussian nature of the soft gluon contribution is thus effectively masked by the $p_\perp$ from the tunneling process, from particle decays and from true hard gluons. The recoil effect on the hadrons in the fragmentation region makes the two jets not completely back-to-back. Since the original jet-axis is not known in e^+e^- annihilation it is not meaningful to specify exactly how the recoil is shared between the two sides. The total recoil from soft gluons is approximately 800 MeV/c at PETRA energies. The shape of the recoil $p_\perp$ distribution is of an almost Gaussian character, with significant deviations only at small $p_\perp$. It is worth noting that the resulting change in the event structure is not all that different from the one obtained with the Field–Feynman recipe [7] of giving also the primary quarks a $p_\perp$ with respect to the jet-direction.

One may note, however, that there is a difference between e^+e^- annihilation and leptoproduction concerning the recoil effect. In the e^+e^- case the gluon cannot unambiguously be associated to the quark or the antiquark, whereas in leptoproduction the $p_\perp$ recoil is always taken by the struck quark. Therefore, if $p_\perp$ is measured with respect to the current direction, the $p_\perp$ recoil is carried by the leading quark in the current fragmentation region and not by the target remnants (even if the gluon is emitted backwards in the hadronic CM frame). We will, in section 4.6.2, see that this will lead to interesting and observable consequences.

We have distinguished the gluons into three classes: true hard gluons, collinear gluons and central soft gluons. For convenience different schemes have been used to represent the effects of these different gluons, but there is no basic difference. In fact, at the price of a considerably more complicated scheme it is possible to simulate the fragmentation of a string which, on a statistical basis, will break either before or after a gluon has lost its energy (see fig. 4.15), with increasing probability for the former if the gluon energy becomes large.

4.6. Comparison with experimental results

Of course, the ultimate test of the different aspects of the hadronization models is to confront them with experimental results. To investigate perturbative QCD, which describes the gluon emission at the parton level, it is also very essential to have a realistic model for the transition to the observable hadron level. This is particularly true at the currently available energies, since effects arising in the hadronization process may often be dominating. In fact, the parton level characteristics are in some cases completely washed out, as will be shown below.

To investigate the features of the gluon emission the transverse properties of the final state particles is the most revealing point. We have already seen, in section 4.3, that the general event structure, arising due to the fact that the string is stretched via the gluon, compares favourably with data. We will, in this subsection, start with a few comparisons with e^+e^- annihilation data and then make a more complete study of $p_\perp$ properties in deep inelastic muon–proton scattering at high energies. This latter process has the advantage that the virtual photon defines an event-axis, the current direction, which gives the longitudinal direction whereas in e^+e^- annihilation this axis must be reconstructed from the measured hadron momenta, which necessarily introduces some uncertainties. In leptoproduction there is on the other hand another contributing source to the final $p_\perp$ of a particle, namely the primordial motion within the target proton, which makes the situation both more complex but also more interesting. The gluon jets that occur in high $p_\perp$ hadron–hadron scattering can also be described with this model but the string structure and colour flow properties are more complicated and will be discussed in section 6.

The features of quark and gluon-jet fragmentation discussed in this paper are all built into the Lund Monte Carlo for jet fragmentation [13], which provides general routines to fragment a specified system of partons. This initial (from a fragmentation point of view) partonic system is then calculated in different programs that use the cross section formulae for the initial interactions, such as e^+e^- annihilation [57], leptoproduction [58] and high $p_\perp$ hadronic reactions [59].

4.6.1. Gluon effects in electron–positron annihilation

The jet structure in e^+e^- annihilation has been analyzed in great detail in many publications and a number of measures of this structure has been used, like planarity, sphericity, thrust etc. Since there exist several reviews on this subject, e.g. [60], we will not go into a detailed discussion here, but rather show a few illustrative examples. Some observables are not sensitive to the differences in different fragmentation models. The planar event structure as shown by the charged particle $p_\perp$ distributions within and out of the event plane (defined by the momentum tensor $\Sigma_i p_i^\alpha p_i^\beta$) can be reasonably well represented by the results of both the Hoyer [45] and Lund [13] Monte Carlo programs, see fig. 4.18 obtained from the CELLO analysis [61] of 34 GeV data. The thrust distributions in the two models are compared with the experimental distribution in fig. 4.19. In other types of analyses different hadronization models will give different results, as e.g. discussed in section 4.3 in relation to the asymmetry

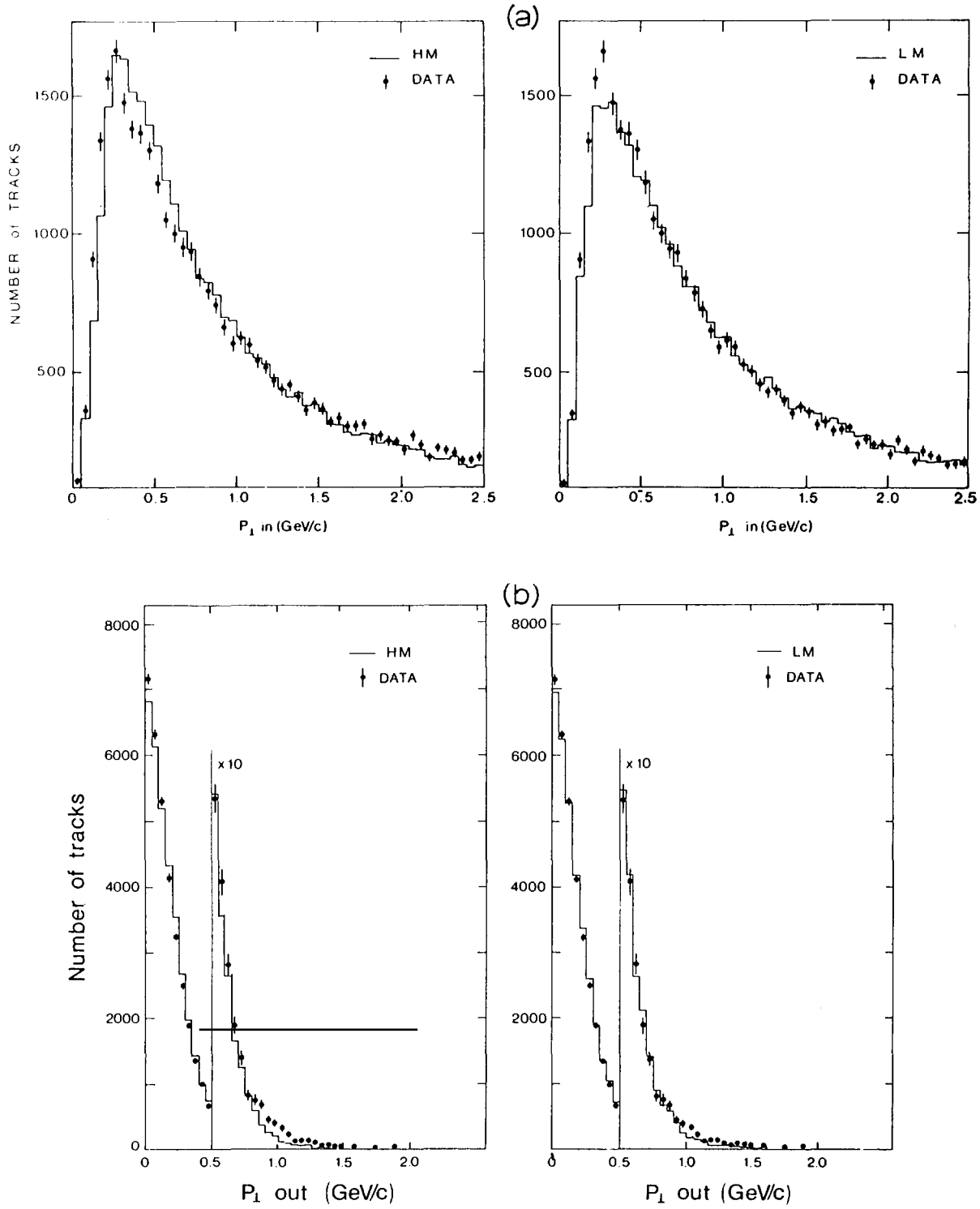

Fig. 4.18. Charged particle $p_\perp$ distributions within (a) and out of (b) the event plane. Data from the CELLO Collaboration [61] are compared with the Hoyer et al. (HM) and Lund (LM) models.

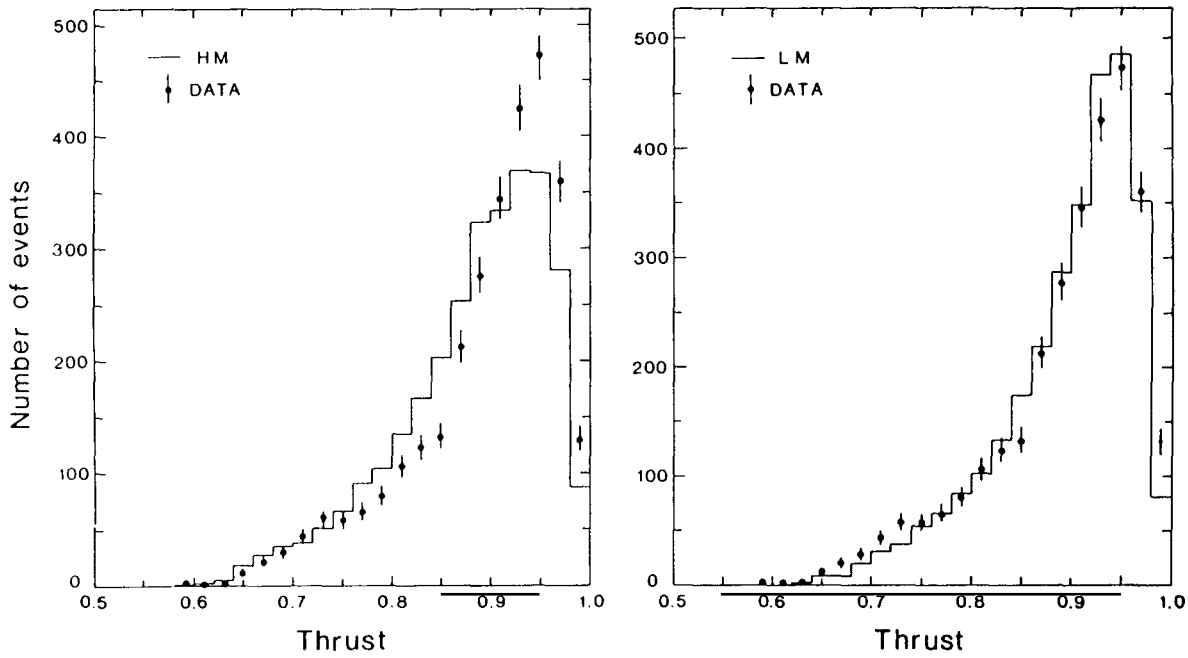

Fig. 4.19. Thrust distribution. Notation as in fig. 4.18.

observed by the JADE group. However, the fact that also observables constructed to be "fragmentation independent" are more sensitive to the hadronization than originally expected, is illustrated by the recent attempts to determine α_s, which we now want to comment.

Given that QCD is the correct theory of the strong interactions, which now seems probable, it is of course interesting to determine the one free parameter of the theory, the running coupling constant α_s or, equivalently, the Λ parameter appearing in the expression for α_s. Now, α_s is (at least at present) only related to the perturbative expansion at high Q^2, while we know that the soft, nonperturbative, fragmentation effects have a major influence on the shape of the hadronic final state. It is therefore difficult to determine α_s without some reference to an explicit model for the fragmentation. Customarily the Hoyer et al. [45] or Ali et al. [46] Monte Carlos have been used for such determinations from e^+e^- data. In a recent CELLO publication [61] it is shown that if the Lund model is used instead, an α_s about 50% higher than in the Hoyer model is necessary in order to fit the data, i.e. typically $\alpha_s = 0.25$ rather than 0.17 (for W around 33 GeV). The other groups at PETRA have since made similar, preliminary observations. What is then the reason for this discrepancy between the models? Actually there is not one single cause, but a number of contributing factors, of varying importance in different methods to determine α_s. Most important is our assumption that the colour field is stretched from the quark via the gluon to the antiquark in a 3-jet event, as discussed above, while in the Hoyer and Ali models the jets are allowed to fragment independently of each other in the CM frame. The resulting difference can be illustrated e.g. for energy–energy correlations, as follows.

Experimentally one can define an energy–energy correlation function $\Sigma(\theta)$

$$\Sigma_{\text{exp}}(\theta) = \frac{1}{N_{\text{event}}} \sum_{\text{events}} \sum_{i>j} \frac{E_i E_j}{W^2} \delta(\theta - \theta_{ij}) \tag{4.36}$$

where the inner sum runs over all particle pairs i, j in an event, with θ_{ij} the angle between the two particles (and the δ function smeared out by the use of some bin size in θ). On the parton level,

$$\Sigma_{\text{parton}}(\theta) = \frac{1}{\sigma_{\text{tot}}} \int \mathrm{d}x_1 \, \mathrm{d}x_2 \, \sigma_0 \frac{2}{3} \frac{\alpha_s}{\pi} \frac{x_1^2 + x_2^2}{(1-x_1)(1-x_2)} \left\{ \frac{x_1 x_2}{4} \delta(\theta - \theta_{12}) + \frac{x_1 x_3}{4} \delta(\theta - \theta_{13}) + \frac{x_2 x_3}{4} \delta(\theta - \theta_{23}) \right\} \tag{4.37}$$

which can be explicitly evaluated [62]. This $\Sigma_{\text{parton}}(\theta)$ is finite for $\theta \neq 0, \neq \pi$ and, neglecting $O(\alpha_s)$ corrections to σ_{tot}, directly proportional to α_s. Since fragmentation effects are considerable, both from two- and three-jet events, Σ_{exp} cannot be equated with Σ_{parton} to yield α_s. However, when the difference

$$\Delta\Sigma(\theta) = \Sigma(\pi - \theta) - \Sigma(\theta) \tag{4.38}$$

is formed, all fragmentation effects symmetric around $\theta = \pi/2$ vanish. If jets fragment *independently* of each other, then the particles in a jet will be symmetrically smeared around the parton-axis, and fragmentation effects will indeed be rather small. Thus $\Delta\Sigma_{\text{parton}}(\theta) \simeq \Delta\Sigma_{\text{exp}}(\theta)$ and α_s may be determined straightforwardly. This conclusion is almost independent of whether the gluon is hard or soft, i.e. allowed to fragment like a quark or to fragment considerably softer. More precisely, fragmentation effects will reduce the observable $\Delta\Sigma$ by a factor 1.1–1.2 compared to the parton level $\Delta\Sigma$ (for $\pi/5 < \theta < 2\pi/5$). (But note that e.g. a naive use of thrust cuts in a Monte Carlo simulation of the matrix element may in itself introduce large errors, which actually increase the observable $\Delta\Sigma$ [63].)

In the Lund model, however, particles in a three-jet event are *not* smeared symmetrically; low-momentum particles will preferentially lie in the q–g and g–$\bar{\text{q}}$ angular regions. This enhances the probability to find two particles with small relative angle and decreases the probability for large relative angle. Thus fragmentation effects reduce $\Delta\Sigma$ by just about a factor 2 at present energies (see [64] for comments on the energy dependence), which has to be compensated by starting out with a higher α_s on the matrix element level. The CELLO result is shown in fig. 4.20, while the fact that this fragmentation effect is associated with the behaviour of low energy particles is illustrated in fig. 4.21. A Montvay type of scheme [47] (see section 4.1) will essentially interpolate between the Lund and the independent jet cases, for $\kappa_g = \kappa$ fragmentation reduces $\Delta\Sigma$ a factor $\simeq 1.4$, for $\kappa_g = 1.5\kappa$ a factor $\simeq 1.65$.

Another way to determine α_s is to count the number of three-jet events, either identified with the use of some cluster algorithm or by making suitable cuts on thrust, oblateness, sphericity or some other variable. In this case fragmentation effects are always large, and an analysis along these lines must be based on comparisons with Monte Carlo results. Again the string picture has clear implications: if e.g. the q–g angle is reasonably small, the breakup of the intervening string will give a number of low to medium energy particles lying between the two jets, so that experimentally one would tend to reconstruct q- and g-axes that are somewhat shifted towards each other (fig. 4.22). Thus three-jet events "look more two-jetlike" [50] in the Lund model than in an independent fragmentation scheme, and a higher α_s is needed to account for a given amount of observable three-jet events.

Since this "hyperbola effect" is associated with low-momentum particles, it will be less important for event measures that depend more on the high-momentum particles. This is illustrated in fig. 4.23, where we show the effects of using measures linear or quadratic in momentum, and of cutting away all particles below some given momentum.

The price to be paid for putting more emphasis on high-momentum particles, however, is to

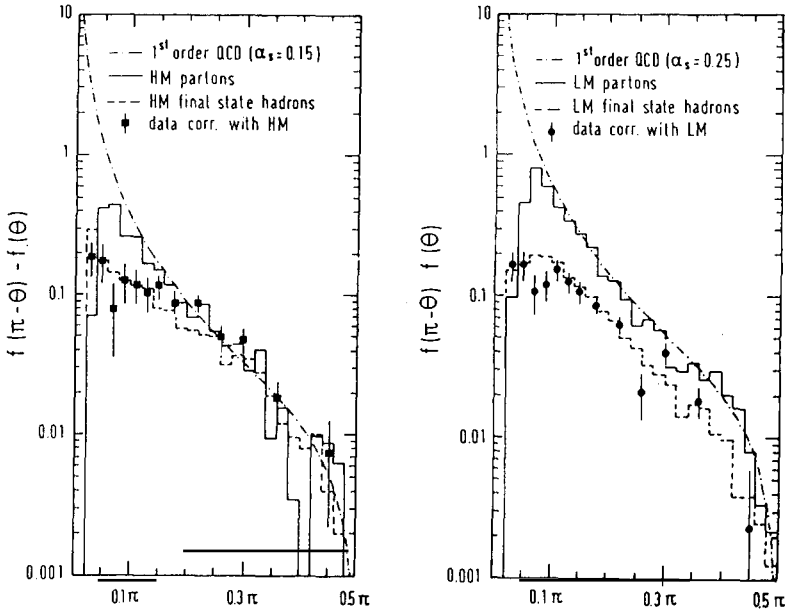

Fig. 4.20. Experimental energy–energy correlation asymmetry $\Delta\Sigma(\theta)$ from CELLO [61] compared to values before and after fragmentation in the Hoyer and Lund Monte Carlos. Note that different α_s have been used.

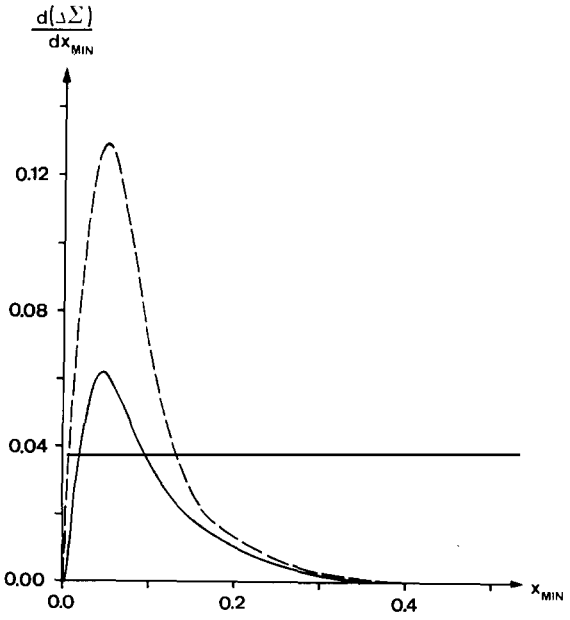

Fig. 4.21. The asymmetry in the interval $\pi/5 < \theta < 2\pi/5$, plotted according to the energy fraction $x = 2E/W$ of the least energetic particle in each pair used in (4.36). The area under the curves, full line for Lund model and dashed for independent fragmentation, give the total asymmetry.

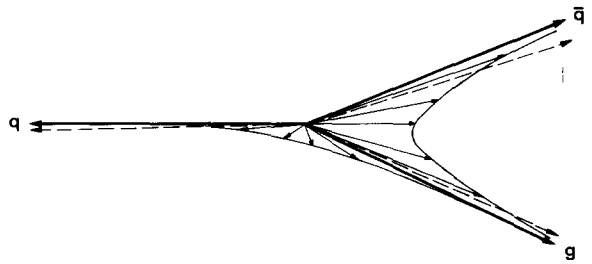

Fig. 4.22. Blowup of the central region of a $q\bar{q}g$ event, schematically illustrating how the fragmentation of the strings give particles between the jets, so that reconstructed parton-axes, dashed, deviate from the true parton directions, full, to give more two-jetlike events.

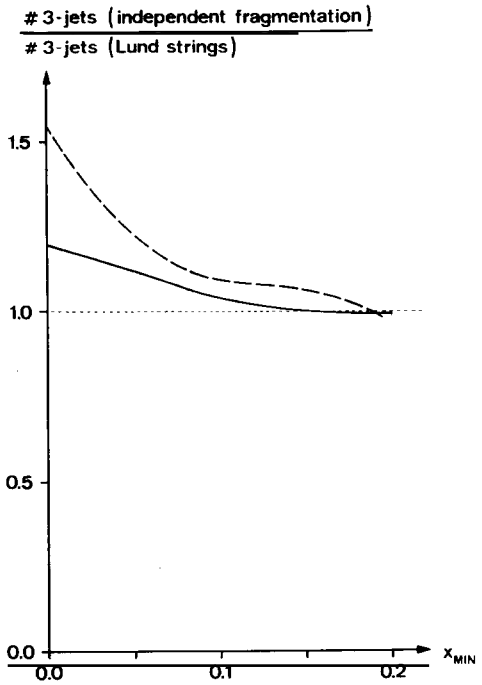

Fig. 4.23. The difference in number of three-jet events between the Lund scheme and a scheme where jets fragment independently (but with the same kind of gluon jet as in the Lund model and the same α_s). The full curve corresponds to using the sphericity measure, the dashed to a "linear sphericity" measure ($(\Sigma p_{i\alpha}p_{i\beta}/p_i)/\Sigma p_i$ is diagonalized rather than $\Sigma p_{i\alpha}p_{i\beta}/\Sigma p_i^2$ [65]). The values at $x_{min} = 0$ correspond to using all particles in the analysis, while nonzero x_{min} means that all particles with $p < x_{min}W/2$ have been cut away.

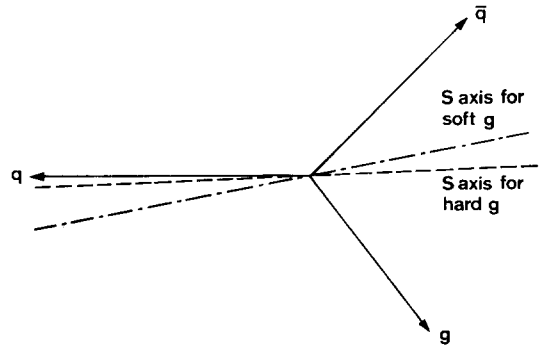

Fig. 4.24. Schematic drawing indicating how different sphericity axes are reconstructed if the gluon fragmentation is hard, dashed line, or soft, dashed-dotted line.

introduce a very strong dependence on the gluon fragmentation function. If the gluon jet is very much soften than a quark jet then the sphericity axis is essentially only determined by the q and $\bar{q}$ directions, and a lower S value will be obtained than for a hard gluon (fig. 4.24). While the gluon fragmentation is simply related to the quark fragmentation in the Lund model, it is completely arbitrary in an independent fragmentation framework. Actually, both the Hoyer and Ali gluon jets, though softer than quark jets, are harder than a Lund gluon jet. Typically this effect may require an α_s 20–30% higher in the Lund model to obtain the same number of three-jet events.

Also a number of other factors may play a rôle in the determination of α_s. So far we have only considered first order QCD, but in second order also events of the type $q\bar{q}gg$ and $q\bar{q}q\bar{q}$ enter, events which no longer need to be planar. If only first order QCD is used then an abnormally large α_s (and/or fragmentation $p_\perp$) is required to fit the out-of-plane momentum spectra. Then more technical differences between the Monte Carlo programs may enter, e.g. the schemes used in the Hoyer and Ali programs to ensure conservation of total energy and momentum, to give different shifts in α_s. Indeed the JADE group finds that for suitably defined cluster thrusts, where dependence on gluon fragmentation functions and momenta out of the plane are reduced, α_s will come out rather similar in the different models [65].

Thus the early expectation, that perturbative QCD and fragmentation effects could be studied

essentially independent of each other, is lost. In the end, our hope is that further studies not only will yield a single number α_s, but also essential information on the fragmentation properties.

4.6.2. Gluon effects in lepton–nucleon scattering

In leptoproduction the "ordinary" type of event is of a 2-jet nature, when viewed in the hadronic CM frame. The forward jet is the quark (or antiquark) which was "kicked out" of the proton by the current. The backward moving jet is the left-over target remnant, which is (usually) a diquark. (We will call this type of event a q-jet event.) From the point of view of colour properties, this diquark is an antitriplet and it will span the same kind of colour flux tube as discussed before. If one does not study the particles in the target fragmentation region one can, as a first approximation, let this diquark be represented by an antiquark, which has the same colour representation. In a more complete study, however, the structure of the diquark has to be taken into account. In the Lund model we have done this as described in section 5.2. The essential feature is that the diquark is assumed to stretch the colour field in a stepwise manner, resulting in a colour flux tube similar to the one in the current fragmentation region. This flux tube is cut into pieces by the production of quark–antiquark pairs as usual. The first rank particle can contain either one or both of the initial quarks, thus forming either a meson or a baryon. If a meson is formed first a baryon will be produced in a later step. This splitting of the diquark occurs in about 40% of the cases.

In perturbative QCD there are, to first order in α_s, two dynamically different 3-jet situations. In the first the quark (or antiquark) radiates off a gluon (fig. 4.25a) and in the second a gluon is split into a quark–antiquark pair (fig. 4.25b). We will call these qg events and $q\bar{q}$ events respectively. The cross sections for these processes can be found in e.g. [66, 67]. In order to evaluate the cross sections it is necessary to make use of the structure functions for the proton constituents. We have mostly used the parametrizations by Glück, Hoffmann and Reya [68]. Several other parametrizations exist, e.g. those in [69], but in general the results do not depend on the particular choice of parametrizations, unless e.g. the softness of the gluon distribution is changed drastically.

A very important point is, of course, that the partons in the jet system should join to form one, or more, colour singlet systems. In the q-jet events there will, of course, only be a simple 2-jet colour flux

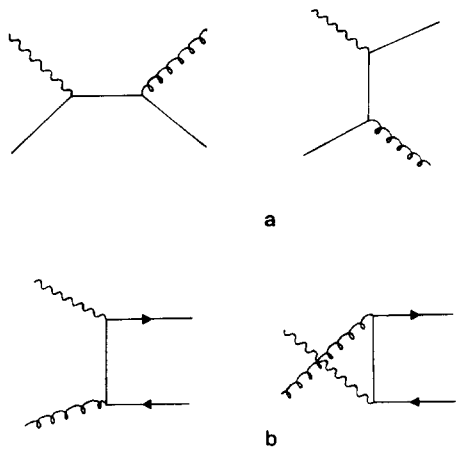

Fig. 4.25. Feynman diagrams giving the correction to order α_s to the pointlike quark-current cross section. The current is denoted by a wavy line, the gluon by a spiralling line and the quarks by straight lines.

tube and in the qg-jet event the string will be spanned from the leading quark via the radiated gluon back to the target diquark in a similar way as in e^+e^- annihilation events. In the $q\bar{q}$-jet events on the other hand, both the produced quark and antiquark will each drag out a string from the target remnant which is in a colour octet state (similar to a gluon) and contains the proton valence quarks. We treat this somewhat more complicated target remnant by dividing it into a diquark to form a colour singlet system together with the produced quark, and a quark to form a colour singlet system together with the produced antiquark. In our calculations the energy-momentum of the target jet is shared so that the diquark in the mean takes two thirds and the quark one third. In this way two separate colour singlet 2-jet systems are produced in this type of $q\bar{q}$ events.

Based on these ingredients (i.e. the differential cross section to choose kinematical variables, proton structure functions, QCD matrix elements and the Lund fragmentation model) a Monte Carlo computer program has been developed [58] and used to study high-energy leptoproduction in general [70] and transverse momentum properties in particular [70, 71]. (Also baryon production has been studied [72].)

The gluon radiation process gives the dominating contribution to the 3-jet events for the larger values of x_B. It is also interesting to note that the probability for these events essentially only depends on the total hadronic CM frame energy W for $x_B > 0.15$. However, since the x_B distribution is peaked at small values one must also take the x_B dependence into account when comparing with data. The energy partition between the jets is uneven so that the gluon has in the mean about half the energy of the quark jet.

The relative cross section for the $q\bar{q}$ events is a complicated function of both W and x_B and they dominate over the qg events at low x_B-values due to the fact that the gluon structure function is very peaked at these values. Usually the energy is very unevenly shared between the two jets, one being very soft as compared to the other (the ratio is in the mean about 1:6). The percentages of the two types of 3-jet events (defined by the cuts in eq. (4.11)) as a function of W is shown in fig. 4.26.

To make a detailed study of the $p_\perp$ properties of the final state hadrons one needs to take the following sources into account:

1. Transverse motions within the target-nucleon, called primordial transverse momentum $\boldsymbol{k}_\perp$, of the parton struck by the current. This is taken into account by letting the jet-axis "swing" around the current direction $\boldsymbol{Q}$ with a Gaussian $\boldsymbol{k}_\perp$ distribution.

2. The first order QCD 3-jet events, that occur at a rate given by α_s, give the partons a $p_\perp$ which essentially depends on the total hadronic mass W [66].

3. The soft gluon emission gives central $p_\perp$ "bumps" and a recoil to the leading quark, as discussed above.

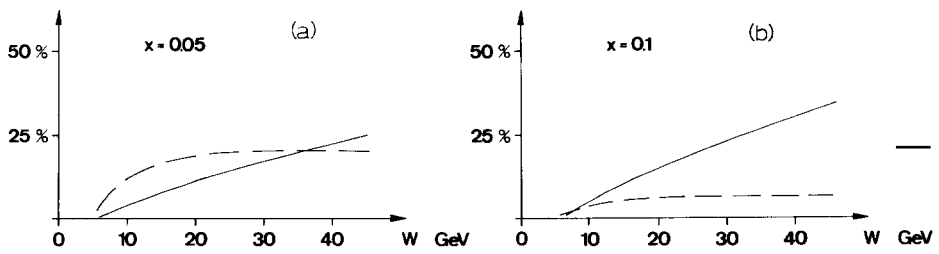

Fig. 4.26. Percentage of qg events (full line) and $q\bar{q}$ events (dashed line) as a function of W for 280 GeV μp scattering with $x = 0.05$ (a) and $x = 0.1$ (b).

4. The Gaussian $p_\perp$ distribution ($\langle p_\perp^2 \rangle = 0.2\,\mathrm{GeV}^2/c^2$) of the $q\bar{q}$-pairs produced in the soft fragmentation process.

5. Decays of unstable particles.

If all but the soft gluon contribution are taken into account, many of the observable features can be well reproduced [70, 73, 74]. It is, however, necessary to use a primordial $k_\perp$ which is too large to be understood as a pure Fermi motion within the target-proton. Furthermore, different values of $k_\perp$ are needed when different physical quantities are studied. To reproduce single particle $p_\perp$ spectra, a larger $k_\perp$ was needed than when reproducing collective $p_\perp$ properties in an event, such as sums of $p_\perp$ or energy flow [73, 74]. When the soft gluon effects are included we find [71] that the same value can be used to represent both kinds of data. We have then chosen a Gaussian $k_\perp$ distribution having the same width as for the fragmentation $p_\perp$, i.e. $\langle k_\perp^2 \rangle = (0.44\,\mathrm{GeV}/c)^2$ or $\langle k_\perp \rangle \simeq 300\,\mathrm{MeV}/c$, which can very well be interpreted as a Fermi motion.

The results we show in this subsection are obtained from the simulation of 280 GeV muon–proton scattering events and imposing cuts on the kinematical variables, $20 < \nu < 260$ GeV, $W^2 > 40\,\mathrm{GeV}^2$ and $Q^2 > 5\,\mathrm{GeV}^2$. These cuts are similar to those used by the European Muon Collaboration, whose data we use for comparison.

According to QCD at the parton level the mean $p_\perp^2$ should increase essentially linearly with W^2 [66]. In fig. 4.27 the resulting W^2 dependence in our model is compared with experimental data [75, 76]. It is

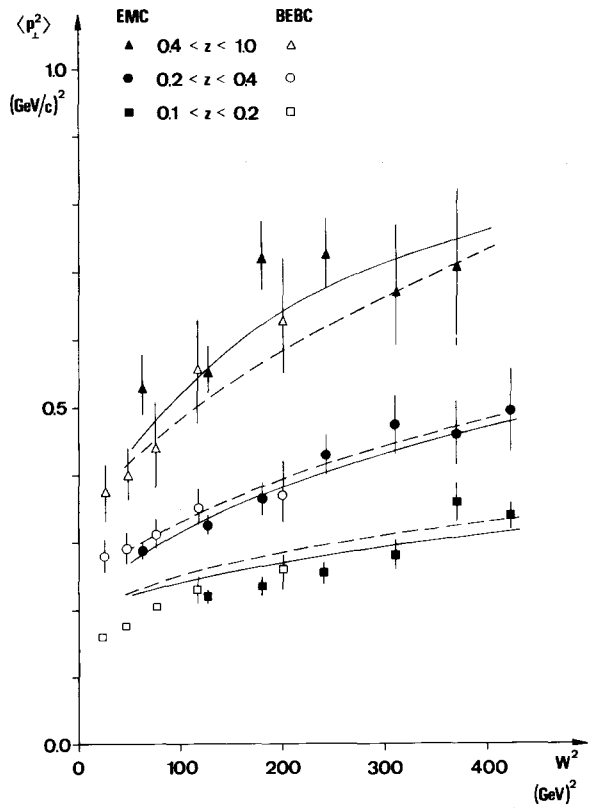

Fig. 4.27. The mean-squared transverse momentum for different z-bins is shown as a function of the squared CM frame hadron energy W^2 together with data from EMC [75] and ABCDLOS [76]. The full lines include soft gluon emission and have $\langle k_\perp^2 \rangle = (0.44\,\mathrm{GeV}/c)^2$. For comparison our old curves (dashed) not including soft gluons and with $\langle k_\perp^2 \rangle = (0.8\,\mathrm{GeV}/c)^2$ are also included.

clearly favourable to include the soft gluon effects both to improve the agreement with data and to avoid an unphysically large primordial $k_\perp$.

The planar structure of the events, due to the occurrence of QCD 3-jet events, is clearly shown in the distributions of the transverse momenta in and out of a determined event plane, fig. 4.28. A single quark-jet, whether "slim" or "fat" cannot describe the data [73].

Since the 3-jet events have larger transverse momenta than the ordinary q-jet events, a simple way to get an enriched sample of 3-jet events for QCD studies is to use a single particle $p_\perp$ trigger condition. In case one triggers on a particle with $z > 0.1$ and $p_\perp > 1.25\,\mathrm{GeV}/c$ the number of 3-jet events will be around 70% instead of 22% without any trigger [70]. This fact has been used by EMC for the energy flow diagrams of fig. 4.29 to clearly show the jet structure in the forward hemisphere of the hadronic CM frame. For more details we refer to EMC's study [73], but the model curves shown here are somewhat improved by the inclusion of the soft gluon effects.

The contributions to the total $p_\perp$ from the different sources mentioned above are shown as a function of the hadron fractional energy, $z = E_h/\nu$, in fig. 4.30. The $p_\perp$ for the leading quark will result in a $p_\perp$ for a fast hadron which is proportional to its energy fraction z. If the soft gluon contribution (IV) is neglected the primordial $k_\perp$ contribution (III) has to be increased to roughly replace curve IV. Hence, the $p_\perp$ of a high-z particle gets a large contribution either from soft gluon emission or primordial $k_\perp$. To differentiate between these two possibilities and test the soft gluon effects more directly, we have suggested [71] a study of the $p_\perp$ balance of a trigger particle with high z. As mentioned above, the main difference between the primordial $k_\perp$ and the soft gluon effect is that in the first case the $p_\perp$ is balanced in the target fragmentation region while in the second case it is balanced in the central plateau. This is seen in fig. 4.31 which shows how the $p_\perp$ compensation by the remaining particles in the event is distributed in pseudorapidity. There is a clear difference in the target fragmentation region which can be studied in the new generation of muon experiments. Due to the large number of particles in the central

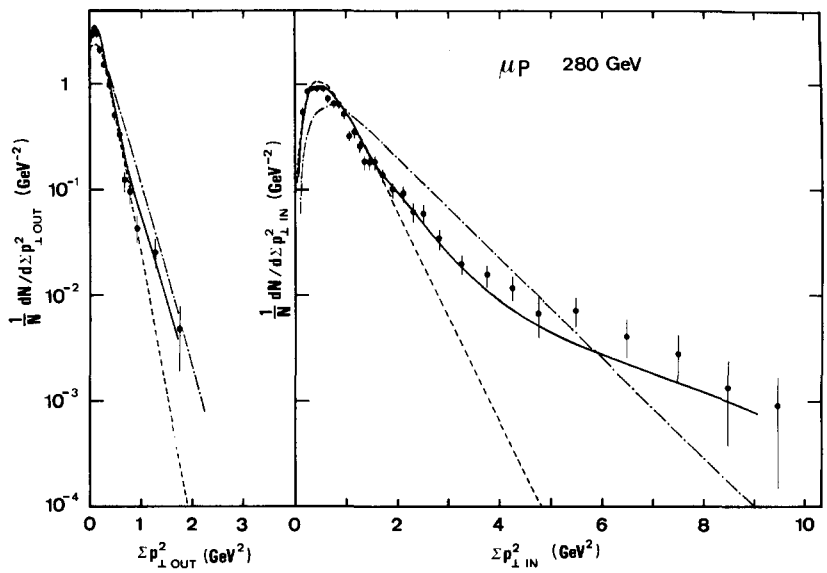

Fig. 4.28. Distributions of $\Sigma p_{\perp in}^2$ and $\Sigma p_{\perp out}^2$ obtained by EMC [73] (events with ≥ 4 charged hadrons with $p_{lab} \geq 6$ GeV). Full line: Lund model including soft gluon emission effects. Dashed line: single quark-jet fragmentation, $\sigma_q = 310$ MeV. Dashed-dotted line: single quark-jet fragmentation, $\sigma_q = 470$ MeV.

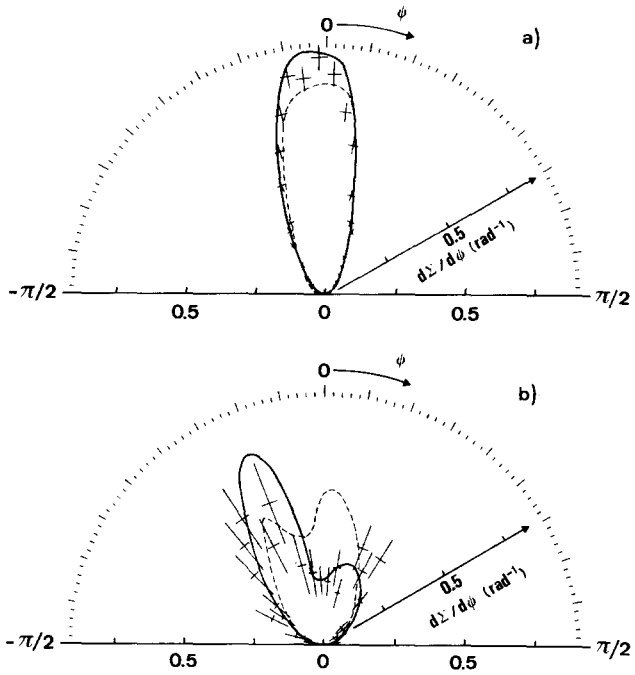

Fig. 4.29. Scaled angular energy flow $d\Sigma/d\psi$ obtained by EMC [73]. Full line: Lund model including soft gluon emission effects. Dashed line: single quark jet fragmentation, $\sigma_q = 470$ MeV. (a) all events having ≥ 4 charged hadrons with $p_{lab} \geq 6$ GeV, (b) subsample with ≥ 1 charged hadron with $p_\perp^2 \geq 2\,\mathrm{GeV}^2$.

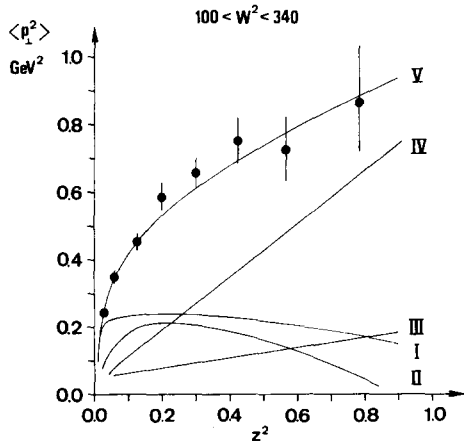

Fig. 4.30. The mean squared transverse momentum as a function of z^2. The curves show the contribution from: (I) the fragmentation process as described by our cascade model, (II) first order QCD processes, (III) primordial transverse momentum, $\langle k_\perp^2 \rangle = (0.44\ \mathrm{GeV}/c)^2$, (IV) soft gluons, (V) our model when all contributions are included. It should be noted that the $p_\perp$ broadening coming from the decay of unstable particles is included in each of the curves, and hence there is some double counting between I, II, III and IV. In fact, the $p_\perp$ broadening coming from decays is a minor effect, but decays must be included to give the correct z spectrum. The data points are from EMC [75].

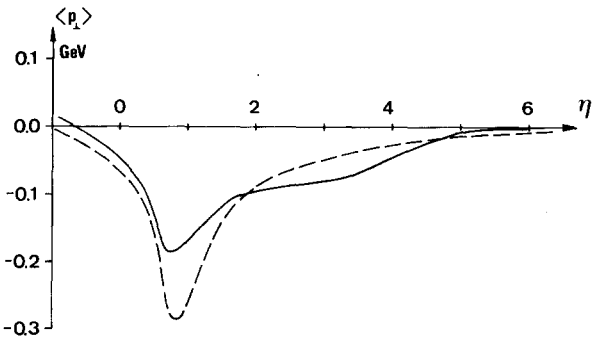

Fig. 4.31. The compensation of the transverse momentum of a fast trigger particle, having $z > 0.5$, by the remaining particles in the event as a function of pseudorapidity in the lab system. $p_\perp$ is measured in a plane spanned by the trigger particle and the virtual photon. A true primordial $k_\perp$ is compensated in the target fragmentation region (dashed line), whereas for soft gluons it is compensated in the central plateau (full line). The mean $k_\perp$ for the two cases are $\langle k_\perp^2 \rangle = (0.8\ \mathrm{GeV}/c)^2$ and $\langle k_\perp^2 \rangle = (0.44\ \mathrm{GeV}/c)^2$.

region it is possible to get a precise value for the mean $p_\perp$ in this region to test this idea even if the target region is not observable. This has been done using EMC data with the result [77] as shown in fig. 4.32. Even if only the forward hemisphere is observable the data clearly favour the soft gluon option. (The drop of the data at $y^* \simeq 0$ is due to the applied momentum cut $p_{\text{lab}} \geq 6$ GeV/c.)

In order to test perturbative QCD there has been a great interest in properties which are insensitive to the hadronization process. The angular energy flow

$$\frac{1}{\Sigma}\frac{\mathrm{d}\Sigma}{\mathrm{d}(\cos\theta)} = \frac{1}{\sigma_{\text{tot}}}\int z\,\frac{\mathrm{d}\sigma(z,\theta)}{\mathrm{d}z\,\mathrm{d}(\cos\theta)}\,\mathrm{d}z \tag{4.39}$$

would have this property if the $p_\perp$ effects arising in the hadronization were sufficiently small to be neglected. It has been shown [78] that QCD gives a characteristic forward-backward asymmetry at the parton level, due to the fact that a radiated gluon is more likely to go along the emitting current quark than along the target jet. Since the amount of 3-jet events is proportional to α_s it has furthermore been

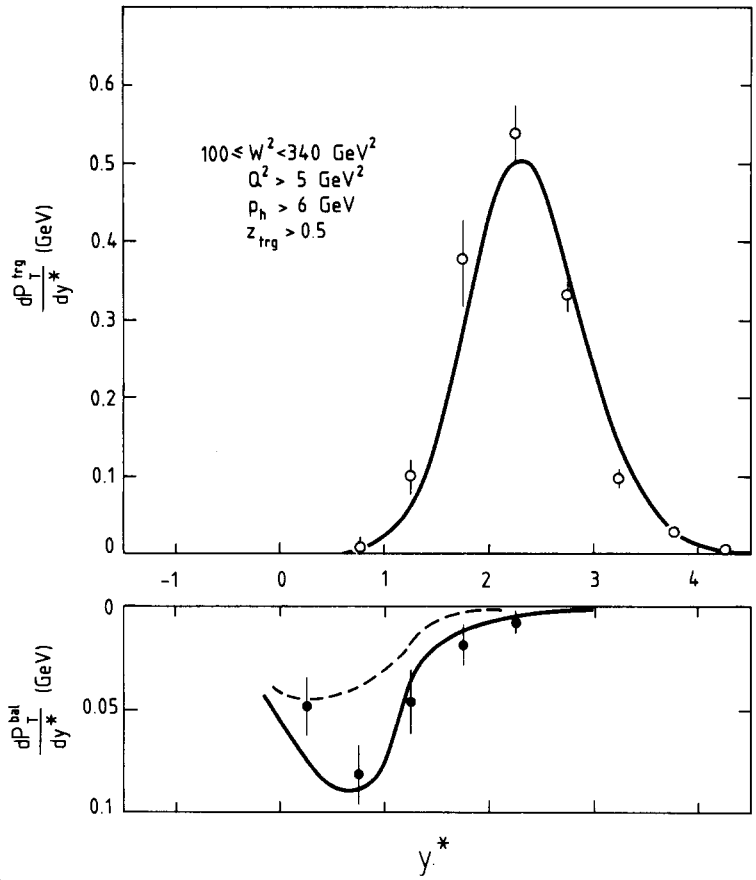

Fig. 4.32. EMC results [77] for the distribution of the transverse momentum flow $p_\perp^{\text{trg}}$ of a trigger particle with $z > 0.5$ (open symbols) and the balancing component $p_\perp^{\text{bal}}$ of further particles in the event as a function of rapidity in the CM frame. The full line is the result of the Lund model including soft gluon emission and a small primordial $k_\perp$. The dashed line is obtained from the model when soft gluon effects are neglected but a large $k_\perp$ is used, $\langle k_\perp^2 \rangle = 0.74$ GeV^2.

suggested that this energy flow could, in particular, be used to measure α_s in leptoproduction experiments. We have, however, in [71] shown that the corrections from the hadronization are, unfortunately, very large at presently available energies.

The dashed curve in fig. 4.33 exhibits the resulting angular distribution of energy flow at the parton level for the 3-jet events in 280 GeV muon–proton scattering. The dip around $\cos\theta = -0.8$ is not due to the QCD matrix elements, but a result of the specific cuts in the string model applied at these relatively low energies. The dash-dotted curve shows the parton level result for a model with independently fragmenting jets using a cut procedure à la Sterman and Weinberg, i.e. to require for a bona fide 3-jet event that a certain energy is outside a given double cone around the current direction. To study the influence of the hadronization process we first consider only the decay of unstable particles, e.g. vector mesons. Therefore, we assume that there is neither any primordial transverse momentum nor any $p_\perp$ introduced in the primary fragmentation process, i.e. in the breakup of the colour field. The resulting energy flow is shown by the dotted curve in fig. 4.33 (soft gluons are neglected here and the diquark in the target fragmentation jet is approximated by an antiquark). The QCD asymmetry is washed out and we notice that the energy flow is also much larger in this case and conclude that the effect is due to the fact that also some 2-jet events can produce particles at large angles to the current direction. The large number of 2-jet events will then completely mask the asymmetry that was produced by the 3-jet events. When the primordial and fragmentation transverse momenta are also taken into account (the former

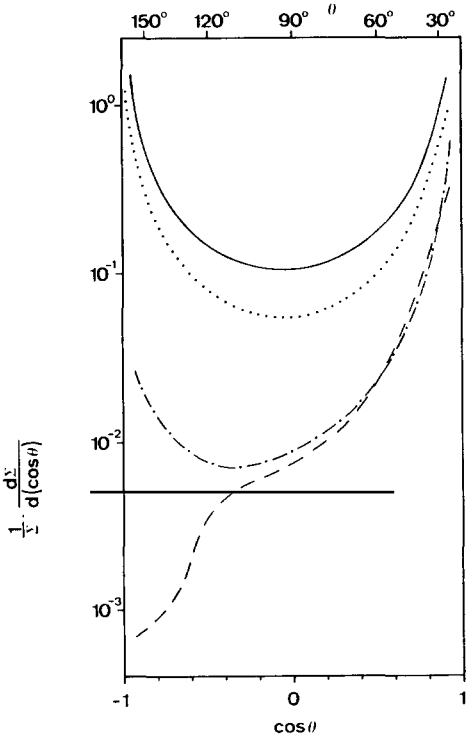

Fig. 4.33. Differential angular energy flow obtained by the Lund model for 280 GeV muon–proton interactions with cuts $Q^2 > 5\,\text{GeV}^2$, $W^2 > 5\,\text{GeV}^2$ and $20 < \nu < 260\,\text{GeV}$. The dashed curve is at the parton level, the dotted/full line is at the particle level excluding/including primordial and fragmentation transverse momentum. The dash-dotted line is the result at the parton level for a model with jets fragmenting independently of each other. At the particle level this model gives the same result as the Lund model.

only gives a very small effect) the result is given by the full line in fig. 4.33. The "independent jet" model gives the same curves on the hadronic level. When using different cuts the resulting energy flow at the parton level might vary somewhat. Very weak cuts will produce jet configurations that are not possible to project onto physical final states due to mass effects. Hence, the same distributions emerge at the particle level.

Let us as a convenient and sensitive measure of the forward-backward asymmetry define

$$A = \frac{E(\theta) - E(\pi - \theta)}{E(\theta) + E(\pi - \theta)}, \qquad 0° < \theta < 90° \tag{4.40}$$

where E is the energy flow at the angle θ in the hadronic CM frame. The dotted lines in fig. 4.34 show this asymmetry when the only source of asymmetry is hard QCD corrections as discussed so far. It is clear, however, that some forward-backward asymmetry will also appear when taking into account that the leading quark can radiate soft gluons and thereby obtain a recoil, as discussed above. The size of this effect when added to the hard processes is shown by the dashed lines in fig. 4.34.

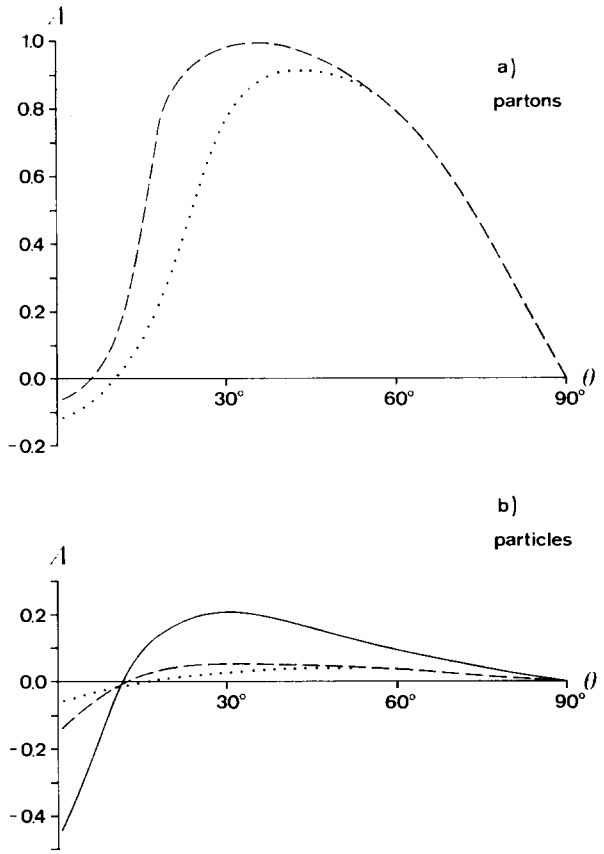

Fig. 4.34. The forward-backward energy flow asymmetry, as defined in (4.40), in the hadronic CM frame at the parton level (a) and particle level (b). The dotted lines give the result of hard QCD processes to first order, dashed lines also include effects from soft gluon emission. The full line shows the resulting asymmetry when the production of a baryon in the target fragmentation jet is also taken into account. The simulated events have the same kinematical constraints as in fig. 4.33.

In our study it turns out, however, that the dominating part of the observable asymmetry arises from the necessity to produce a baryon in the target fragmentation region. This introduces an asymmetry between the forward and the backward jet which cannot be calculated from basic principles, but can be estimated by the diquark jet model based on experimental observations. The result, which is given by the full line in fig. 4.34b, is essentially caused by the fact that a leading baryon, in general, takes a larger fraction of the jet energy than a meson does. This larger energy fraction is partly due to pure mass effects but depends also on the model for diquark fragmentation and is enhanced by the different behaviour in the decay of unstable baryons and mesons. For a more detailed discussion we refer to [71].

By using trigger conditions, like the $p_\perp$ trigger mentioned above, it is possible to get a sample of events with an increased fraction of 3-jet events which will show the QCD properties more clearly. The assumed hadronization independence of the energy flow is, however, lost by requiring a specific particle property. In [71] we show the result of the energy flow asymmetry using such a $p_\perp$ trigger and also indicate the energy dependence of the asymmetry.

4.7. Onium decays into gluons

For heavy onium states ($J^{PC} = 1^{--}$ resonances) the dominant decay mode is expected to be the three-gluon decay. In these decays we expect the string pieces between the gluons to form an expanding triangle with the gluons at the corners, fig. 4.35. Even if the matrix element for the decay [79] does not have the kind of singularities encountered in e.g. the $q\bar{q}g$ matrix element, cuts are still necessary in order to make it possible for the system to fragment. In case a three-gluon configuration fails to fulfill the cuts, there is still a definite three-gluon colour structure, but two gluons lie so close that they effectively give a single, somewhat broader jet. Hence we can, in this case, allow the ggg system to fragment as a two-gluon system [57]. Unfortunately, this procedure is not suitable for Υ decays since, with the usual cuts, all three-gluon decays are reduced to gg events, in disagreement with experimental data. For toponium (and beyond) there are, however, no such problems with this kind of model.

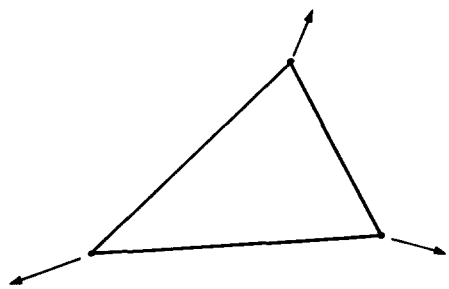

Fig. 4.35. For the three-gluon decay of a heavy onium state, like upsilon and toponium, a triangular shape of a closed string is expected. The three kink-singularities at the corners carry the energy-momentum of the gluons.

5. Hadron fragmentation in hadronic collisions and DIS

If we study the distribution in x_F of all particles (both baryons and mesons) in the following cases:

(1) quark fragmentation in e^+e^- annihilation and leptoproduction (DIS)
(2) meson fragmentation in hadronic collisions
(3) proton fragmentation in hadronic collisions
(4) proton fragmentation in DIS (diquark fragmentation)

we observe a very large similarity. It is therefore tempting to assume a common underlying production mechanism – that particles in all cases are produced in a stretched-out colour triplet field.

In sections 5.1 and 5.2 we discuss a reaction mechanism which leads to an essentially linear colour field in the fragmentation regions, and in section 5.3 we show how this is also obtained in a string picture in which e.g. a baryon is treated as three quarks connected by a Y-shaped string. Perhaps the strongest evidence in favour of this picture is the observed polarization of Σ^- particles, as will be discussed in section 5.6.

5.1. Meson fragmentation

The resemblance between (1) and (2) was noted in ref. [80]. The fragmentation of a meson in an ordinary low-$p_\perp$ (nondiffractive) hadronic collision looks very much like the average of the fragmentation of its constituent quarks. Thus we have e.g. for π^+ fragmenting into hadron h:

$$\frac{1}{\sigma}\frac{\mathrm{d}\sigma}{\mathrm{d}x}(\pi^+ \to \mathrm{h}) \simeq \tfrac{1}{2}(D(\mathrm{u} \to \mathrm{h}) + D(\bar{\mathrm{d}} \to \mathrm{h})) . \tag{5.1}$$

(Here σ denotes the inelastic nondiffractive cross section.) This has been called the fragmentation model, and some comparisons between early data are shown in fig. 5.1.

A possible reaction mechanism which reproduces this property is pictured in fig. 5.3 [81]. The colour of a quark is, due to asymptotic freedom, not well localized, but rather distributed like a blob around the quark. A meson can be imagined as two blobs confined in a bag as in fig. 5.2. It is thus e.g. red in one end, antired in the other, and "white" in the middle.

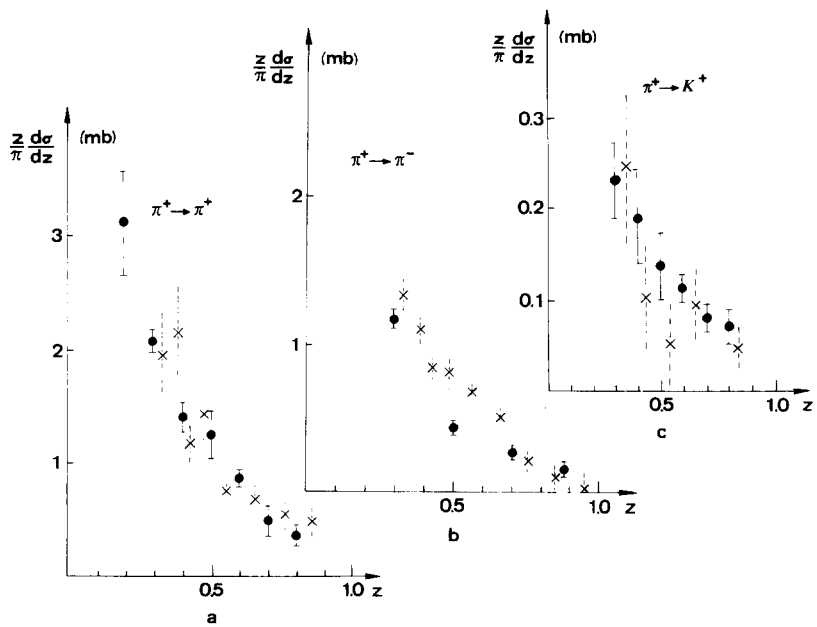

Fig. 5.1. The distributions $(z/\pi)\,\mathrm{d}\sigma/\mathrm{d}z$ for $\pi^+ \to \pi^+$, π^- and K^-. ●: data for $\pi^+ p \to hX$ from ref. [82], for $\pi^+ \to \pi^+$, the diffractive peak is subtracted. ×: predictions according to eq. (5.1) with quark fragmentation functions from refs. [14, 83] and $\sigma = 18.0$ mb.

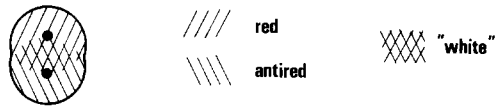

Fig. 5.2. The colour of a quark is, due to asymptotic freedom, not well localized, but rather distributed like a blob around the quark. A meson can be imagined as two blobs confined in a bag as shown in the figure. It is thus, e.g., red in one end. antired in the other, and "white" in the middle.

In fig. 5.3 we show two meson bags approaching each other. (They are Lorentz contracted.) If the coloured parts overlap, the two bags can unite to form one larger bag. This bag is stretched to a colour flux tube as in fig. 5.3. The bag pressure, or alternatively the force in the stringlike colour force-field, retards the meson remnants. As seen in fig. 5.3 the colliding "blob" will lose its momentum first, and when it is stopped, the other blob will be retarded. The bag is thus stretched to the same length as if all the energy were carried by one of the valence quarks. Although the dynamics is very different, when the energy in the colour field is divided into final state hadrons we obtain essentially the same result as for a quark jet, with one of the original valence quarks in the first rank meson.

In this picture the two valence quarks cooperate to stretch one colour field in the fragmentation region. The result will to some extent depend on the position of the interacting quark (called the I-quark) along the field, expressed by the scaled parameter x_I. The I-quark loses its initial colour in the interaction, whereas its energy is only gradually stored in the colour field. When the field is stretched the fraction x_I of its full length, the I-quark is stopped and the other quark (called L for leading) continues and stretches the remaining fraction $1 - x_I$ of the colour field. When the field breaks into pieces, the value of x_I determines which hadron will contain the I-quark flavour.

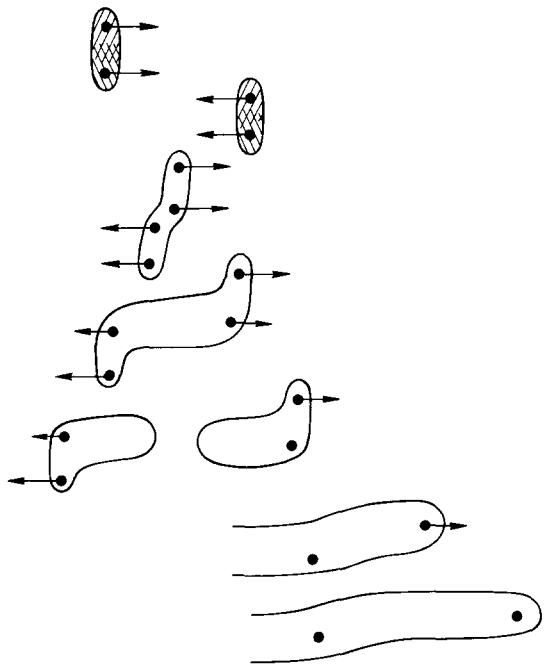

Fig. 5.3. Consider two meson bags approaching each other (the bags are Lorentz contracted). If the coloured parts overlap, the two bags can unite to form one larger bag, which is stretched to a colour flux tube. The bag pressure retards the meson remnants. The colliding blob will lose all its momentum before the other blob will be retarded. The bag is thus stretched to the same length as if all the energy were carried by one of the valence quarks.

The relation in eq. (5.1) obviously corresponds to $x_I = 0$. The probability for x_I having larger values is related to the wavefunction of the incoming meson. For pion fragmentation so many new u- and d-quarks are produced in the process that it is difficult to see the effect of the I-quark. Actually, Monte Carlo studies to be discussed below show that it is mainly seen in the possibility for the first rank hadron to contain both the flavours of the incoming meson. This happens if z for the produced hadron and x_I are large, so that $z + x_I > 1$. Unfortunately this enhancement of fast particles with the flavour of the incoming meson is in phase-space situated below the diffractive peak, and is therefore difficult to study experimentally.

For kaon fragmentation, the result is somewhat more sensitive to the x_I-distribution when the I-quark is a strange quark. Direct application of eq. (5.1) (corresponding to $x_I = 0$) will give too small a probability for a meson in the fragmentation region ($z \gtrsim 0.2$) to carry the initial strangeness. In fig. 5.4 we show some results assuming the following probability distribution for x_I

$$dP/dx_I = 3(1 - x_I)^2 . \tag{5.2}$$

We have here assumed equal probabilities for the two valence quarks in the initial kaon to be the

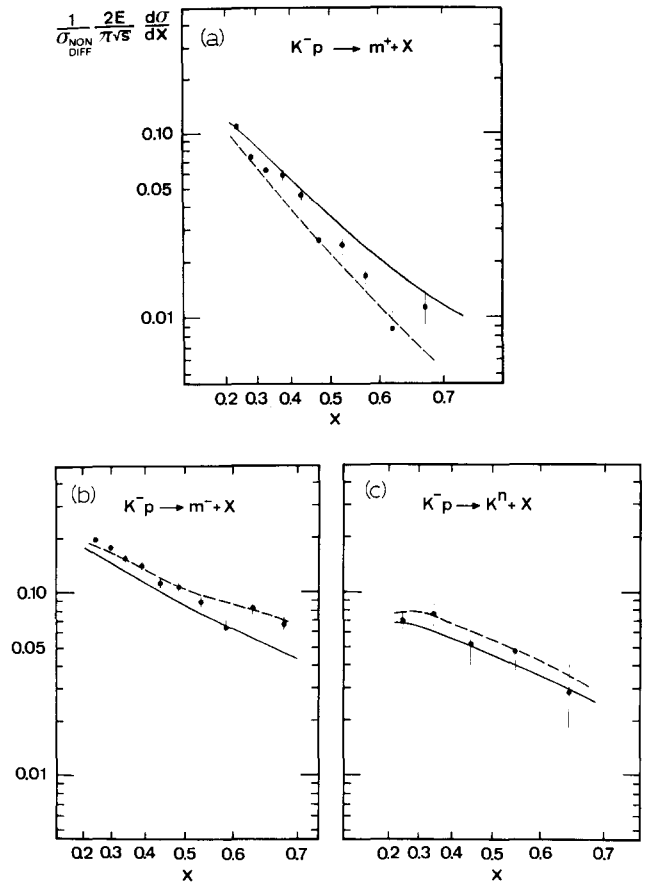

Fig. 5.4. The distributions $(1/\sigma)(z/\pi)\,d\sigma/dz$ for (a) $K^-p \to m^+X$, (b) $K^-p \to m^-X$, (c) $K^-p \to K^nX$, data from ref. [84]. The solid line corresponds to eq. (5.1), i.e. to $x_I = 0$, while the dashed line is the result with dP/dx_I given in eq. (5.2).

I-quark. An increased probability for the strange quark to be at larger z is also obtained if the nonstrange one more often is the I-quark. This could be the case if the difference between the kaon and pion cross sections is due to a smaller probability for the strange quark to interact, as in the additive quark model. However, this will not reproduce the data for the reaction $K^- \to m^+$ equally well (see fig. 5.4). In the bag model, the kaon bag is smaller than the pion bag. The more massive s-quark limits the motion of the nonstrange quark. The different kaon and pion cross sections should then not be related to different fixed cross sections for the strange and nonstrange quarks.

The result in eq. (5.1) is also obtained in the dual topological expansion scheme, where the original valence quarks stretch two different colour-fields, but where the meson energy is very unevenly shared, so that one of the valence quarks takes most of the energy [85]. In this scheme the leading meson can never contain both valence quarks of the incoming meson. However, as mentioned above this is difficult to study since it is masked under the diffractive peak.

Perhaps the strongest evidence for a picture where the particles are produced in the same kind of colour force-field as in a quark jet, is the agreement for the reaction $K^+ \to \bar{\Lambda}$. Baryon–antibaryon pairs are produced in e^+e^--annihilation, and we thus expect this to be possible also in meson fragmentation. In section 3.4 we showed that $q\bar{q}$–$q\bar{q}$ pair production in the colour field can reproduce the observed variation with W and x_F in e^+e^- annihilation. In fig. 5.5 we show results for $K^+ \to \bar{\Lambda}$ assuming (anti)diquarks to be produced in the same way in the colour field behind a leading $\bar{s}$-quark. The same mechanism will also give the process $K^- \to \Lambda$; however the agreement for $K^+ \to \bar{\Lambda}$ is more striking because here it cannot be a spill-over of the baryon number from the target fragmentation region.

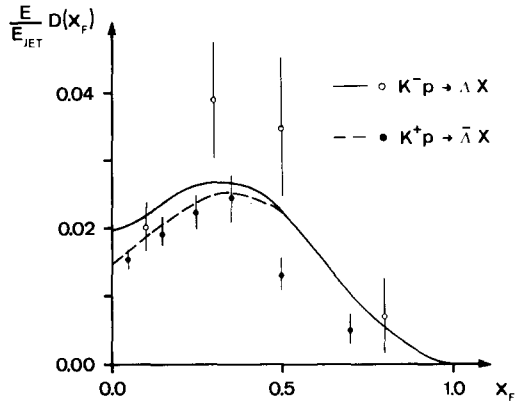

Fig. 5.5. The distribution $x_F \cdot D(x_F)$ for $K^-p \to \Lambda X$ (110 GeV/c) and $K^+p \to \bar{\Lambda} X$ (70 GeV); data from ref. [114].

5.2. Proton fragmentation

If we apply these ideas to proton interactions we expect that when one valence quark from a proton interacts with another hadron (case (3) above) or is hit by a lepton (case (4)), the rest of the proton (a diquark) continues and fragments in similar ways [80, 81]. As mentioned above, not only are cases (3) and (4) similar, they also resemble cases (1) and (2) if all particles, both mesons and baryons, are included. This suggests that also in proton fragmentation an essentially linear colour triplet field is stretched. If one of the valence quarks interacts with a virtual photon, a $W^{\pm}$ or another hadron, we can imagine a reaction as shown in fig. 5.6. A colour field or flux tube is stretched in a stepwise manner such

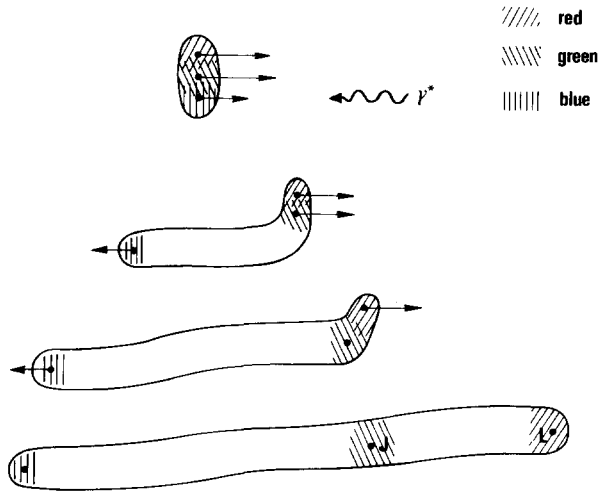

Fig. 5.6. One quark in a proton is hit by a virtual photon (or a W or another hadron), and a colour flux tube is stretched in a stepwise manner (cf. fig. 5.3).

that one valence quark (called L) is at the end of the force field followed by a partner (called J for "junction") in a diquark. In the case of a hadronic collision, the interacting quark (the I-quark) will not stop immediately but follow after the J-quark. The colour field between the separated colours will be as shown in fig. 5.7 and assuming that the linear properties of the force field are the most important it will break into pieces as in fig. 5.8. (Although not shown in fig. 5.6, it will of course start to break long before it is fully stretched out.) In that way we obtain a linear force-field with the same strength as in a quark jet.

If the L-quark is red as in fig. 5.7, the I- and J-quarks are together antired, and the field between the L- and J-quarks will be antired–red. Similarly the J- and L-quarks are together antiblue and the field between I and J is blue–antiblue. We notice that the field changes direction at the J-quark so that when a $q\bar{q}$-pair is produced in the field, the quark is always pulled towards (and the antiquark away from) the J-quark. Thus if the linear properties of the force field are most important we expect the jet to fragment into hadrons in much the same way as a quark jet, with the exception that the part which happens to contain the J-quark becomes a baryon instead of a meson. This is illustrated in fig. 5.8 in case there is one break in the field between J and L.

We use the same production mechanism for quark–antiquark pairs as for a quark jet described in section 2. Evidently the result will depend on the position of the J-quark along the field (in scaled units x_J). For the situation in fig. 5.8 one $q\bar{q}$-pair is produced between J and L, and the first rank hadron is a

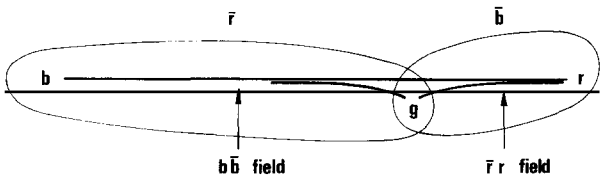

Fig. 5.7. The force field between the separated colours. The blue and green quarks act together as an antitriplet, antired in colour, while the green and red quarks act as an antiblue colour antitriplet.

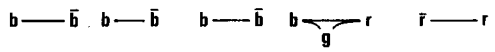

Fig. 5.8. The resulting breakup structure in the baryon fragmentation region.

meson, containing the L-flavour. If the first break occurs instead behind the J-quark, then the first rank hadron becomes a baryon containing the original diquark JL. Figures 5.9 and 5.10 show the analogues of figs. 2.4 and 2.7. The treatment of the J-quark position in terms of a single scale invariant coordinate x_J means that it after turning is moving with a very large velocity in the rest frame of the original proton (fig. 5.10) or with a finite velocity in the total CM frame (fig. 5.9). We will return to this question below.

In this way the original LJ diquark structure is treated by a probability distribution to find the J-quark at x_J. This is related to the wavefunction of the initial proton. Thus the I- and J-quarks together stretch the fraction x_J and the L-quark stretches the remaining fraction $(1 - x_J)$ of the full field length. From the resulting pion spectra we find that the distribution must vanish for $x_J = 0$ and $x_J = 1$. We have not tried to make a best fit to experimental data but merely used the simple normalized distribution

$$dP/dx_J = 6x_J(1 - x_J). \tag{5.3}$$

We also note that the final state distributions are rather insensitive to variations around this shape. With our recipe to divide the force field into hadrons, this implies around 40% probability for a break between the L- and J-quarks. Thus we have about equal probabilities that the final state baryon will contain one or both of the initial flavours related to the L- and J-quarks; in this scheme it obviously always takes at least one.

For hadronic collisions we assume, as in fig. 5.3 for meson collisions, that the I-quark is not immediately stopped. For simplicity we assume that its orbit is parallel to J and that its scaled position variable x_I is evenly distributed between 0 and x_J. This implies that the x_I-distribution will be

$$dP/dx_I = 3(1 - x_I)^2. \tag{5.4}$$

In that way the probability to find an original flavour in a central unit of rapidity space will decrease as $\approx 3m_\perp/\sqrt{s}$. This number is compatible with the charge asymmetry between pp and $\bar{p}p$ collisions at the ISR [86].

In principle we could expect different x_J-distributions in hadronic collisions and in leptoproduction where the I-quark is directly kicked and moving at the other end of the force field. However, due to lack of experimental information we assume the same x_J-distribution in both cases.

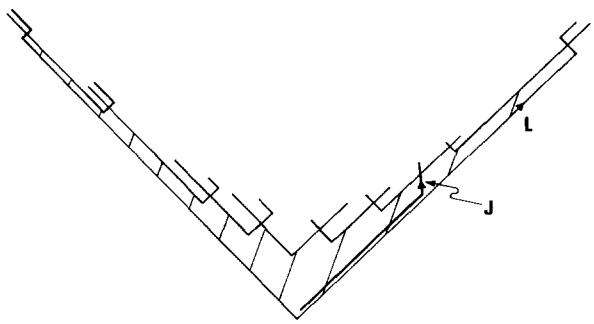

Fig. 5.9. The analogue of fig. 2.4 for baryon fragmentation. The trajectory of the J-quark is indicated. In this case it happens to go into the second rank hadron, which thus becomes a baryon.

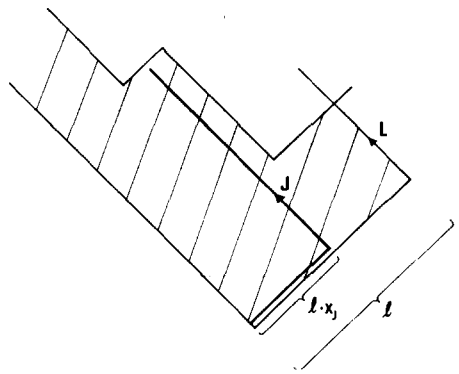

Fig. 5.10. The analogue of fig. 2.7 for baryon fragmentation. In this Lorentz frame the J-quark moves "backwards" with very large velocity, i.e., close to the light cone.

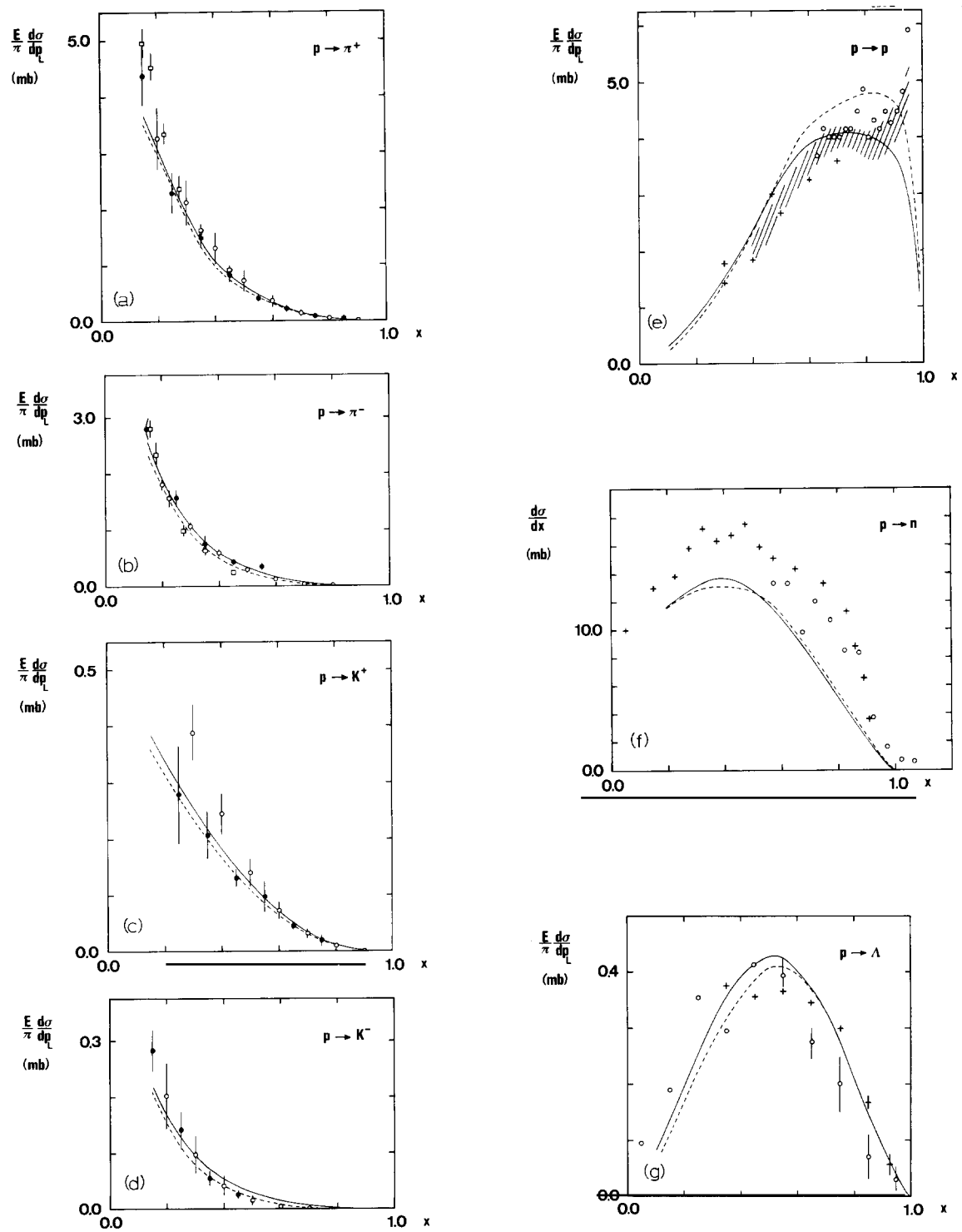

Fig. 5.11. Inclusive particle spectra in proton fragmentation [81]. Meson data from ref. [110] (□), ref. [111] (●), ref. [88] (○). Proton data from ref. [112] (○), ref. [113] (+), ref. [88] (///). Neutron data from ref. [89] (○) (actually pn → pX), ref. [90] (+). Λ data from ref. [91] (○), ref. [92] (+). Data from refs. [111, 88, 112] are integrated over $p_\perp$ and for the proton data from ref. [88] the $p_\perp$-integration is estimated. The solid line is the model calculation. The dashed line is obtained with a modification of the effect caused by finite colour-field lengths [81].

An important point is the fact that the produced baryon has to be a symmetric state of three quarks with regards to flavour and spin. As for $B\bar{B}$ production (section 3.4), we assume the production of each baryon type to be weighted by the probability to find three quarks in a *symmetric* state with the proper quantum numbers, if the new quarks are produced with random spin and flavour (except for the suppression of s-quarks).

As before we also neglect particles with orbital angular momentum $\neq 0$ and only take into account the ground state 56-multiplet. In the same way as vector mesons are suppressed relative to pseudoscalar mesons, we also expect a suppression of the decuplet relative to the octet (cf. section 3.4). However, this suppression will only give very small changes in the results presented in figs. 5.11 and 5.12.

For a leptoproduction event the flavour of the interacting quark is determined by the structure functions (and the quark charges). For a hadronic reaction we expect equal probabilities for the three valence quarks in the proton to correspond to the I-quark. As mentioned above, in about 60% of the events the leading LJ-diquark is not split but goes into one baryon. In these events we assume that it does not change its isospin and spin; we thus assume this diquark to be in the states uu ($S = 1$); ud ($I = S = 0$), and ud ($I = S = 1$) with the probabilities 1/3, 1/2 and 1/6 respectively, as given by SU(6).

A ud ($I = S = 0$) diquark is expected to be a more tightly bound system than the $I = S = 1$ diquarks. (This is connected to the $\Lambda^0 - \Sigma^0$ mass difference and probably to the difference in the u- and d-quark structure functions for $x_B \sim 1$ [87].) Thus if an interacting u-quark (I-quark) originally forms a ud ($I = S = 0$) with the d-quark in the proton, we expect this d-quark to be the J-quark, whereas the other u-quark, which is more loosely bound to the I-quark, will be the leading quark (L-quark) at the end of the force field. With SU(6) ratios for different diquarks we thus find the probabilities 1/12 and 11/12 for the L-quark to be a d- or u-quark respectively. It is obvious that with equal probabilities for the three

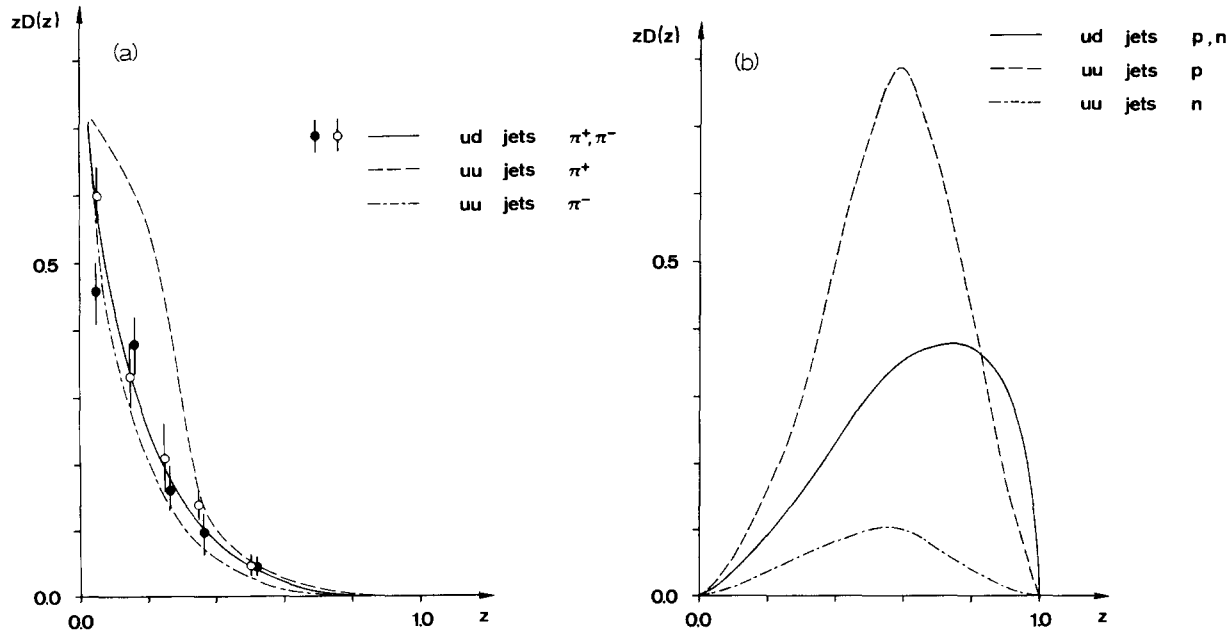

Fig. 5.12. Diquark fragmentation functions into mesons (a) and baryons (b). The experimental data on ud→ π^+, π^- come from the reaction $\bar{\nu}p \to \pi X$ in ref. [93]. Note that $z \to 1$ corresponds to the target fragmentation region in this case. In connection with the baryon fragmentation distributions, baryon–antibaryon production along the field is not included.

valence quarks to be the L-quark, one could never reproduce the experimental result that $\pi^+/\pi^- \sim 5$ for large z. This must be a reflection of an asymmetry between the u- and d-quarks in the proton wavefunction (related to the proton structure functions).

In contrast, for a leptoproduction event we expect that when one quark is kicked out of the proton with a large momentum transfer, it loses its memory about to which of the two remaining quarks it was more tightly bound. Thus we assume equal probabilities for the remaining quarks to be the L- and the J-quark.

Our model is now fully determined (apart from transverse momentum properties discussed in sections 5.3 and 5.4), and via a Monte Carlo program it is possible to study not only inclusive particle spectra but also any kind of correlation. Some examples are presented in figs. 5.11 and 5.12 and we note generally a very good agreement between the model and experimental data.

As discussed above (in section 2.5) we want to emphasize that low-energy jet systems, like in neutrino interactions where the mean W is around 5 GeV, are naturally very sensitive to kinematical effects. In particular the production of a heavy particle, a baryon, in the target fragmentation jet may influence the forward jet also since the forward and backward jets are not well separated, in e.g. rapidity. In fig. 5.13 we compare the momentum spectrum of protons in νp and $\bar{\nu}$p interactions with data from BEBC and note the importance of taking the limited experimental acceptance into account. After all, our jet model works surprisingly well also at low energies (see also fig. 2.12).

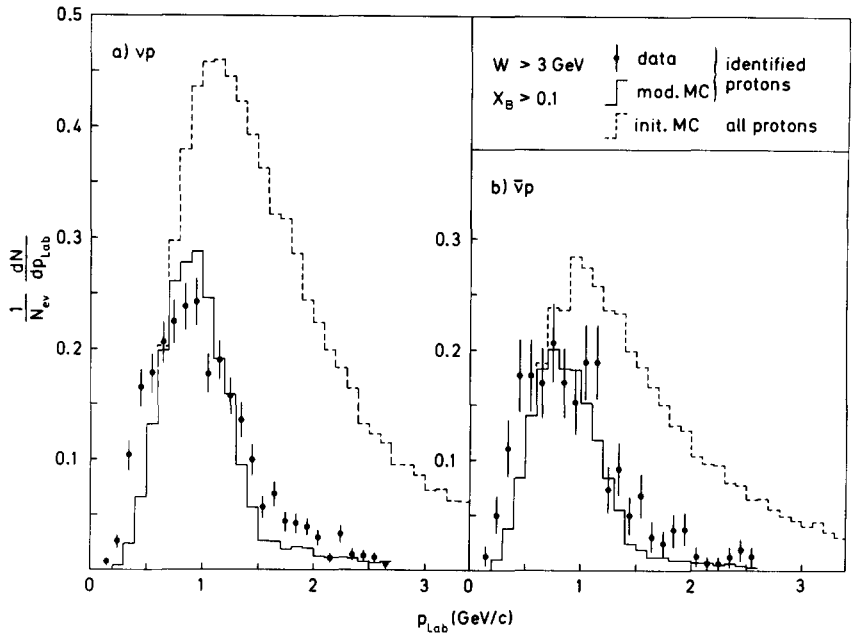

Fig. 5.13. Proton production in νp scattering. Data from BEBC [115] compared to model calculations.

5.3. *String picture of hadron fragmentation*

In section 2 we studied particle production in a straight smooth colour-field, and above we have applied these results to the case when one quark is kicked out of a hadron. Due to the relative motion of the quarks in the initial hadron, the colour field will not be completely straight. In this subsection we

study the situation when the initial hadron is described by massless quarks connected by a string in a yo-yo mode (for a meson) or by a Y-shaped string (for a baryon). We will see that if one of the quarks is kicked out, the string will be stretched and fragment in the way described above. In particular for a baryon one quark will be close to the junction which leads to the essentially linear picture described above.

5.3.1. A model for meson fragmentation [108]

We start by treating a meson and assume that initially, before one of the quarks is kicked out, it consists of a quark and an antiquark in a yo-yo mode. The results can also easily be generalized to more complicated initial states. Thus, just before the interaction, the q- and $\bar{q}$-particles are moving along the string with momenta $\boldsymbol{k}$ and $-\boldsymbol{k}$ at a distance $2l$ and after the momentum transfer the q-particle will obtain the momentum $\boldsymbol{Q}+\boldsymbol{k}$. The subsequent motion shown in fig. 5.14 will be [108]:

1. The q-particle will move along the direction $\boldsymbol{Q}+\boldsymbol{k}$ (having angle α with respect to the original string direction) with the velocity of light and with constantly decreasing momentum.

2. A straight section L (with angle $(\pi-\alpha)/2$ with respect to the string) is formed and a disturbance (a "corner") A moves along the string at the velocity of light (carrying no momentum, however). The transverse velocity of L is $v_\perp = \cos(\alpha/2)$.

3. The $\bar{q}$-particle is at first accelerated along the original string. When it meets a corner A, a new straight section L′ is formed and $\bar{q}$ is decelerated until its momentum is zero. The transverse velocity of L′ is $v'_\perp = \sin(\alpha/2)$.

4. The $\bar{q}$-particle is now pulled back along the string and in the lab frame $\bar{q}$ will move along a line parallel to $\boldsymbol{Q}+\boldsymbol{k}$ (the dashed line in fig. 5.14). In a Lorentz frame in which L′ has $v_\perp = 0$, $\bar{q}$ moves in and out along the string L′. The angle between the string segments L and L′ is $\pi/2$ in the rest frame of the original meson.

The string system will now move as a rigid body along $\boldsymbol{Q}+\boldsymbol{k}$, q is losing while $\bar{q}$ is gaining momentum. The situation is evidently rather similar to the situation in fig. 2.7 when q_0 has turned around and $\bar{q}$ is moving with a constant relative distance.

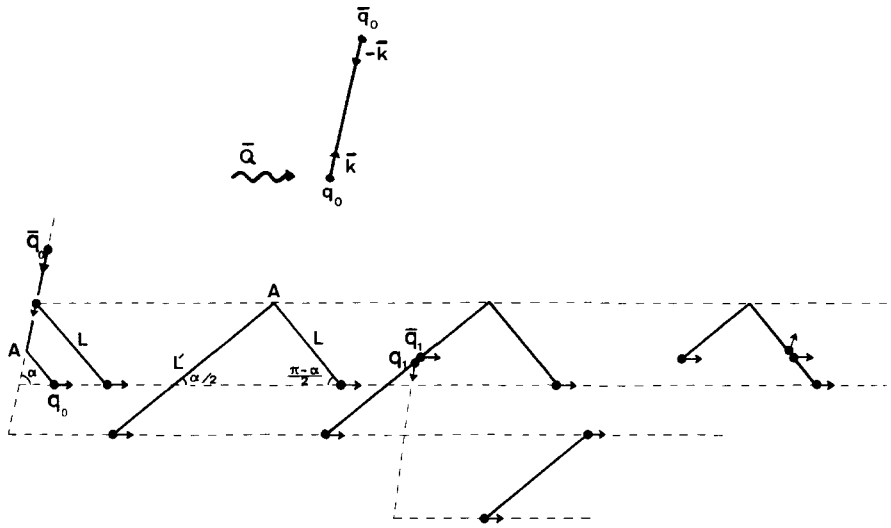

Fig. 5.14. The subsequent motion and decay of an initial quark–antiquark yo-yo state when the quark q_0 is given a momentum transfer.

The main difference is that the string segments L and L′ carry momentum. Thus a piece dl along L′ will have a momentum d$\boldsymbol{p}$ with components d$p_\perp$ transverse to $\boldsymbol{Q}+\boldsymbol{k}$ and dp_l along $\boldsymbol{Q}+\boldsymbol{k}$ and an energy dE [12, 108]

$$\begin{aligned} \mathrm{d}p_\perp &= \kappa\, \mathrm{d}l\, \mathrm{tg}(\alpha/2)\sin(\alpha/2)\,, \\ \mathrm{d}p_l &= \kappa\, \mathrm{d}l\, \sin(\alpha/2)\,, \qquad \mathrm{d}E = \kappa\, \mathrm{d}l/\cos(\alpha/2)\,. \end{aligned} \tag{5.5}$$

There are similar relations for a piece along L.

Nevertheless, as we will show below, all the quantities relevant to the decay, depend only on the "longitudinal projections", i.e. only on the projections upon the direction $\boldsymbol{Q}+\boldsymbol{k}$. Further, when the string breaks up by the formation of q$\bar{\mathrm{q}}$-pairs along the string segments L and L′ then (with one exception) the new subsystems are all left in yo-yo modes. The exception is the system containing the corner A.

To see this, consider the production of a first pair $\mathrm{q}_1\bar{\mathrm{q}}_1$, for simplicity assumed to be along L′ at a distance l' from the $\bar{\mathrm{q}}_0$-particle at the endpoint. According to the results above, q_1 will be accelerated along the dashed line indicated in fig. 5.14 forming a yo-yo system together with $\bar{\mathrm{q}}_0$.

The energy and momentum of the system are in general small as compared to the energy and momentum of the whole original system. The relevant variable in the target fragmentation region is the lightcone variable

$$z^- = (E - p_l)/(E - p_l)_{\mathrm{tot}} \tag{5.6}$$

which for large energies coincides with the ordinary Feynman scaling variable. From eqs. (5.5) we obtain that for the system $\mathrm{q}_1\bar{\mathrm{q}}_0$ and l'

$$E - p_l = \kappa\, l' \cos(\alpha/2) \equiv \kappa\, l'_\parallel \tag{5.7}$$

i.e. $(E - p_l)$ only depends upon the projection of the string-piece l' along $\boldsymbol{Q}+\boldsymbol{k}$. Actually we immediately obtain that

$$l'_\parallel = z^- L_\parallel \tag{5.8}$$

where $L_\parallel$ is the corresponding longitudinal size of the whole system.

The remainder system containing q_0, the string-segments L and the remaining piece of L′ and the new endpoint $\bar{\mathrm{q}}_1$ will continue to move as a rigid triangle with $\bar{\mathrm{q}}_1$ accelerated parallel to $\boldsymbol{Q}+\boldsymbol{k}$. For the mass of this system, M, we obtain by applying the same considerations as above for a large total cm energy W:

$$M^2 \approx (1 - z^-)W^2\,. \tag{5.9}$$

Further we note that if the production probability per unit time for a q$\bar{\mathrm{q}}$-pair is known in the rest frame of the string, due to time dilatation it is proportional to $\sqrt{1 - v_\perp^2}$ in a frame where the string moves with transverse velocity $v_\perp$. This implies that the production probability is also proportional to the tension $T = \kappa\sqrt{1 - v_\perp^2}$. Thus the probability to produce a pair in the string-element dl in L′ is

proportional to

$$\sqrt{1-v_\perp^2}\,\mathrm{d}l = \mathrm{d}l\cos(\alpha/2) = \mathrm{d}l_\parallel\,. \tag{5.10}$$

Comparing the results in eqs. (5.8), (5.9) and (5.10) to the eqs. (2.26)–(2.29) of section 2.3 we conclude that the only difference is that all the relevant quantities are determined by the projections on the direction $\boldsymbol{Q}+\boldsymbol{k}$. The same results would apply also if the meson $\bar{q}_0q_1$ contained the corner A. Then the remainder system would move as a rigid stick. Actually this part of the system is then in a yo-yo mode, Lorentz transformed at an angle to the string direction.

As in the one-dimensional case more and more mesons will break off, and the string-pieces corresponding to these mesons will become shorter and shorter while the corresponding momenta become larger and larger. In the current fragmentation region, where the mesons have z^+-values of the order 1, we obtain from the relation

$$z^+ \cdot z^- = m_\perp^2/W^2 \tag{5.11}$$

that z^- is of the order $m_\perp^2/W^2$. Consequently the size of the string-pieces is correspondingly small (cf. eq. (5.8)).

All the meson states are in the yo-yo mode except for the one in the target fragmentation region which contains the corner A in fig. 5.14. Actually, in this case the quark and antiquark will move along the sides of a triangle (in the CM frame) [108]. Therefore, if the projection of this triangular mode upon a physical meson state is similar to the projection of the yo-yo mode, then the breakup distributions in the target fragmentation region are not different from the ones obtained in the one-dimensional model.

With regard to the transverse degrees of motion (with respect to the direction $\boldsymbol{Q}+\boldsymbol{k}$) we note from eq. (5.5) that the string-pieces carry transverse momentum proportional to the size of the string at the time of production. Since the mesons in the current fragmentation region take very short pieces (in the lab system), they will obtain transverse momenta from this source only to the order $m_\perp^2/W^2$. The total transverse momentum of the string system, equal to $-\boldsymbol{k}_\perp$, is therefore partitioned among the mesons of the target fragmentation region. The particles with largest z^- will take the main part, but the precise properties of this distribution also depend on our assumption that the original state before the transfer of $\boldsymbol{Q}$ is a yo-yo mode. For a more complicated state we will obtain a different shape of the string. This will, however, not affect the properties of the current fragmentation region because the mesons in this part of the phase space stem from a very small piece close to the end of the string.

Thus we conclude that if a quark in a mesonic system is hit by a virtual photon or weak interaction probe with momentum $\boldsymbol{Q}$, we obtain a quark jet with momentum $\boldsymbol{Q}+\boldsymbol{k}$ of the same nature as in e^+e^- annihilation. This happens in spite of the fact that the string has a finite angle to the jet direction, even at infinite energies. (This angle is small, however, in a Lorentz frame in which the mesons in the current fragmentation region have low momenta.) Here $\boldsymbol{k}$ is the momentum of the quark at the time it is hit. The remaining momentum in the system, $-\boldsymbol{k}$, is divided among the particles in the target fragmentation region in a manner such that a particle with a large z^- takes a large fraction.

5.3.2. A model for baryon fragmentation [94]

We now turn to the case of an initial baryon. We will assume that the (massless) quarks move symmetrically at the ends of three string-pieces, joined in a junction as shown in fig. 5.15. The junction itself will in this picture not carry any energy-momentum – it is only a device which moves in such a way

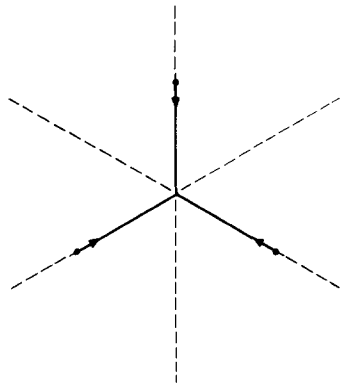

Fig. 5.15. A Y-shaped baryon string model in the rest system. The quarks are at the endpoints of the string.

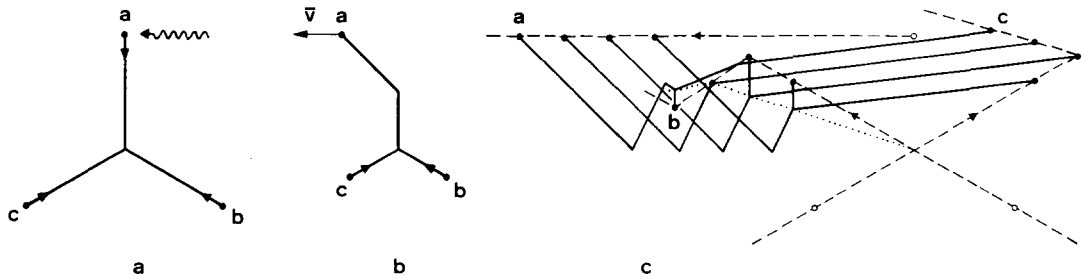

Fig. 5.16. The motion of the Y-shaped baryon string in case the quark marked a is made to move along the direction $\boldsymbol{V}$ by an interaction (a). In this example the angles θ and φ in eq. (5.12) are $\pi/2$ and 0 respectively. In (b) the quark a moves away along $\boldsymbol{V}$ with an adjoining string segment, and a corner moves with the velocity of light towards the junction. In (c) a set of positions in time are marked out with the strings marked by full lines, the quark trajectories with dashed lines and the trajectory of the junction by a dotted line. In position 2 the quarks b and c are at the "old" turning points and will henceforth be accelerated in new directions.

that the total tension at rest of the three string-pieces vanishes. It is not difficult to show that, on the average, half of the energy of the system is kinetic energy of the quarks and the other half potential energy in the strings ("glue"). In fig. 5.16 we show the motion of this system if one of the valence quarks is made to move in the direction $\boldsymbol{V}$ due to an interaction with another hadron or with a lepton in a deep inelastic scattering event. When the quark a moves away, a bend on its adjoining string-piece will move towards the junction with the velocity of light. It reaches the junction at the same time as the other two quarks (provided the three quarks are moving *towards* the junction at the moment of the collision). After this the junction will move with a constant velocity $\bar{v}_j$, which depends on the direction $\bar{V}$ of the quark a. We note that the force from a string on a massless quark is always along the quark motion and the quarks b and c will continue to the "old" turning points (position 2). When they turn around they will, however, be accelerated in a new direction, such that in a Lorentz frame in which the adjoining string-piece is at rest, the quark will just move along the string. We note that when they stop, one of the quarks (b in fig. 5.16) is close to the junction whereas the other one (c) is much farther away. A simple calculation tells us that the energy available in the string-piece adjoining c is in general large enough to produce $q\bar{q}$ pairs, thereby producing a meson containing the quark c.

For the quark b, however, the situation is always such that it will end up too close to the junction for any possible particle production. Thus the quark b and the junction will always end up in the same final state hadron which then becomes a baryon.

We have only discussed the situation when all the quarks are moving "inwards" at the time of the interaction with a. The other situation when all move "outwards" will result in an almost identical final state situation.

We have evidently in this semi-classical model obtained a dynamical situation very similar to the one described in section 5.2, with a, b and c taking the roles of I, J and L respectively. There are, however, two differences. First, there will be a piece of the string between the quark b and the junction where the string cannot break. This will have the same effect as if the J-quark had a finite mass. If we interpret fig. 5.10 as a picture in momentum-space rather than in coordinate-space, there will be a narrow region around the J-quark trajectory where new pairs cannot be produced. We will here neglect this effect.

More important is that the junction moves with a finite velocity. If the string does not break, the b-quark will move back and forth through the junction a number of times, but after some time the c-quark, which moves with the velocity of light, will catch up. If the string has not broken before, we will assume that it will no more be possible to break it between the c-quark and the junction.

As will be discussed in sections 5.5 and 5.6 this is important for the possibility to produce the heavier strange quarks or quarks with large $p_\perp$ in the region between J and L.

The velocity of the junction will depend on the direction $\bar{V}$ of the "kick" in fig. 5.16. Let this direction be described by the polar angles θ and φ in a frame where the kicked quark initially moved along the z-direction and the other two quarks in the xz-plane. Then the velocity v_j of the junction (in the original proton rest frame) after it has been passed by the quarks and the bend in fig. 5.16 is given by the expression

$$v_j^2 = \frac{9\sin^2\theta\sin^2\varphi + \frac{9}{4}\sin^2\theta\cos^2\varphi + 1 + 2\cos\theta + \cos^2\theta}{(\cos\theta - \frac{1}{2})^2}. \tag{5.12}$$

Thus we find that the average value of v_j^2 is given by

$$\langle v_j^2 \rangle \simeq (0.69)^2. \tag{5.13}$$

It turns out that a velocity-change from $v_j = 1$ to $v_j = 0.7$ hardly affects the possibility to produce nonstrange quarks with ordinary $p_\perp$. Thus the particle spectra in figs. 5.11 and 5.12 will not be noticeably changed, only the size of the Λ production spectrum will be a bit smaller. However, the small fraction of events with production of heavier strange quarks or quarks with large $k_\perp$ will be suppressed. This will be discussed further in section 5.5 and will have important consequences for the polarization of hyperons as will be discussed in section 5.6.

5.4. Transverse momentum properties

In sections 5.1 and 5.2 we presented inclusive spectra for various reactions integrated over $p_\perp$. In this subsection we will consider the transverse momentum properties in the proton fragmentation region in some detail.

In addition to the $p_\perp$ of the produced $q\bar{q}$-pairs we also have to consider the primordial $k_\perp$, i.e. the transverse momentum of the valence constituents in the original hadronic bound state. To account fully for the properties of these contributions one needs a complete picture of the baryon wavefunction. Lacking such a picture we will be satisfied with the following simplified assumptions compatible with the hadron-string models presented above.

(1) The three valence-constituents, which in accordance with the considerations in the first two subsections will end up as the L-, J- and I-quark along the force field, will each be given a Gaussian transverse momentum distribution

$$dP_j = d^2k_\perp \exp -(\boldsymbol{k}_\perp^2/\sigma'^2), \qquad j = \mathrm{I, J, L} \tag{5.14}$$

with the constraint that

$$\boldsymbol{k}_{\perp\mathrm{I}} + \boldsymbol{k}_{\perp\mathrm{J}} + \boldsymbol{k}_{\perp\mathrm{L}} = 0\,. \tag{5.15}$$

We will in that way have a parametrization with in principle a parameter σ' at our disposal.

(2) This primordial transverse momentum is transferred to the final state hadron in the same way as the tunneling contribution. Thus the $p_\perp$ of a hadron is the vector sum of the $\bar{k}_\perp$ of its two (for a meson) or three (for a baryon) constituents.

In fig. 5.17 we present the $p_\perp$-spectrum for protons and Λ-particles obtained with a value of σ' such that

$$\langle k_\perp^2\rangle_{\mathrm{I,J\,or\,L}} = \tfrac{2}{3}\sigma'^2 = (0.4\ \mathrm{GeV}/c)^2\,. \tag{5.16}$$

We note that this is consistent with the primordial $k_\perp$ carried by a quark in a DIS-event (cf. section 4.6.2) (when also soft gluon emission is accounted for). As a further check of the x_F and $p_\perp$-distributions we present in fig. 5.18 the baryonic jet profile defined in accordance with the Ochs–Stodolsky considerations [96]. The variable λ is defined as

$$\lambda = x_\mathrm{F}/p_\perp \tag{5.17}$$

with x_F the ordinary Feynman scaling variable.

We compare the results to experimental data and note a general good agreement.

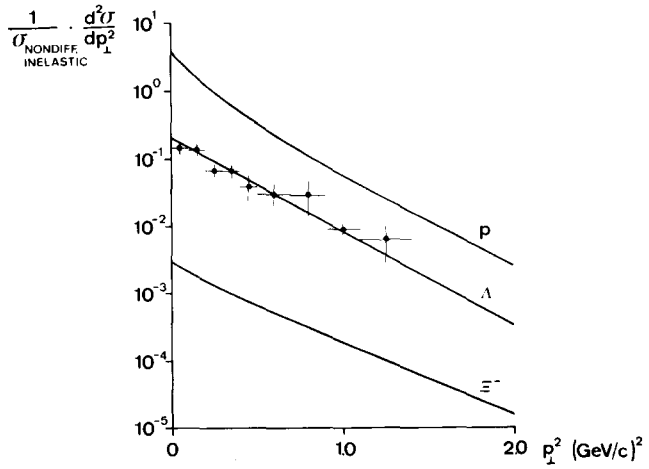

Fig. 5.17. The transverse momentum distribution of the protons, Λ- and Ξ^--particles in a baryon fragmentation region according to the model. Experimental results for Λ from ref. [95] are normalized with $\sigma_{\mathrm{nondiff,\,inelastic}} = 26$ mb.

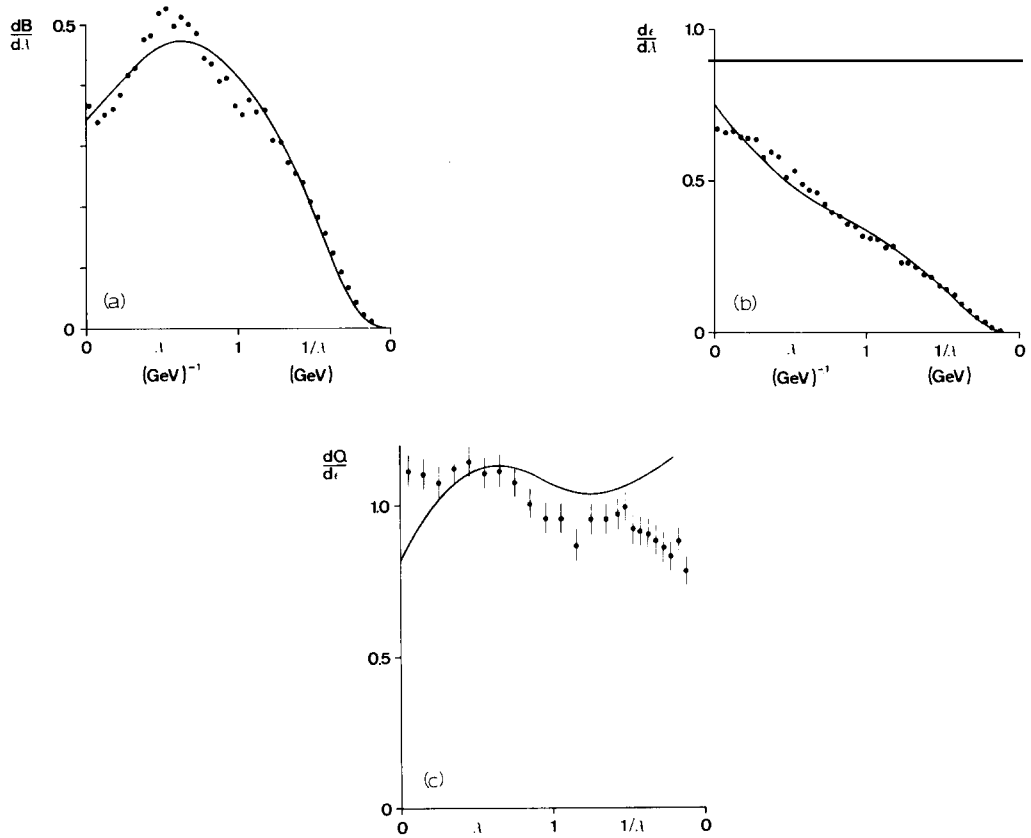

Fig. 5.18. The Ochs–Stodolsky jet profiles for baryon number $dB/d\lambda$, energy fraction $d\varepsilon/d\lambda$ and charge (displayed as $dQ/d\varepsilon$) with $\lambda = x_F/p_\perp$. Experimental data from [96, 97]. The curves are calculated for the experimental beam momentum, 24 GeV/c.

5.5. Suppression of strange quarks and large $k_\perp$ between the leading quarks

In the string picture developed in section 5.3 the junction and the J-quark move with a finite velocity. To see the significance of this effect it is useful to consider fig. 5.19. We note that in order to produce a first rank π- or K-meson a new $q\bar{q}$-pair must be produced along the hyperbolae marked π and K respectively. If the J-quark (and the junction) moves with a velocity close to the velocity of light (fig. 5.19a), then both pions and kaons can be produced with values of z between 0 and $(1 - x_j)$. When the junction moves with a finite velocity (fig. 5.19b) then it is obvious that the more massive kaons will have a much more restricted z-range available.

In the string picture there will be a correlation between the velocity of the junction (which depends on the direction $\bar{V}$ of the "kick" in fig. 5.16) and the value of x_j (which however also depends on the phase in the quark motion at the time of the "kick"). We will study the string motion and these correlations in more detail in future work. For the studies presented here we assume that it is sufficient to give the junction a constant velocity $v_{\text{effective}}$ in the rest frame of the initial proton. For the results presented below we have been guided by the string picture and used (cf. eq. (5.13))

$$v_{\text{eff}} = \sqrt{\langle v_j^2 \rangle} \simeq 0.69\,. \tag{5.18}$$

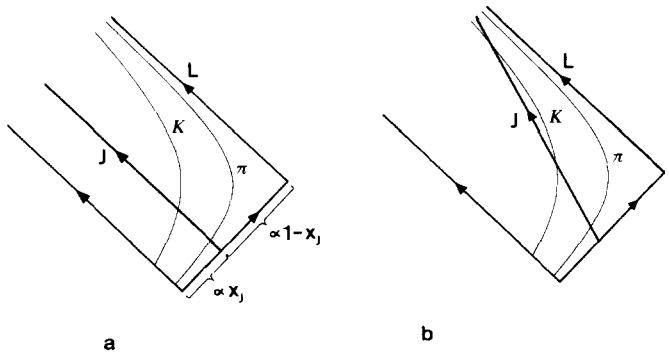

Fig. 5.19. A final state pion or kaon can be formed by the L-quark and an antiquark produced along the hyperbola marked π or K respectively. If the J-quark moves with very large velocity in the initial proton rest frame (a), both pions and kaons can be produced with z-values between 0 and $1 - x_J$. If the J-quark moves with lower velocity (b) the z-range for kaons in particular is more restricted.

The way this suppresses the production of strange quarks can be understood from fig. 5.26 below. To produce a Σ^- particle, two new quarks, one s and one d, have to be produced, one on each side of the J-quark. In fig. 5.26 the fraction of events in which the new quark between J and L is the s- or the d-quark is denoted by V and Ib respectively. Curve IV describes the fraction corresponding to $B\bar{B}$-pair production.

Similarly the production of quark-pairs with large transverse momenta is suppressed between J and L. A larger transverse mass for the first rank meson is suppressed just as the kaon is suppressed according to fig. 5.19. Also the suppression of large Γ in eq. (3.20) will suppress large $k_\perp$ in the small string segment between J and L. According to our Monte Carlo simulations the $k_\perp$-distributions turn out to be effectively Gaussian, with widths such that

$$\langle k_\perp^2 \rangle_{\text{LJ segment}} = 0.09(\text{GeV}/c)^2 ; \qquad \langle k_\perp^2 \rangle_{\text{behind J}} = 0.18(\text{GeV}/c)^2 . \tag{5.19}$$

These results are obtained for both strange and nonstrange quarks.

5.6. Hyperon polarization in proton fragmentation

Since momentum distributions of the produced hadrons often are largely governed by the longitudinal phase-space, polarization phenomena offer an extra tool to gain insight into the hadronization process. Polarization effects were commonly expected to die away quickly with increasing energy and it came as a surprise when strong polarization effects in the inclusive production of Λ-particles were observed even at FNAL and ISR energies. This cannot be explained from hard scattering processes as calculated in perturbative QCD, and therefore it must be a result of the soft confining interactions. We also note that the observed polarization is not a large angle phenomenon; instead it seems to saturate already at $p_\perp \sim 1$ GeV/c.

5.6.1. Polarization mechanism [98]

When a quark–antiquark pair is produced in a colour field, we note that (cf. section 3) while a massless pair can classically be produced in a single point in space-time and afterwards be dragged apart by the force field, a pair with (transverse) masses $\mu_\perp$ must classically be produced at a distance $2l$ such that the field energy in between equals the produced masses (cf. eq. (3.2)).

If the colour field has no transverse excitations, then transverse momentum must be conserved and the $q\bar{q}$-pair is produced with equal and opposite $k_\perp$. Quantum mechanically the pair production can be treated as a tunneling phenomenon with a (virtual) pair produced in a space-time point and afterwards tunneling out through a linear potential. As discussed in section 3, this leads to a Gaussian distribution in $k_\perp$.

From fig. 5.20 it is evident that such a pair will carry an orbital angular momentum $\bar{L}$ of the order

$$|\bar{L}| \simeq 2lk_\perp \simeq 2k_\perp \mu_\perp/\kappa\,. \tag{5.20}$$

If the force field is nonexcited with respect to transverse degrees of freedom, the orbital angular momentum $\bar{L}$ must be compensated by the pair becoming polarized in the opposite direction. We note that in order for this description to be consistent it is necessary that the $k_\perp$-distribution is such that angular momenta $L > 1$ are suppressed. Since eq. (5.20) implies that $L \approx 1$ for $k_\perp \approx 0.3\,\mathrm{GeV}/c$ this is indeed the case.

A similar result is also obtained if quarks are more frequently produced in spin states which are energetically favoured by the Thomas precession term in the Hamiltonian [99]. In the following we study how this polarization effect can be observed in the polarization of hyperons produced in proton fragmentation. Most experimental data are for pp-collisions but our model predicts similar effects for leptoproduction.

5.6.2. Λ-polarization

The Λ-particle is particularly easy to study. Firstly, in the constituent quark model it contains beside the strange quark a ud-pair which has spin zero, thus the spin of the Λ is the spin of the s-quark. Secondly a Λ-particle clearly exhibits its polarization via its weak decay.

If we look at a Λ-particle produced with large z it is according to our model usually formed by producing a strange quark in the field behind a ud-diquark from the initial proton. In refs. [98, 94] we studied the polarization of Λ-particles produced by this mechanism, which should dominate in the large-x_F limit.

For the polarization of the s-quark we assumed that it increased with the orbital angular momentum L of the produced $s\bar{s}$-pair according to the relation

$$p_q = L/(\beta + L) \tag{5.21}$$

where the parameter β is expected to be in the range 1–2.

If the Λ is produced with a definite $\bar{p}_\perp(\Lambda)$ also the s-quark tends to have its transverse momentum in this direction. We note that if both the s-quark and the ud-diquark have Gaussian distributions (as is

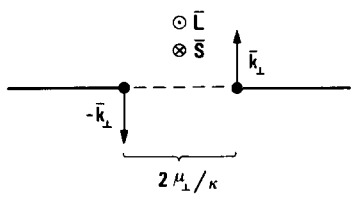

Fig. 5.20. A quark and an antiquark with transverse momenta $\bar{k}_\perp$ and $-\bar{k}_\perp$ are produced at a distance $2\mu_\perp/\kappa$ from each other. They carry an orbital angular momentum $\bar{L}$ which is compensated if the spins are polarized in the opposite direction.

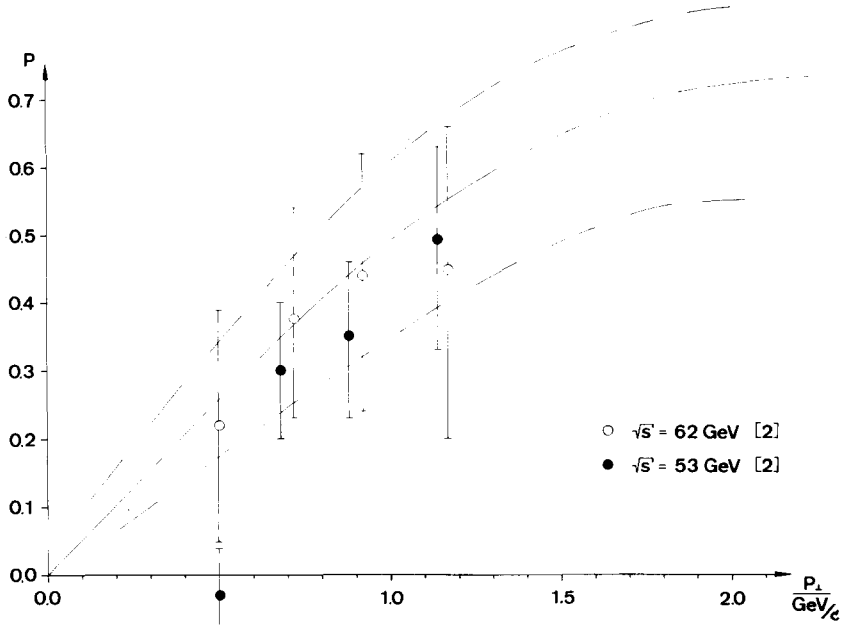

Fig. 5.21. The polarization of Λ-particles (along $\bar{p}_\Lambda \times \bar{p}_p$) in proton fragmentation regions as a function of $p_\perp$. Data from ref. [100] and the dashed lines correspond to upper and lower limit for model predictions for large x_F.

assumed above) with widths σ_q and σ_{qq} respectively we find

$$\left\langle p_\perp(s) \frac{\boldsymbol{p}_{\perp\Lambda}}{|\boldsymbol{p}_{\perp\Lambda}|} \right\rangle = \frac{\sigma_q^2}{\sigma_q^2 + \sigma_{qq}^2} |\boldsymbol{p}_{\perp\Lambda}| \,. \tag{5.22}$$

The resulting polarization for Λ-particles as a function of $p_\perp$ is shown in fig. 5.21 and we note a good agreement with ISR-data obtained at large x_F-values.

For lower values of x_F, Λ-particles can in our model be produced by the following different mechanisms:

(Ia) The Λ-particle stems from a $(ud)_0$ composed of the L- and J-quarks with the *s-quark* produced *behind* the J-quark.

(Ib) The Λ-particle stems from a $(ud)_0$ composed of the J-quark and another (u or d) quark from a piece produced between L and J together with and *s-quark* produced *behind* the J-quark.

(II) The Λ-particle stems from a $(ud)_0$ built from the J-quark and a (u or d) quark produced behind it (or possibly the I-quark) while the *s-quark* stems from the field in *between the J- and L-quark.*

(III) The Λ-particle stems from the decay of a primarily produced Σ^0 or a Y*.

(IV) The Λ-particle is one of a pair from baryon–antibaryon production along the force field. $B\bar{B}$-pairs can be produced when a diquark–antidiquark pair (colour $\bar{3}$–3) is produced in the field. We assume that this occurs with the same probability as in a quark jet as described in ref. [41].

In fig. 5.22 we exhibit the fractional Λ-particle production according to the mechanisms (I)–(IV) (f_I–f_{IV}) as a function of x_F for large energies. (For this purpose we do not differ between (Ia) and (Ib).)

According to our production model the x_F- and the $p_\perp$-distributions do to a large extent factorize for a given production mechanism. Due to the Gaussian character of the $k_\perp$-distributions both for the tunneling production and for the primordial contributions, the mean s-quark transverse momentum is

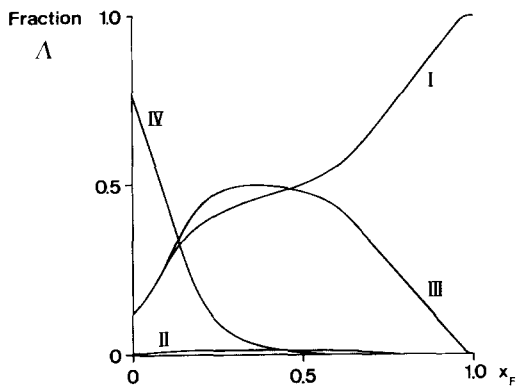

Fig. 5.22. The fractions of Λ-particles produced with the mechanisms I–IV in the main text as functions of x_F in a proton fragmentation region. (The calculations are for 400 GeV/c proton lab. momentum.)

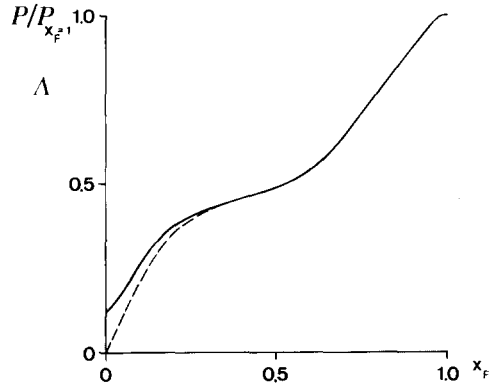

Fig. 5.23. The ratio in eq. (5.23) is shown as the full line corresponding to the model prediction for Λ-polarization normalized to 1 at $x_F = 1$. In e.g. a proton–proton interaction, Λ's stemming from the opposite hemisphere ($x_F < 0$) are polarized oppositely and the resulting subtracted prediction is shown by a dashed line.

proportional to the Λ transverse momentum. For the production mechanisms (Ia) and (Ib) the s-quark and therefore also the Λ-particle should be polarized along the direction $\boldsymbol{p}_\Lambda \times \boldsymbol{p}_{\text{proton}}$. For the production mechanism (II), where the s-quark will be pulled by the field in the opposite direction, the polarization should be opposite to $\boldsymbol{p}_\Lambda \times \boldsymbol{p}_p$.

Λ-particles stemming from the decay of Σ^0 and Y* should retain some part of the original particle polarization. This contribution will be rather small – although we expect it to be in the same directions as the one from production mechanisms (Ia) and (Ib) – and we will neglect it henceforth.

Finally, for the reaction mechanism (IV) we do not expect any Λ polarization, at least not along the normal to the beam–Λ-plane. In fig. 5.23 we plot the ratio

$$\frac{f_{\text{I}} - f_{\text{II}}}{f_{\text{I}} + f_{\text{II}} + f_{\text{III}} + f_{\text{IV}}} \tag{5.23}$$

as a function of x_F and we expect that for a fixed $p_\perp$ and with the absolute size of Λ polarization given at $x_F = 1$ this should provide a prediction for the Λ polarization in the whole fragmentation region. We note that the dependence on x_F is almost linear, as is also indicated by the experimental data [101]

5.6.3. Σ^0, Σ^+ polarization

In the constituent quark model the Σ^0 and Σ^+ are $((ud)_1 s)$ and $((uu)_1 s)$ states respectively with the index on the diquark corresponding to spin and isospin 1. Since the Σ^0 and Σ^+ are both spin 1/2 particles, their polarization will be *opposite* to the produced s-quark polarization and its size will depend upon to what extent the corresponding spin-1 diquark is polarized by itself. These diquarks are often "spectators" in the ordinary notation, i.e. they may stem from the original proton wavefunctions, and therefore they should exhibit no polarization according to conventional wisdom. There are in our opinion reasons to believe that the production mechanisms will favour spectator polarizations [99, 109]. If we neglect the question of the absolute size of the Σ^0 polarization, we may, however, estimate the x_F-dependence just as for the Λ-particle. The production mechanisms (I)–(IV) discussed above are available also for the Σ^0- and Σ^+-particles, and in fig. 5.24 we depict the relative fractions for different

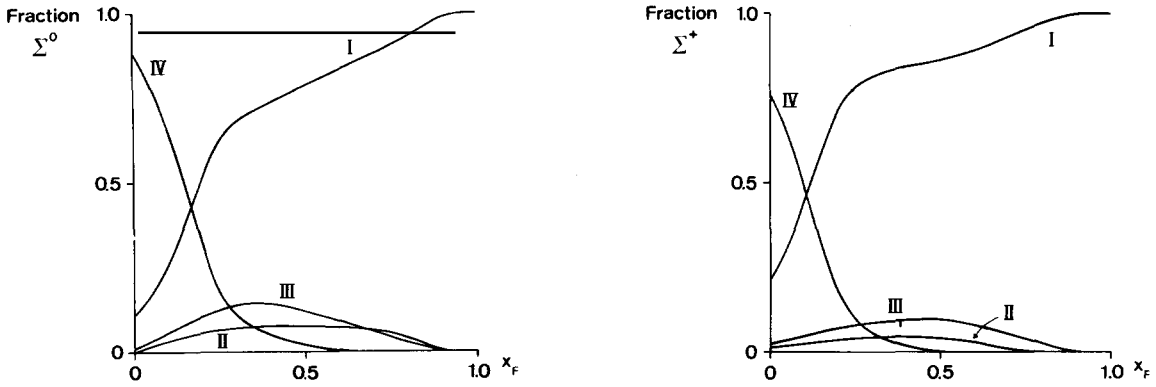

Fig. 5.24. The fractions for Σ^0 and Σ^+ corresponding to fig. 5.22 for the Λ-particles.

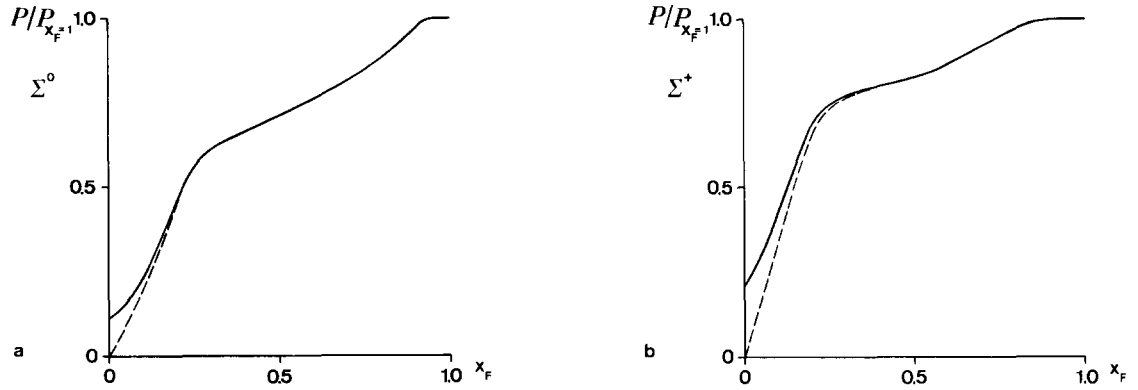

Fig. 5.25. The ratio in fig. 5.23 for the Λ-particles shown for Σ^0 and Σ^+.

x_F-values. We also show in fig. 5.25 the ratio (5.23) as a measure of the expected Σ^0 and Σ^+ polarizations along the direction $\boldsymbol{p}_{\text{proton}} \times \boldsymbol{p}_{\Sigma}$.

5.6.4. Σ^- polarizations

In order to produce $\Sigma^-((dd)_1s)$ or $\Xi\{(ss)_1d$ or $(ss)_1u\}$ in a proton fragmentation region, it is necessary to produce at least two new quarks for the hyperon. For Σ^- it is possible to take one of the d-quarks from the initial proton. In our model this quark is then the J-quark and we have the following possibilities:

(Ib) The *s-quark* stems from *behind* the J-quark and the new d-quark from the string segment between J and L.

(V) The *s-quark* stems from *between J and L* and the new d-quark from behind J.

(III) Decay of Y*-particles.

(IV) Σ^--particles produced via the $B\bar{B}$-pair production mechanism.

According to our model the produced Σ^--particles will be polarized upwards (i.e. along $\bar{p}_{\text{proton}} \times \bar{p}_{\Sigma^-}$) as the combined effect of the following properties

1: The quark behind the J-quark (s or d in case (Ib) and (V) respectively) is polarized upwards and

the quark between J and L (s or d) is polarized downwards, because it is pulled in the opposite direction by the colour field.

2: Mechanism (Ib) dominates over (V).

As discussed in section 5.5 the production of strange quarks is suppressed in the LJ segment of the string. In fig. 5.26 we show the fractions of produced Σ^- according to the mechanisms (Ib), (IV) and (V).

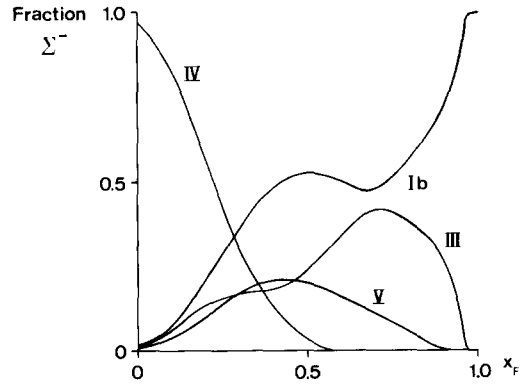

Fig. 5.26. The fractions for Σ^- from the different reaction mechanisms described in the main text.

Because the $p_\perp$-spectra for the produced quarks are approximately Gaussian (cf. eq. (5.19)), the transverse momentum and thereby the polarizations of the produced quarks will increase linearly with the transverse momentum of the Σ^-. We note that according to the additive quark model, the different possible quark polarizations will affect the final state Σ^- in different ways. To see that we assume that the three quarks, d (and J-quark), d (the produced d-quark) and s have polarizations α_1, α_2 and α_3 ($-1 \le \alpha_i \le 1$, $i = 1, 2, 3$) respectively. The spin wavefunction for a Σ^- with spin up ($m_s = +1/2$) is given by

$$\psi_{\Sigma^-}(+) = \sqrt{\tfrac{2}{3}}|{+}{+}{-}\rangle - \sqrt{\tfrac{1}{6}}|{+}{-}{+}\rangle - \sqrt{\tfrac{1}{6}}|{-}{+}{+}\rangle \tag{5.24}$$

in easily understood notation. With the quark polarization given above and with the assumption that all phases are randomly distributed, the probability that the spins add up to a total spin 1/2 pointing upwards, i.e. give a Σ^- with spin up, is given by

$$\frac{2}{3}\left(\frac{1+\alpha_1}{2}\right)\left(\frac{1+\alpha_2}{2}\right)\left(\frac{1-\alpha_3}{2}\right) + \frac{1}{6}\left(\frac{1+\alpha_1}{2}\right)\left(\frac{1-\alpha_2}{2}\right)\left(\frac{1+\alpha_3}{2}\right) + \frac{1}{6}\left(\frac{1-\alpha_1}{2}\right)\left(\frac{1+\alpha_2}{2}\right)\left(\frac{1+\alpha_3}{2}\right). \tag{5.25}$$

Consequently, the resulting Σ^- polarization, P_{Σ^-}, is

$$P_{\Sigma^-} = \frac{2(\alpha_1+\alpha_2) - \alpha_3 - 3\alpha_1\alpha_2\alpha_3}{3 + \alpha_1\alpha_2 - 2\alpha_3(\alpha_1+\alpha_2)}. \tag{5.26}$$

This result is illustrated in fig. 5.27. In fig. 5.27a we assume that the spectator J-quark is unpolarized ($\alpha_1 = 0$) and show the Σ^- polarization, P_{Σ^-}, as a function of the polarization of the other two quarks, α_2 and α_3. We note that the production mechanism (Ib) ($\alpha_2 > 0$, $\alpha_3 < 0$) will give $P > 0$ and mechanism (V)

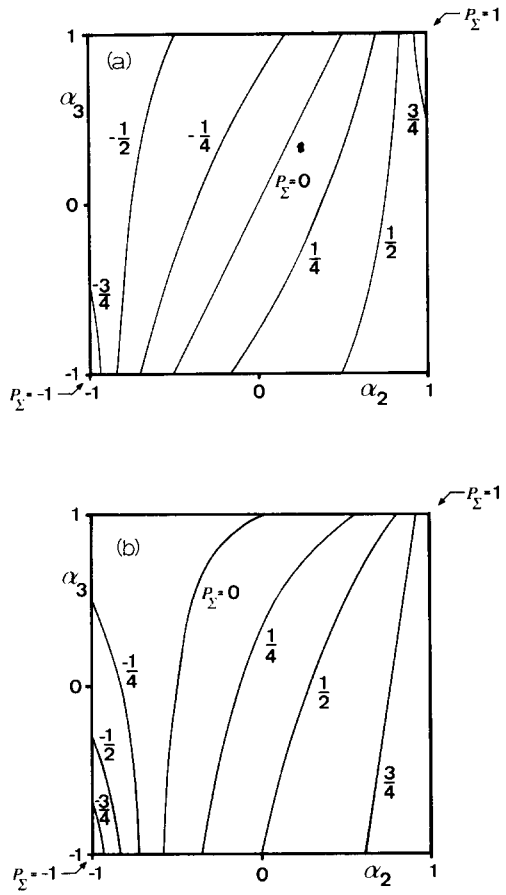

Fig. 5.27. Level curves for fixed polarization of Σ^- as functions of the polarization of the produced d- (α_2) and s-quarks (α_3) when the polarization of the J-quark is $\alpha_1 = 0$ (a) and $\alpha_1 = 0.5$ (b).

($\alpha_2 < 0, \alpha_3 > 0$) will give $P < 0$. We also note that the influence of the d-quark polarization (α_2) is stronger than that of the s-quark. If mechanism (Ib) dominates over (V), obviously Σ^- will be polarized upwards.

As mentioned above it is possible that the initial J-quark is polarized upwards. In fig. 5.27b we show the Σ^- polarization assuming that $\alpha_1 = 0.5$ (50% polarization). We note that this will increase the Σ^- polarization but it will not change the sign. Thus without a detailed model for the possible polarization of the J-quark it is not possible to give a quantitative prediction for the Σ^- polarization, although qualitatively we obtain Σ^- polarization in the same direction as for Σ^+ and Σ^0. This was pointed out already in ref. [102].

We note that in case both the produced quarks for the Σ^- stem from a field behind the J-quark like in a recombination model [103], then a Thomas precession mechanism [99] would give both $\alpha_2 < 0$ and $\alpha_3 < 0$. According to fig. 5.27 this mechanism would then result in a Σ^- polarization which is either very small or in the opposite direction from the one found for Σ^+ and Σ^0. Experimental results show that this is not the case [104] and this fact provides a strong indication for the essentially one-dimensional force-field production presented here, where the new quarks stem from both sides of the J-quark.

Ξ polarization

To produce a Ξ it is necessary to produce two new s-quarks. In our model one is produced on each side of the J-quark, and therefore they tend to be polarized in opposite directions. On the other hand, to form a Ξ the s-quarks must form a triplet spin state, an $(ss)_1$. If one of the two s-quarks has larger $k_\perp$ it will thus have a strong polarization effect and the whole ss-pair will be polarized accordingly. The combined polarization property of the pair is related to the sum of the orbital angular momenta obtained according to fig. 5.20, i.e.

$$L_{1z} + L_{2z} = 2(\mu_{1\perp}k_{1x} - \mu_{2\perp}k_{2x})/\kappa\,. \tag{5.27}$$

Here the x-direction is chosen along $\vec{p}_{\perp\Xi}$ and z along $\vec{p}_{\text{proton}} \times \vec{p}_{\Xi}$. Since $k_{\perp 1}$ and $k_{\perp 2}$ have approximately Gaussian distributions we obtain

$$\langle k_{1x} - k_{2x}\rangle_{p_{\perp\Xi}\,\text{fixed}} = \frac{\langle k_{\perp 1}^2\rangle - \langle k_{\perp 2}^2\rangle}{\langle k_{\perp 1}^2\rangle + \langle k_{\perp 2}^2\rangle}\, p_{\perp\Xi}\,. \tag{5.28}$$

With the widths given in eq. (5.19) we have $\langle k_{\perp 1}^2\rangle \approx 2\langle k_{\perp 2}^2\rangle$. Therefore an estimate of the angular momentum in accordance with eqs. (5.26) and (5.27) would be a linear rise with $p_{\perp\Xi}$:

$$L_{1z} + L_{2z} \simeq \tfrac{2}{3}\langle\mu_\perp\rangle p_{\perp\Xi}/\kappa\,. \tag{5.29}$$

Thus due to the smaller mass available in the string-segment between the L- and J-quark we expect the Ξ-particle to be polarized in the same direction as a Λ-particle.

Once again in case the J-quark is polarized upwards the Ξ polarization will increase but not change its direction.

6. High-$p_\perp$ scattering and topological properties of the colour field

In the Lund model hadrons are produced from the energy in the colour field. Thus in processes with many quarks and gluons the way these are connected by the confining colour-field is important for the way the final state hadrons are produced. This field topology must be taken into account because a confining field cannot be described solely in terms of the positions of the colour charges, as is the case for Coulomb potentials in electrodynamics.

As an example, in an $e^+e^- \to q\bar{q}gg$ event the colour field can be stretched in two different ways as shown in fig. 6.1. We note that this problem is not specific for the Lund model where the gluons are treated as kinks on the stringlike field. The same ambiguity is present also if the gluon is attached to an octet field as in fig. 6.2. Another example is shown in fig. 6.3 which describes the process $gg \to gg$ in a high-$p_\perp$ event. Here the final state contains also the remnants of the incoming hadrons which, due to the emission of the scattered gluons, are colour octets just like gluons. Thus the final state contains four colour octets which can be connected in six different ways. We note that the orientation of the field (defined such that when a $q\bar{q}$-pair is produced the q is pulled along and the $\bar{q}$ against the field direction) is significant and in principle measurable via e.g. $K\bar{K}$ correlations.

In perturbative QCD it is possible to compute amplitudes for the different colour combinations of the partons which can be associated with the different configurations for the colour fields [105].

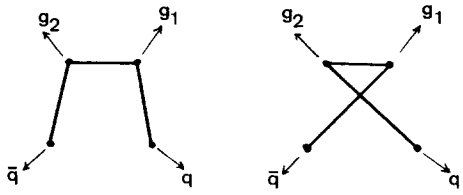

Fig. 6.1. In an $e^+e^- \to q\bar{q}gg$ event the colour field can be stretched in two different ways.

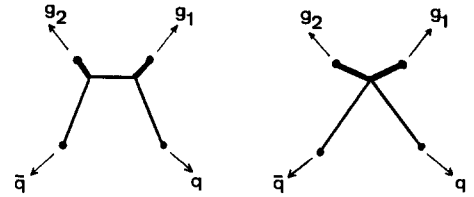

Fig. 6.2. Colour-field configurations as in fig. 6.1 but with a Montvay-gluon (cf. section 4). The heavy lines denote colour octet fields.

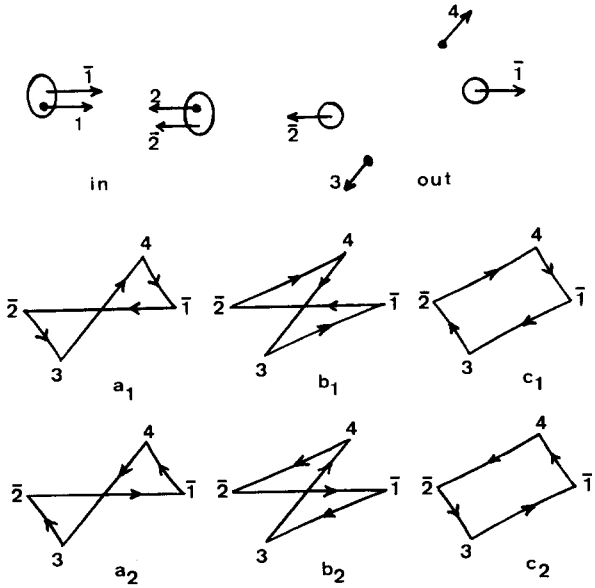

Fig. 6.3. Gluon–gluon scattering in a high-$p_\perp$ event. The incoming (outgoing) gluons are called 1, 2 (3, 4). The hadron remnants $\bar{1}$ and $\bar{2}$ are also colour octets and continue stretching the colour field in the same way as gluons. The colour field between the four outgoing octets can be stretched in six different ways.

However we note that this way to identify noninterfering amplitudes for the different configurations is only unique in the case with infinitely many colours.

In e.g. a high-$p_\perp$ event the fast hadrons in the different jets are insensitive to the way the jets are connected. The distributions of these hadrons have been studied extensively in the literature by many authors. However, if we want to describe the whole event, including the particles with smaller momenta, we must for each subprocess ($qq \to qq$, $qq \to gg$, $qg \to qg$ etc.) compute the amplitudes for all the possible field configurations [106].

Another problem arises because we expect a smooth transition between high-$p_\perp$ and low-$p_\perp$ events. As discussed in section 5 it seems as if in a low-$p_\perp$ event a colour triplet field is stretched in the fragmentation region of an initial proton or meson. In the gg-scattering event illustrated in fig. 6.3 the initial hadron has lost a gluon and continues as a colour octet, stretching a colour octet field or two colour triplet fields. It is then natural to expect that these two triplet fields are not stretched all the way to the end, and that e.g. the field in fig. 6.3 has to be modified as shown in fig. 6.4. In this way it would be possible to obtain a smooth transition between low $p_\perp$ and high $p_\perp$.

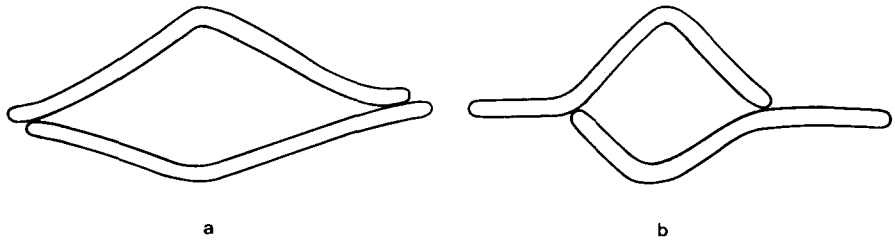

Fig. 6.4. If the colour flux tubes in (a) (the configuration in fig. 6.3 case c) are modified as in (b), it is possible to get a smooth transition between high-$p_\perp$ events and low-$p_\perp$ events as described in section 5.

Thus extensive studies of high-$p_\perp$ events, including low-momentum particles and correlations, are important in order to learn how the confining fields are stretched. However the problem is complicated both due to the amount of competing subprocesses and because the observable effects are in general rather small. A simpler situation with fewer subprocesses, but where the same problems appear, is offered by direct photon production, which thus could give valuable information. In ref. [107] it is demonstrated that in this case multiplicity- and $p_\perp$-spectra show sizeable, experimentally measurable asymmetries. In fig. 6.5 we show a forward–backward asymmetry for the associated hadrons when triggering on a high-$p_\perp$ photon in the direction $\theta_\gamma \sim 20°$. This result is obtained assuming that the colour field is stretched by the initial proton remnant as shown in fig. 6.4a, and a smaller asymmetry at *lower* values of $p_{\perp \text{in}}$ would indicate that the field is stretched more like in fig. 6.4b.

However since very little experimental information is available at present, we will not go into the details here but refer the reader to the original literature [106, 107].

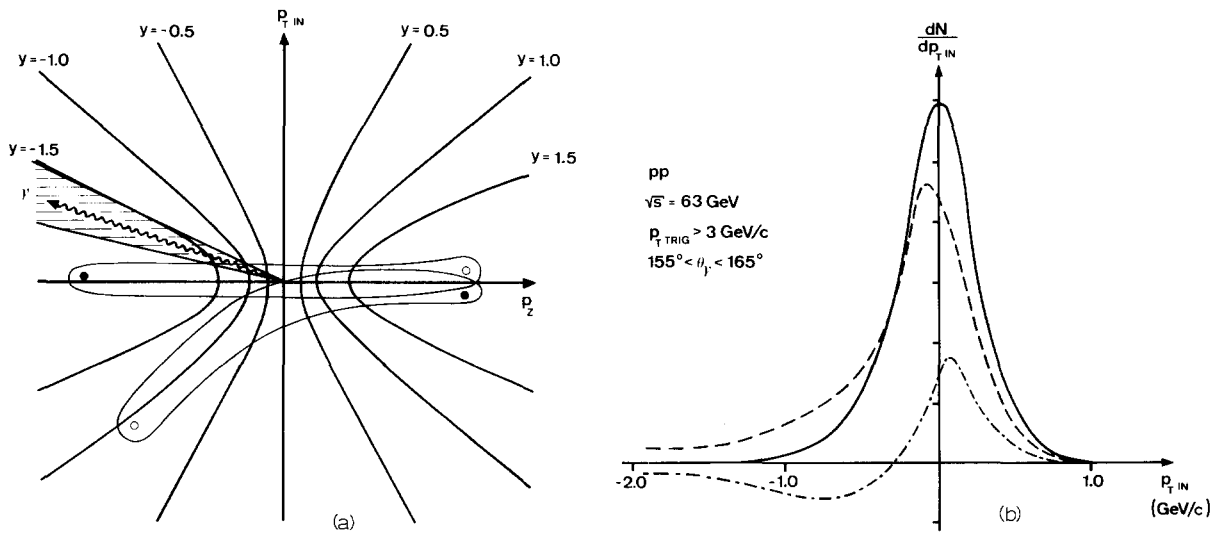

Fig. 6.5. $p_\perp$-compensation for a prompt photon trigger with polar angle between 155° and 165° and with $p_\perp = 3\,\text{GeV}/c$, in pp scattering at $\sqrt{s} = 63\,\text{GeV}$. (a) indicates how the particles are produced in momentum space from the colour fields if the photon is produced in the hard reaction $qg \to q\gamma$. Due to the softer gluon structure function, the photon is usually emitted opposite to the incoming gluon direction. (b) shows $dN/dp_\perp$ for hadrons with $1.0 < y < 1.5$ (full line) and hadrons with $-1.5 < y < -1.0$ (dashed line), and the difference between these distributions (dash-dotted line).

Acknowledgements

We would like to thank the other previous and present members of the Lund group who have contributed to this work, in particular H.-U. Bengtsson, I. Holgersson, O. Månsson, C. Peterson and B. Söderberg.

We would also like to thank those experimental colleagues who kindly have helped us with many of the experimental figures presented here.

Finally we are in great debt to Mrs M. Bergsten for all her help, in particular her ability to type our barely readable manuscripts.

References

[1] G. 't Hooft, Marseille Conference on Yang–Mills fields (1972);
D.J. Gross and F. Wilczek, Phys. Rev. Lett. 30 (1973) 1343;
H.D. Politzer, Phys. Rev. Lett. 30 (1973) 1346.
[2] R.D. Field and R.P. Feynman, Nucl. Phys. B136 (1978) 1;
T. Sjöstrand, Computer Phys. Comm. 27 (1982) 243;
P. Hoyer et al., Nucl. Phys. B161 (1979) 349;
A. Ali et al., Phys. Lett. 93B (1980) 155.
[3] K. Gottfried and F.E. Low, Phys. Rev. D17 (1978) 2487.
[4] A. Krzywicki and B. Petersson, Phys. Rev. D6 (1972) 924.
[5] F. Niedermayer, Nucl. Phys. B79 (1974) 355.
[6] J.D. Bjorken, in: Proc. SLAC Summer Institute on Particle Physics, SLAC-167 (1973) Vol. I, p. 1.
[7] R.D. Field and R.P. Feynman, Nucl. Phys. B136 (1978) 1.
[8] B. Andersson, G. Gustafson and C. Peterson, Nucl. Phys. B135 (1978) 273.
[9] J. Schwinger, Phys. Rev. 128 (1962) 2425; in: Theoretical Physics, Trieste Lectures, 1962 (IAEA Vienna 1963) p. 89.
[10] A. Casher, J. Kogut and L. Susskind, Phys. Rev. D10 (1974) 732.
[11] B. Andersson, G. Gustafson and C. Peterson, Z. Physik C1 (1979) 105.
[12] X. Artru, Physics Reports, next part.
[13] T. Sjöstrand, Computer Phys. Comm. 27 (1982) 243.
[14] G. Drews et al., Phys. Rev. Lett. 41 (1978) 1433;
I. Cohen et al., DESY 80/26 and Cornell CLNS 80/449.
[15] TASSO Collaboration, R. Brandelik et al., Phys. Lett. 117B (1982) 135.
[16] Amsterdam-Bergen-Bologna-Padova-Pisa-Saclay-Torino Collaboration (WA 25), Fragmentation of the Hadronic System in a ($\bar{\nu}$) Deuterium Experiment; Comparison with the Lund Model, paper presented at Paris Conf. 1982.
[17] DASP Collaboration, R. Brandelik et al., Nucl. Phys. B148 (1979) 189.
[18] TASSO Collaboration, R. Brandelik et al., Phys. Lett. 89B (1980) 418.
[19] TASSO Collaboration, M. Althoff et al., Z. Physik C17 (1983) 5.
[20] B. Andersson, G. Gustafson and B. Söderberg, Lund preprint LU TP 83-2.
[21] PLUTO Collaboration, Ch. Berger et al., DESY 82-058;
W. Koch, DESY 82-072, to be published in: Proc. Multiparticle Conference, Volendam 1982.
[22] X. Artru and G. Mennessier, Nucl. Phys. B70 (1974) 93.
[23] M.G. Bowler, Z. Physik C11 (1981) 169.
[24] R. Hagedorn, CERN report 71-12; 2.
[25] K.G. Wilson, Phys. Rev. D10 (1974) 2445.
[26] J.D. Bjorken, Phys. Rev. D17 (1978) 171.
[27] CDHS Collaboration, H. Abramowicz et al., Z. Physik C15 (1982) 19.
[28] S.M. Errede, RX-966 (Ohio-State) 1981, Ph.D. Thesis, unpublished.
[29] Mark II Collaboration, J.M. Yelton et al., Phys. Rev. Lett. 49 (1982) 430.
[30] D. Lüke, in: 21st Intern. Conf. on High Energy Physics, eds. P. Petiau and M. Porneuf, Journal de Physique 43 (1982) C3-67.
[31] J. Kirkby, ibid C3-45.
[32] CLEO Collaboration, C. Bebek et al., Phys. Rev. Lett. 49 (1982) 610.
[33] W. Heisenberg and H. Euler, Z. Physik 98 (1936) 714;
J. Schwinger, Phys. Rev. 82 (1951) 664.

[34] E. Brezin and C. Itzykson, Phys. Rev. D2 (1970) 1191.
[35] A. Casher, H. Neuberger and S. Nussinov, Phys. Rev. D20 (1979) 179.
[36] B. Andersson, G. Gustafson and T. Sjöstrand, Z. Physik C6 (1980) 235.
[37] B. Andersson and G. Gustafson, Lund preprint LU TP 82-5.
[38] I. Cohen et al., Phys. Rev. D25 (1982) 634.
[39] H.E. Montgomery, Proc. 1981 Int. Symp. on Lepton and Photon Interactions, Bonn 1981;
EMC Collaboration, J.J. Aubert et al., Phys. Lett. 103B (1981) 388.
[40] G. Wolf, in: 21st. Int. Conf. on High Energy Physics, eds. P. Petiau and M. Porneuf, Journal de Physique 43 (1982) C3-525;
B. Foster, Invited talk at Europhysics Study Conf., Erice, Sicily, 1981;
JADE Collaboration, W. Bartel et al., Phys. Lett. 104B (1981) 325;
TASSO Collaboration, ref. [19].
[41] B. Andersson, G. Gustafson and T. Sjöstrand, Nucl. Phys. B197 (1982) 45.
[42] T. Meyer, Z. Physik C12 (1982) 77.
[43] K.W. Bell et al., Rutherford preprint RL-82-011.
[44] M. Piccolo et al., Phys. Rev. Lett. 39 (1977) 1503;
G.S. Abrams et al., Phys. Rev. Lett. 44 (1980) 10.
[45] P. Hoyer, P. Osland, H.G. Sander, T.F. Walsh and P.M. Zerwas, Nucl. Phys. B161 (1979) 349.
[46] A. Ali, E. Pietarinen, G. Kramer and J. Willrodt, Phys. Lett. 93B (1980) 155.
[47] I. Montvay, Phys. Lett. 84B (1979) 331.
[48] C. Peterson and T.F. Walsh, Phys. Lett. 91B (1980) 455.
[49] B. Andersson, G. Gustafson and T. Sjöstrand, Phys. Lett. 94B (1980) 211.
[50] JADE Collaboration, W. Bartel et al., Phys. Lett. 101B (1981) 129;
A. Petersen, Moriond Proceedings 1983.
[51] JADE Collaboration, W. Bartel et al., preprint DESY 82-086.
[52] J. Ellis, M.K. Gaillard and G.G. Ross, Nucl. Phys. B111 (1976) 253.
[53] P. Söding, Rapporteur talk at the EPS Intern. Conf. on High Energy Interactions, Geneva 1979;
B. Wiik, Rapporteur talk at the Madison Conference 1980.
[54] G. Parisi and R. Petronzio, Nucl. Phys. B154 (1979) 427.
[55] Yu. Dokshitzer, D. Dyakonov and S. Troyan, Proc. 13th Winter School, Leningrad 1978.
[56] B. Andersson, G. Gustafson and T. Sjöstrand, Z. Phys. C12 (1982) 49.
[57] T. Sjöstrand, The Lund Monte Carlo for e^+e^- jet physics, Lund preprint LU TP 82-7, to be published in Comp. Phys. Comm.
[58] G. Ingelman and T. Sjöstrand, A Monte Carlo program for leptoproduction, Lund preprint LU TP 80-12.
[59] H.-U. Bengtsson, The Lund Monte Carlo for high-$p_\perp$ physics, Lund preprint LU TP 82-15.
[60] G. Wolf, Selected topics on e^+e^- physics, preprint DESY 80/13;
P. Duinker, Rev. Mod. Phys. 54 (1982) 325.
[61] CELLO Collaboration, preprint DESY 82-061.
[62] C. Basham, L. Brown, S. Ellis and S. Love, Phys. Rev. Lett. 41 (1978) 1585; Phys. Rev. D19 (1979) 2018; Phys. Rev. D24 (1981) 2382.
[63] A. Ali and F. Barreiro, Phys. Lett. 118B (1982) 155.
[64] S.D. Ellis, Phys. Lett. 117B (1982) 333.
[65] JADE Collaboration, W. Bartel et al., Phys. Lett. 119B (1982) 239.
[66] G. Altarelli and G. Martinelli, Phys. Lett. 76B (1978) 89.
[67] A. Méndez, Nucl. Phys. B145 (1978) 199;
R.D. Peccei and R. Rückl, Nucl. Phys. B162 (1980) 125.
[68] M. Glück, E. Hoffman and E. Reya, Z. Phys. C13 (1982) 119.
[69] A.J. Buras and K.J.F. Gaemers, Nucl. Phys. B132 (1978) 249;
M. Glück and E. Reya, Nucl. Phys. B130 (1977) 76;
J.F. Owens and E. Reya, Phys. Rev. D17 (1978) 3003.
[70] B. Andersson, G. Gustafson, G. Ingelman and T. Sjöstrand, Z. Phys. C9 (1981) 233.
[71] G. Ingelman, B. Andersson, G. Gustafson and T. Sjöstrand, Nucl. Phys. B206 (1982) 239.
[72] B. Andersson, G. Gustafson, G. Ingelman and T. Sjöstrand, Z. Phys. C13 (1982) 361.
[73] EMC Collaboration, J.J. Aubert et al., Phys. Lett. 100B (1981) 433.
[74] J. Gayler, preprint DESY 81-063.
[75] EMC Collaboration, J.J. Aubert et al., Phys. Lett. 95B (1980) 306.
[76] ABCDLOS Collaboration, Preprint CERN-EP/80-66.
[77] EMC Collaboration, J.J. Aubert et al., Phys. Lett. 119B (1982) 233.
[78] E.K. Manesis and N.A. Papadopoulos, Phys. Lett. 86B (1979) 361; Nucl. Phys. B174 (1980) 300; QCD and hadronic energy flow at SPS and HERA energies, Johannes Gutenberg Universität, Mainz preprint MZ-TH 80/7;
F. Halzen and D.M. Scott, in: Proc. XIth Intern. Symp. on Multiparticle Dynamics, Brugge, Belgium, 1982.
[79] K. Koller and T.F. Walsh, Nucl. Phys. B140 (1978) 449.
[80] B. Andersson, G. Gustafson and C. Peterson, Phys. Lett. 69B (1977) 221; 71B (1977) 337.

[81] B. Andersson, G. Gustafson, I. Holgersson and O. Månsson, Nucl. Phys. B178 (1981) 242.
[82] Single Arm Spectrometer Data, W.M. Troy Thesis MIT (1978).
[83] I. Cohen et al., Phys. Rev. Lett. 40 (1978) 1614.
[84] R. Göttgens et al., Z. Physik C9 (1981) 21.
[85] A. Capella, U. Sukhatme, Chung-I. Tan and J. Tran Thanh Van, Phys. Lett. 81B (1979) 68.
[86] Axial Field Spectrometer Collaboration, Phys. Lett. 108B (1982) 58;
A. Capella, J. Tran Thanh Van and U.P. Sukhatme, Orsay preprint 82/31.
[87] R.P. Feynman, Photon–Hadron Interactions (New York, Benjamin, 1972).
[88] J.R. Johnson et al., Phys. Rev. D17 (1978) 1292.
[89] Y. Eisenberg et al., Nucl. Phys. B135 (1978) 189.
[90] V. Blobel et al., Nucl. Phys. B135 (1978) 379.
[91] H. Kichini et al., Phys. Rev. D20 (1979) 37.
[92] S. Erhan et al., Phys. Lett. 85B (1979) 447.
[93] M. Derrick et al., Phys. Rev. D17 (1978) 1.
[94] B. Andersson, G. Gustafson and O. Månsson, Lund preprint LU TP 82-13.
[95] D. Brick et al., Nucl. Phys. B164 (1980) 1.
[96] W. Ochs and L. Stodolsky, Phys. Lett. 69B (1977) 225.
[97] H. Fesefeldt, W. Ochs and L. Stodolsky, Phys. Lett. 74B (1978) 389;
W. Ochs and T. Shimada, Z. Phys. C4 (1980) 141.
[98] B. Andersson, G. Gustafson and G. Ingelman, Phys. Lett. 85B (1979) 417.
[99] T. de Grand et al., Phys. Rev. D23 (1981) 1227.
[100] S. Erhan et al., Phys. Lett. 82B (1979) 301.
[101] K. Heller, Talk presented at the 5th Intern. Symp. on High Energy Spin Physics, Brookhaven, 1982.
[102] G. Gustafson, in: Proc. 1980 Intern. Symp. on High Energy Spin Physics, Lausanne, 1980.
[103] K.P. Das and R.C. Hwa, Phys. Lett. 68B (1977) 459.
[104] B. Lundberg, Talk presented at the 5th Intern. Symp. on High Energy Spin Physics, Brookhaven, 1982.
[105] G. Gustafson, Z. Phys. C15 (1982) 155.
[106] H.-U. Bengtsson and O. Månsson, Lund preprint LU TP 82-14.
[107] B. Andersson, H.-U. Bengtsson and G. Gustafson, Lund preprint LU TP 82-10.
[108] B. Andersson and G. Gustafson, Z. Phys. C3 (1980) 22.
[109] G. Gustafson, Talk presented at the 5th Intern. Symp. on High Energy Spin Physics, Brookhaven, 1982.
[110] T. Kafka et al., Phys. Rev. D16 (1977) 1261.
[111] F.E. Taylor et al., Phys. Rev. D14 (1976) 1217.
[112] P. Capiluppi et al., Nucl. Phys. B70 (1974) 1;
M.G. Albrow et al., Nucl. Phys. B73 (1974) 40;
P. Capiluppi et al., Nucl. Phys. B79 (1974) 189.
[113] P.D. Higgins et al., Phys. Rev. D19 (1979) 731.
[114] M. Barth et al., Z. Phys. C10 (1981) 205;
P.R.S. Wright et al., CERN EP 81-2.
[115] Aachen-Bonn-CERN-München-Oxford Collaboration, P. Allen et al., Max-Planck-Institut preprint MPI-PAE/Exp. El. 106.
[116] D. Gross, Phys. Rev. Lett. 32 (1974) 1071;
K. Konishi, A. Ukawa and G. Veneziano, Nucl. Phys. B157 (1979) 45.